**Atmospheric
Chemistry
and Physics**

Validation of NO$_2$ and NO from the Atmospheric Chemistry Experiment (ACE)

T. Kerzenmacher[1], M. A. Wolff[1], K. Strong[1], E. Dupuy[2], K. A. Walker[1,2], L. K. Amekudzi[3], R. L. Batchelor[1], P. F. Bernath[4,2], G. Berthet[5], T. Blumenstock[6], C. D. Boone[2], K. Bramstedt[3], C. Brogniez[7], S. Brohede[8], J. P. Burrows[3], V. Catoire[5], J. Dodion[9], J. R. Drummond[10,1], D. G. Dufour[11], B. Funke[12], D. Fussen[9], F. Goutail[13], D. W. T. Griffith[14], C. S. Haley[15], F. Hendrick[9], M. Höpfner[6], N. Huret[5], N. Jones[14], J. Kar[1], I. Kramer[6], E. J. Llewellyn[16], M. López-Puertas[12], G. Manney[17,18], C. T. McElroy[19,1], C. A. McLinden[19], S. Melo[20], S. Mikuteit[6], D. Murtagh[8], F. Nichitiu[1], J. Notholt[3], C. Nowlan[1], C. Piccolo[21], J.-P. Pommereau[13], C. Randall[22], P. Raspollini[23], M. Ridolfi[24], A. Richter[3], M. Schneider[6], O. Schrems[25], M. Silicani[20], G. P. Stiller[6], J. Taylor[1], C. Tétard[7], M. Toohey[1], F. Vanhellemont[9], T. Warneke[3], J. M. Zawodny[26], and J. Zou[1]

[1]Department of Physics, University of Toronto, Toronto, Ontario, Canada
[2]Department of Chemistry, University of Waterloo, Waterloo, Ontario, Canada
[3]Institute of Environmental Physics, Institute of Remote Sensing, Universität Bremen, Bremen, Germany
[4]Department of Chemistry, University of York, Heslington, York, UK
[5]Laboratoire de Physique et Chimie de l'Environnement, CNRS–Université d'Orléans, Orléans, France
[6]Forschungszentrum Karlsruhe und Universität Karlsruhe, Inst. für Meteorologie und Klimaforschung (IMK), Karlsruhe, Germany
[7]Laboratoire d'Optique Atmosphérique, Université des sciences et technologies de Lille, Villeneuve d'Ascq, France
[8]Department of Radio and Space Science, Chalmers University of Technology, Göteborg, Sweden
[9]Belgisch Instituut voor Ruimte-Aëronomie–Institut d'Aéronomie Spatiale de Belgique (IASB-BIRA), Bruxelles, Belgium
[10]Department of Physics & Atmospheric Science, Dalhousie University, Halifax, Nova Scotia, Canada
[11]Picomole Instruments Inc., Edmonton, Alberta, Canada
[12]Instituto de Astrofísica de Andalucía, CSIC, Granada, Spain
[13]Service d'Aéronomie–CNRS, Verrières-le-Buisson, France
[14]School of Chemistry, University of Wollongong, Wollongong, Australia
[15]Centre for Research in Earth and Space Science, York University, Toronto, Ontario, Canada
[16]Institute of Space and Atmospheric Studies, University of Saskatchewan, Saskatoon, Saskatchewan, Canada
[17]Jet Propulsion Laboratory, California Institute of Technology, Pasadena, CA, USA
[18]New Mexico Institute of Mining and Technology, Socorro, NM, USA
[19]Environment Canada, Downsview, Ontario, Canada
[20]Canadian Space Agency, St Hubert, Quebec, Canada
[21]Atmospheric, Oceanic and Planetary Physics, University of Oxford, Oxford, UK
[22]Laboratory for Atmospheric and Space Physics & Department of Atmospheric and Oceanic Sciences, University of Colorado, Boulder, CO, USA
[23]Istituto di Fisica Applicata "Nello Carrara" (IFAC) del Consiglio Nazionale delle Ricerche (CNR), Firenze, Italy
[24]Dipartimento di Chimica Fisica e Inorganica, Universitá di Bologna, Bologna, Italy
[25]Alfred Wegener Institute for Polar and Marine Research, Bremerhaven, Germany
[26]NASA Langley Research Center, Hampton, VA, USA

Correspondence to: T. Kerzenmacher
(tobias@atmosp.physics.utoronto.ca)

Abstract. Vertical profiles of NO$_2$ and NO have been obtained from solar occultation measurements by the Atmospheric Chemistry Experiment (ACE), using an infrared Fourier Transform Spectrometer (ACE-FTS) and (for NO$_2$) an ultraviolet-visible-near-infrared spectrometer, MAESTRO (Measurement of Aerosol Extinction in the Stratosphere and Troposphere Retrieved by Occultation). In this paper, the quality of the ACE-FTS version 2.2 NO$_2$ and NO and the MAESTRO version 1.2 NO$_2$ data are assessed using other solar occultation measurements (HALOE, SAGE II, SAGE III, POAM III, SCIAMACHY), stellar occultation measurements (GOMOS), limb measurements (MIPAS, OSIRIS), nadir measurements (SCIAMACHY), balloon-borne measurements (SPIRALE, SAOZ) and ground-based measurements (UV-VIS, FTIR). Time differences between the comparison measurements were reduced using either a tight coincidence criterion, or where possible, chemical box models. ACE-FTS NO$_2$ and NO and the MAESTRO NO$_2$ are generally consistent with the correlative data. The ACE-FTS and MAESTRO NO$_2$ volume mixing ratio (VMR) profiles agree with the profiles from other satellite data sets to within about 20% between 25 and 40 km, with the exception of MIPAS ESA (for ACE-FTS) and SAGE II (for ACE-FTS (sunrise) and MAESTRO) and suggest a negative bias between 23 and 40 km of about 10%. MAESTRO reports larger VMR values than the ACE-FTS. In comparisons with HALOE, ACE-FTS NO VMRs typically (on average) agree to ±8% from 22 to 64 km and to +10% from 93 to 105 km, with maxima of 21% and 36%, respectively. Partial column comparisons for NO$_2$ show that there is quite good agreement between the ACE instruments and the FTIRs, with a mean difference of +7.3% for ACE-FTS and +12.8% for MAESTRO.

1 Introduction

This is one of two papers describing the validation of NO$_y$ species measured by the Atmospheric Chemistry Experiment (ACE) through comparisons with coincident measurements. The total reactive nitrogen, or NO$_y$, family consists of active nitrogen, NO$_x$ (NO+NO$_2$), and all oxidized nitrogen species, including NO$_3$, HNO$_3$, HNO$_4$, ClONO$_2$, BrONO$_2$ and N$_2$O$_5$. The ACE-Fourier Transform Spectrometer (ACE-FTS) measures all of these species, with the exception of NO$_3$ and BrONO$_2$, while the Measurement of Aerosol Extinction in the Stratosphere and Troposphere Retrieved by Occultation (ACE-MAESTRO, referred to as MAESTRO in this paper) measures NO$_2$. The species NO$_2$ and NO are two of the 14 primary target species for the ACE mission. In this study, the quality of ACE-FTS version 2.2 nitrogen dioxide (NO$_2$) and nitric oxide (NO) and MAESTRO version 1.2 NO$_2$ are assessed prior to their public release. A companion paper by Wolff et al. (2008) provides an assessment of

the ACE-FTS version 2.2 nitric acid (HNO$_3$), chlorine nitrate (ClONO$_2$) and updated version 2.2 dinitrogen pentoxide (N$_2$O$_5$). Validation of ACE-FTS version 2.2 measurements of nitrous oxide (N$_2$O), the source gas for NO$_y$, is discussed by Strong et al. (2008).

NO$_2$ and NO are rapidly interconverted and closely linked through photochemical reactions in the atmosphere. As NO$_x$, they have a maximum lifetime of 10 to 50 h in the stratosphere between 20 and 50 km under midlatitude equinox conditions (Dessler, 2000). The NO$_x$ gas phase catalytic cycle destroys odd oxygen in the stratosphere, while NO$_2$ and NO also have important roles determining the polar ozone budget.

Remote sensing measurements of NO$_2$ and NO have been performed since the early 1970s (e.g. Murcray et al., 1968; Ackermann and Muller, 1972; Brewer et al., 1973; Burkhardt et al., 1975; Fontanella et al., 1975; Noxon, 1975). Satellite instruments have been regularly measuring these species since the launch of Nimbus-7 in 1979, which carried the Stratospheric and Mesospheric Sounder (SAMS) for NO (Drummond et al., 1980) and the Limb Infrared Monitor of the Stratosphere (LIMS) for NO and NO$_2$ (Gille et al., 1980). There was a visible light spectrometer on board the Solar Mesosphere Explorer (SME) spacecraft, which also made early measurements of NO and NO$_2$ (Mount et al., 1984). The launch of the Upper Atmosphere Research Satellite (UARS) in 1991 provided measurements from the Improved Stratospheric and Mesospheric Sounder (ISAMS) (Taylor et al., 1993), the Cryogenic Limb Array Etalon Spectrometer (CLAES) (Roche et al., 1993) and the HALogen Occultation Experiment (HALOE) (Russell et al., 1993).

The ACE mission builds on the heritage of a number of previous solar occultation missions, including the Atmospheric Trace MOlecule Spectroscopy (ATMOS) instrument (Abrams et al., 1996; Gunson et al., 1996; Newchurch et al., 1996; Manney et al., 1999), which flew on four Space Shuttle flights between 1985 and 1994. The three Stratospheric Aerosol and Gas Experiment instruments, SAGE I (McCormick et al., 1979; Chu and McCormick, 1979, 1986), SAGE II (Mauldin et al., 1985) and SAGE III (SAGE ATBD Team, 2002) all used ultraviolet-visible (UV-VIS) solar occultation to measure NO$_2$, as did the second Polar Ozone and Aerosol Measurement (POAM II) (Glaccum et al., 1996) and POAM III (Lucke et al., 1999; Randall et al., 2002). The Improved Limb Atmospheric Spectrometers (ILAS) I and II were infrared solar occultation instruments that also measured NO$_2$ (e.g. Sasano et al., 1999; Nakajima et al., 2006; Irie et al., 2002; Wetzel et al., 2006). In addition to the ACE instruments, there are currently two instruments in orbit measuring NO$_2$ using the occultation technique: SCIAMACHY (SCanning Imaging Absorption spectroMeter for Atmospheric CHartographY), doing solar occultation measurements, (which is its secondary measurement mode) (Bovensmann et al., 1999) and the stellar occultation instrument GOMOS (Global Ozone Monitoring by

the Occultation of Stars) (Kyrölä et al., 2004, and references therein).

Space-based measurements of NO$_2$ are also being made using several other techniques. The Global Ozone Monitoring Experiment GOME (Burrows et al., 1999), SCIA-MACHY (Bovensmann et al., 1999), GOME-2 (Callies et al., 2004), and the Ozone Monitoring Instrument (OMI) (Levelt et al., 2006) all retrieve NO$_2$ total columns from nadir-viewing observations at visible wavelengths. Also using this spectral range for NO$_2$, but in limb-scattering mode, is the Optical Spectrograph and Infra-Red Imager System, or OSIRIS, (Llewellyn et al., 2004) and SCIAMACHY (Bovensmann et al., 1999) in limb mode. The Michelson Interferometer for Passive Atmospheric Sounding (MIPAS) detects both NO$_x$ species and is the only instrument besides ACE-FTS that is currently measuring stratospheric NO from orbit (Fischer and Oelhaf, 1996; Fischer et al., 2008). Recent validation studies of NO$_2$ have been performed by Brohede et al. (2007a) for OSIRIS and Wetzel et al. (2007) for MIPAS Environmental Satellite (Envisat) operational data; the latter included a comparison with the ACE-FTS v2.2 data. In addition, measurements of NO$_2$ by GOMOS, MIPAS and SCIA-MACHY, all on Envisat, were compared by Bracher et al. (2005a).

In this paper, we assess the quality of the ACE-FTS version 2.2 NO$_2$ and NO data and the MAESTRO version 1.2 NO$_2$ data through comparisons with available coincident measurements. The paper is organized as follows. In Sect. 2, the ACE mission and the retrievals of these two species by ACE-FTS and MAESTRO are presented. Section 3 describes all of the satellite, balloon-borne and ground-based instruments used in this study. The validation methodology and the use of a chemical box model to account for the diurnal variability of NO$_2$ and NO are discussed in Sect. 4. In Sect. 5, the results of vertical profile and partial column comparisons for NO$_2$ are given, while Sect. 6 focuses on the results of the NO and NO$_x$ comparisons. Finally, the results are summarized and conclusions regarding the quality of the ACE NO$_2$ and NO data are provided in Sect. 7.

2 The Atmospheric Chemistry Experiment

The ACE satellite mission, in orbit since 12 August 2003, carries two instruments, the ACE-FTS (Bernath et al., 2005) and a dual spectrometer, MAESTRO (McElroy et al., 2007). Both instruments record solar occultation spectra, ACE-FTS in the infrared and MAESTRO in the UV-VIS-near-infrared, from which vertical profiles of atmospheric trace gases, temperature and aerosol extinction are retrieved. The SCISAT spacecraft is in a circular orbit at an altitude of 650 km, with a 74° inclination angle (Bernath et al., 2005), providing up to 15 sunrise and 15 sunset solar occultations per day. The choice of orbital parameters results in coverage of the tropics, midlatitudes and polar regions with an annually repeat-
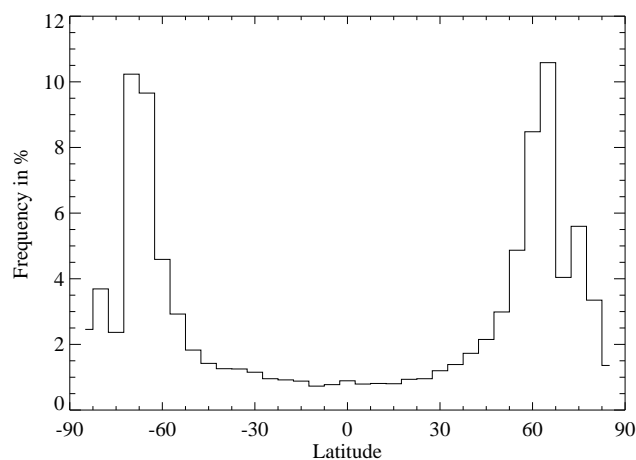

Fig. 1. Sampling frequency of 11,111 ACE satellite measurements (February 2004 to December 2007) using 5° latitude bins.

ing pattern, and a sampling frequency that is greatest over the Arctic and Antarctic (see Fig. 1). The primary scientific objective of the ACE mission is to understand the chemical and dynamical processes that control the distribution of ozone in the stratosphere and upper troposphere, particularly in the Arctic (Bernath et al., 2005; Bernath, 2006, and references therein).

In previous studies McHugh et al. (2005) compared ACE-FTS v1.0 NO$_2$ to HALOE v19 NO$_2$ and found a low bias of 0 to 10% from 22 to 35 km, and a high bias of 0 to 50% below 22 km. Comparisons between HALOE v19 and ACE-FTS v1.0 NO data were described by McHugh et al. (2005), who found that ACE-FTS NO was 10 to 20% smaller than HALOE from 25 to 55 km. Large uncertainties were present from 65 to 90 km, and ACE-FTS NO was approximately 50% smaller than HALOE above 90 km. ACE-FTS and MAESTRO NO$_2$ profiles have been compared with data from POAM III and SAGE III (Kar et al., 2007) and partial columns have been compared with those retrieved using the Portable Atmospheric Research Interferometric Spectrometer for the InfraRed (PARIS-IR), a ground-based adaptation of ACE-FTS and other ground-based spectrometers during the spring 2004 to 2006 Canadian Arctic ACE validation campaigns (Kerzenmacher et al., 2005; Fraser et al., 2008; Sung et al., 2008[1]; Fu et al., 2008). ACE-FTS NO$_x$ profiles have been used in high energy particle precipitation studies (Rinsland et al., 2005; Randall et al., 2007).

---

[1]Sung, K., Strong, K., Mittermeier, R. L., Walker K. A., Fu, D., Kerzenmacher, T., Fast, H., Bernath, P., F., Boone, C. D., Daffer, W. H., Drummond, J. R., Kolonjari, F., Loewen, P., MacQuarrie, K., and Manney, G. L.: Ground-based column measurements at Eureka, Nunavut, made using two Fourier transform infrared spectrometers in spring 2004 and 2005, and comparison with the Atmospheric Chemistry Experiment, in preparation, 2008.
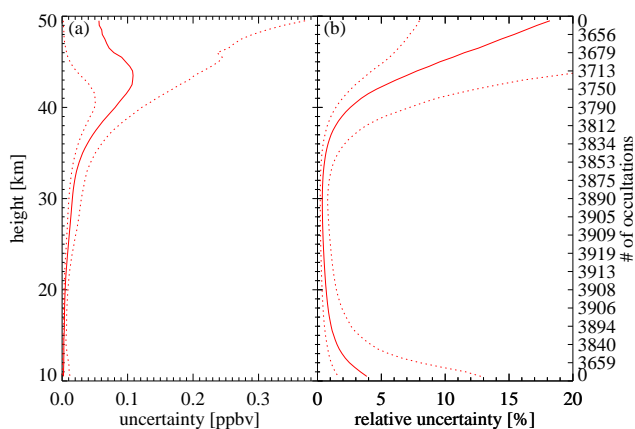
Fig. 2. MAESTRO uncertainties for NO$_2$ using all available data from 2005. Profiles are shown for the median (solid), and 16th and 84th percentiles (dotted) of the **(a)** absolute and **(b)** relative uncertainties.

2.1 ACE-MAESTRO

MAESTRO is based on the Meteorological Service of Canada's SunPhotoSpectrometer (McElroy, 1995; McElroy et al., 1995) that flew on the Space Shuttle in 1992 and was used as part of the NASA ER-2 stratospheric chemistry research program (McElroy et al., 2007). It incorporates two instruments: the UV-VIS instrument that covers the range 285 to 565 nm with a full width at half intensity resolution of 1.5 nm and the visible-near-infrared instrument that measures spectra in the 515 to 1015 nm range with a resolution of 2.0 nm. For the retrievals, GOME flight model NO$_2$ (221 K) and O$_3$ (202 K) absorption cross-sections (Burrows et al., 1998; Burrows et al., 1999) are used. The spectral fits are performed across a wide range of wavelengths, from 420 to 545 nm in the UV and 530 to 755 nm in the visible, and are modelled at a wavelength spacing of 0.1 nm.

NO$_2$ is fit using a differential optical absorption spectroscopy method (e.g. Platt, 1994; Platt and Stutz, 2008), combined with an iterative Chahine (1970) relaxation inversion algorithm. A detailed description of how the retrievals are performed can be found in McElroy et al. (2007). No diurnal corrections were made to the retrieved VMR profiles.

Kar et al. (2007) present errors for the NO$_2$ profiles. In summary, there is an estimated uncertainty due to fitting errors of <5% between 20 and 40 km, which is found by propagating the estimated uncertainty through the spectral retrieval process. Additionally there is a systematic error of about 2% due to uncertainties in NO$_2$ cross sections and 5 to 10% systematic error due to not accounting for temperature effects in the NO$_2$ cross sections. The error due to temperature effects in the O$_3$ cross sections is smaller than 1%. Figure 2 shows the median of the MAESTRO fitting error uncertainties for all retrieved NO$_2$ profiles over the year 2005. The retrieval

program propagates estimated uncertainty through the spectral retrieval process. This is a good proccess for the linear inversion algorithm but does not work well for the Chahine method. For the version 1.2 retrievals, the Chahine method is used, and the uncertainties are propagated with a simplified algorithm. These uncertainties are, therefore, not very accurate but they provide some relative estimate and serve as a rough guide to the relative uncertainties of the MAESTRO measurements. The median relative uncertainties increase exponentially with altitude for NO$_2$. The magnitude of the relative uncertainties is a function of the retrieval errors and the VMR profiles. The median relative uncertainties are <5% from 20 to 40 km, increasing to 18% at 49 km.

The MAESTRO data products are reported on two vertical grids: VMR as a function of tangent altitude and VMR as a function of altitude interpolated onto a 0.5-km grid with the same interpolation method used in the optical model. The full width at half maximum slit size results in an instrument field-of-view of 1.2 km in the vertical and approximately 35 (UV-VIS) and 45 km (VIS-near infrared) in the horizontal for a tangent altitude of 22 km. During an occultation, the signal comes only from the solar disk and the signal extent in the horizontal is then 25 km (McElroy et al., 2007). The altitude resolution of MAESTRO profiles is in the range 1 to 2 km. This was concluded by Kar et al. (2007) based on comparisons of MAESTRO observations with coincident ozonesonde profiles. For the MAESTRO analysis, pressure-temperature profiles are needed. For the version 1.2 MAESTRO data, these are taken from the ACE-FTS retrieval. The altitude-time sequence from the ACE-FTS measurements is used for altitude assignment in the MAESTRO retrievals. The comparisons in this work are made with version 1.2 of the MAESTRO data on the 0.5-km grid.

2.2 ACE-FTS

ACE-FTS measures atmospheric spectra between 750 and 4400 cm^{-1} (2.2 to 13 μm) at a resolution of 0.02 cm^{-1} (Bernath et al., 2005). From these spectra, pressure, temperature and VMR profiles of over 30 trace gases are retrieved as functions of altitude. Typical signal-to-noise ratios are more than 300 from ~900 to 3700 cm^{-1}. The instrument field-of-view (1.25 mrad) corresponds to a maximum vertical resolution of 3 to 4 km (Boone et al., 2005). The vertical spacing between consecutive 2-second ACE-FTS measurements depends on the satellite's orbit geometry during the occultation and can vary from 1.5 to 6 km. The altitude coverage of the measurements extends from the cloud tops to between ~100 and 150 km.

The approach used for the retrieval of VMR profiles and other details of the ACE-FTS processing are described by Boone et al. (2005). A brief description of the retrieval process is given here. A non-linear least squares global fitting technique is employed to analyze selected microwindows (0.3 to 30 cm^{-1} wide portions of the spectrum containing
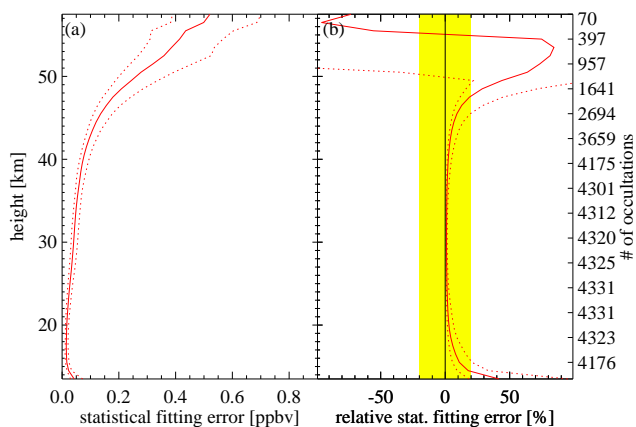
Fig. 3. ACE-FTS statistical fitting errors for NO_2 using all available data from 2005. Profiles are shown for the median (solid), and 16th and 84th percentiles (dotted) of the **(a)** absolute and **(b)** relative statistical fitting errors.

Fig. 4. Same as Fig. 3 but for ACE-FTS NO.

spectral features for the target molecule). Prior to performing VMR retrievals, pressure and temperature as a function of altitude are determined through the analysis of CO_2 lines in the spectra. Forward model calculations employ the spectroscopic constants and cross section measurements from the HITRAN 2004 line list (Rothman et al., 2005).

For the purpose of generating calculated spectra (i.e. performing forward model calculations), quantities are interpolated from the measurement grid onto a standard 1-km grid using piecewise quadratic interpolation. The comparisons in this work use the VMRs on the 1-km grid. Retrieved quantities are determined at the measurement heights.

The retrieval for NO_2 employs 21 microwindows ranging from 1581 to 1642 cm^{-1}, covering an altitude range of 13 to 58 km. There are minor interferences from various isotopologues of H_2O in these microwindows, but no interferers are retrieved. For NO_2, the wavenumber ranges for the microwindows remained the same between versions 1.0 and 2.2, but the altitude limits changed. The lower altitude limit was raised from 10 km in version 1.0 to 13 km in version 2.2 to avoid saturation of the spectral region that occurred at low altitudes in tropical occultations. The upper altitude limit was raised from 45 km in version 1.0 to 58 km in version 2.2 to capture enhancements in NO_2 at high altitudes during polar spring (e.g. Rinsland et al., 2005; Randall et al., 2007). For occultations with no enhancements at high altitudes, the top portion of the retrieved NO_2 VMR profile will be mostly fitting noise. The precision of the ACE-FTS NO_2 VMRs is defined as the 1σ statistical fitting errors from the least-squares process, assuming a normal distribution of random errors (Boone et al., 2005).

Version 2.2 ACE-FTS microwindows for NO range from 1842.9 to 1923.5 cm^{-1} covering an altitude range from 15 to
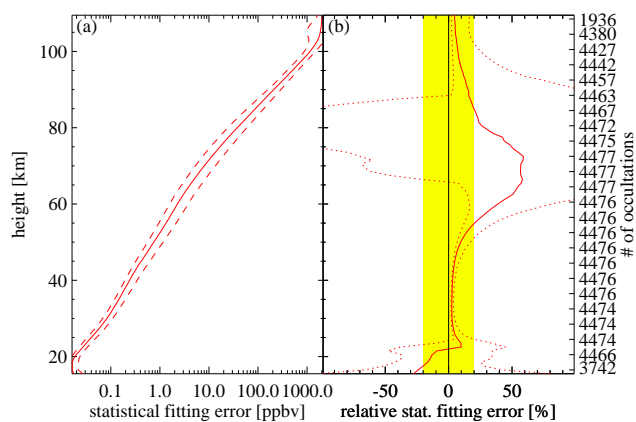
110 km. A total of 20 microwindows were used for the retrieval of NO. For NO, the upper altitude limit for retrievals was lowered from 115 km in version 1.0 to 110 km in version 2.2, and the lower altitude limit was raised from 12 to 15 km. Two NO microwindows from version 1.0, in the wavenumber range 1820 to 1830 cm^{-1}, were in the overlap region between the MCT and InSb detectors. As a result, these two microwindows suffered from elevated noise and were therefore removed from version 2.2 processing. Five new microwindows were added for version 2.2 NO retrievals. For version 1.0, there were four interfering species for NO retrievals (H_2O, CO_2, O_3 and N_2O). For version 2.2, the microwindow altitude ranges were selected such that there was only one interfering species (O_3).

The other interferers were fixed to the results of previous retrievals. The NO VMR profile has orders of magnitude larger VMR values at high altitudes (upper mesosphere and thermosphere) compared to low altitudes. The retrieved NO VMR profiles often exhibit a negative spike in the transition region between large and small VMR. This unphysical result is a consequence of insufficient altitude sampling in the region where the NO VMR profile goes through a minimum. Another known issue in the ACE-FTS version 2.2 NO data set occurs at low altitudes (below about 25 km). Small, negative VMR values are often retrieved in this altitude region. Preliminary investigations suggest that neglecting diurnal effects in the NO retrievals may be the cause of these negative VMR values at low altitudes. No diurnal effect corrections were made to the retrieved VMR profiles for either NO or NO_2.

Figures 3 and 4 show the statistical fitting errors for the ACE-FTS NO_2 and NO profiles, respectively. These errors are calculated as the square root of the diagonal elements of the covariance matrix used in the least squares fitting procedure. If the measurement errors are normally distributed and one ignores correlations between the parameters, this represents the 1σ statistical fitting errors. The median

relative statistical fitting error for NO_2 is <2.5% from 20 to 40 km, increasing to 85% at 53 km where the NO_2 VMR is small. Likewise, the median relative statistical fitting error of NO is <10% from 22 to 50 km, increasing to 58% at 66 km where the NO VMR is small. The median relative statistical fitting error falls back below 10% for altitudes above 80 km, as the NO VMR profile increases. Negative relative statistical fitting error values are apparent at very high altitudes for NO_2 and low altitudes for NO, and are a byproduct of negative retrieved VMRs at these altitudes.

3 Validation instruments

A variety of different measurements from ground-based, airborne and satellite instruments exist for NO_2 and fewer for NO. These instruments are described in this section. Measurements from solar occultation satellite instruments are important for the comparisons because the ACE satellite instruments measure in solar occultation mode, therefore differences due to measurement mode can be excluded. There are, however, data available from other measurement modes (stellar occultation, limb scatter and emission) that provide additional coincident measurements with ACE. Nadir measurements have limited vertical resolution and are therefore useful in only a limited way. Only one nadir satellite product has been included in this study. Other comparisons are made with ground-based FTIR measurements that use a solar absorption measurement technique similar to that of ACE-FTS, and with ground-based UV-VIS balloon-borne and ground-based instruments that use a similar measurement technique to MAESTRO. One comparison is made with an in-situ balloon instrument that provides very high vertical resolution.

3.1 Satellite instruments

In this work, we present comparisons of NO_2 with ten NO_2 satellite products available from eight instruments. Only HALOE and MIPAS IMK-IAA provide NO.

3.1.1 HALOE, SAGE II, SAGE III and POAM III

A number of solar occultation instruments were measuring at the same time as ACE-FTS and MAESTRO. These include HALOE (Russell et al., 1993), SAGE II (Mauldin et al., 1985), SAGE III (SAGE ATBD Team, 2002) and POAM III (Lucke et al., 1999). These instruments ceased operations in August 2005 (SAGE II), November 2005 (HALOE), December 2005 (POAM III) and March 2006 (SAGE III), so they operated throughout most of the first two years of the ACE mission.

SAGE II and HALOE were in mid-inclination orbits, with occultation locations spanning a range from about 75° N to 75° S in around a month with a resolution of ~2 km. The POAM III instrument was in a near-polar sun-synchronous 10:30 (local time) orbit, so its measurements remained in

the polar regions year-round, from about 54° N to 71° N and 63° to 88° S. The SAGE III instrument was also in a near-polar sun-synchronous orbit, but its equator crossing time was 09:00 (local time). Its measurement locations thus ranged from about 48° N to 81° N and 37° S to 59° S. Both POAM III and SAGE III have high vertical resolutions of ~2 km.

The versions of the data used in this work are the following: version 19 retrievals from HALOE, version 4.0 retrievals from POAM III, version 6.2 retrievals from SAGE II and version 3.00 retrievals from SAGE III.

Version 17 HALOE NO_2 was validated by Gordley et al. (1996), showing mean differences with correlative measurements of about 10 to 15% in the middle stratosphere. Randall et al. (2002) compared POAM III v3.0 NO_2 to HALOE v19 showing agreement to within 6%, with no systematic bias, from 20 to 33 km. POAM III exhibited a high bias relative to HALOE at higher altitudes, up to about 12%. The upper limit on POAM III NO_2 retrievals is 45 km. Comparisons between the most recent versions of all data sets were shown by Randall et al. (2005b). POAM III v4.0 NO_2 has a positive bias relative to HALOE of 20% from 20 to 23 km and 10 to 15% near 40 km. POAM III NO_2 agrees with SAGE III NO_2 to within ±5% from 25 to 40 km. As expected from this, comparisons between NO_2 profiles from SAGE III and HALOE are similar to those between POAM III and HALOE. Differences are within ±10% from about 23 to 35 km, with SAGE III higher than HALOE below 24 km and above 35 km. It is important to note that the HALOE retrievals include corrections for diurnal variations along the line of sight, whereas the SAGE III and POAM III retrievals do not. This could be one explanation for the differences below 25 km (see Newchurch et al., 1996).

Neither HALOE, POAM III nor SAGE III are thought to have significant sunrise/sunset biases. However, comparisons between SAGE II v6.2 and SAGE III, HALOE and POAM III indicate a significant sunrise/sunset bias in the SAGE II data, with more reasonable results for the sunset occultations (Randall et al., 2005b). SAGE II sunset NO_2 agrees to within ±15% with POAM III and SAGE III from about 25 to 38 km.

From the results quoted above, confidence at about the 15% level can be placed on the correlative data in the middle stratosphere (25 to 40 km), but accuracies at lower and higher altitudes are less certain.

For the HALOE NO comparisons, version 17 data was found to agree with correlative measurements to within about 10 to 15% in the middle stratosphere, but with a low bias as high as 35% between 30 and 60 km with some correlative data sets. Average agreement with the ATMOS instrument was within 15% above 65 km (Gordley et al., 1996).

3.1.2 SCIAMACHY, GOMOS and MIPAS on Envisat

The European Space Agency (ESA) Envisat mission was launched on 1 March 2002, carrying three instruments dedicated to atmospheric science: SCIAMACHY, GOMOS and MIPAS. Currently, extension of the mission until 2013 is under consideration. Envisat is in a quasi-polar, sun-synchronous orbit at an altitude of 800 km, with an inclination of 98.6°, a descending node crossing time of 10:00 and an ascending node crossing at 22:00 (local time).

SCIAMACHY is a passive moderate-resolution UV-VIS-near-infrared imaging spectrometer. Its wavelength range is 240 to 2380 nm and the resolution is 0.2 to 1.5 nm. SCIAMACHY observes the Earth's atmosphere in nadir, limb and solar/lunar occultation geometries and provides column and profile information of atmospheric trace gases of relevance to ozone chemistry, air pollution, and climate monitoring issues (Bovensmann et al., 1999; Gottwald et al., 2006). The primary measurements during daytime are alternate nadir and limb measurements.

SCIAMACHY solar occultation measurements are performed every orbit between 49° N and 69° N depending on season. Although from the instruments' point of view, the sun rises above the horizon, the local time at the tangent point corresponds to a sunset event. In southern latitudes (40° S to 90° S) SCIAMACHY also performs lunar occultation measurements, depending on visibility and phase of the moon (Amekudzi et al., 2005). The SCIATRAN version 2.1 radiative transfer code (Rozanov et al., 2005) is used for forward modeling and retrieval. An optimal estimation approach with Twomey-Tikhonov regularization is used to fit NO$_2$ in the spectral window from 425 to 453 nm simultaneously with ozone (524 to 590 nm) at the spectral resolution of the instrument. A detailed algorithm description can be found in Meyer et al. (2005). Recent validation results are given in Amekudzi et al. (2007) and updated for NO$_2$ in Bramstedt et al. (2007). Precise tangent height information is derived geometrically using the sun as a well-characterized target (Bramstedt et al., 2007).

SCIAMACHY nadir measurements provide atmospheric NO$_2$ columns with good spatial coverage, providing a large number of coincidences at all seasons for comparison with ACE measurements. Here, we use the University of Bremen scientific NO$_2$ product v2.0, which is similar to the GOME columns described in Richter et al. (2005) without the normalisation necessary to correct for a diffuser plate problem in the GOME instrument. Briefly, the NO$_2$ columns are retrieved with the Differential Optical Absorption Spectroscopy (DOAS) method in the wavelength interval 425 to 450 nm and corrected for light path enhancement using radiative transfer calculations based on the stratospheric part of the US standard atmosphere. When comparing SCIAMACHY columns and ACE measurements, three problems arise. First, the time of measurement is different as Envisat is in a morning orbit and most nadir measurements are not performed during twilight. This time difference has to be accounted for explicitly by correcting for the diurnal variation of NO$_2$ (see Fig. 6). Second, the diurnal effect will lead to a positive bias in the ACE partial columns. Finally, the SCIAMACHY columns include tropospheric NO$_2$, which can be large in polluted situations. While polluted measurements have been removed from the data set used, the tropospheric background is included, which is of the order of 0.3 to 0.7×10^{14} molec/cm^2 depending on location and season.

GOMOS is a stellar occultation experiment (Kyrölä et al., 2004, and references therein). The instrument is a grating spectrometer capable of observing about 100 000 star occultations per year in different UV-VIS-near-infrared spectral ranges with a vertical sampling better than 1.7 km between two consecutive acquisitions. Global coverage can be achieved in about three days, depending on the season of the year and the available stars. The precision of GOMOS is strongly influenced by both star magnitude and star temperature, which impact the signal-to-noise ratio in the useful spectral range. This is also influenced by the obliquity of the occultations, which does not allow a complete correction of the star scintillation produced by atmospheric turbulence. GOMOS can sound the atmosphere at different local solar times depending on the star position.

MIPAS is a limb-sounding emission Fourier transform spectrometer operating in the mid-infrared spectral region (Fischer and Oelhaf, 1996; Fischer et al., 2008). Spectra are acquired over the range 685 to 2410 cm^{-1} (14.5 to 4.1 μm), which includes the vibration-rotation bands of many molecules of interest. MIPAS operated from July 2002 to March 2004 at its full spectral resolution of 0.025 cm^{-1} (0.05 cm^{-1} apodized with the strong Norton and Beer (1976) function). MIPAS observes the atmosphere during day and night with daily coverage from pole to pole and thus provides trace gas distributions during polar night. Within its full-resolution standard observation mode, MIPAS covered the altitude range from 6 to 68 km, with tangent altitudes every 3 km from 6 to 42 km, and further tangent altitudes at 47, 52, 60, and 68 km, generating profiles spaced approximately every 500 km along the orbit. MIPAS passes the equator in a southerly direction at 10:00 local time 14.3 times a day. During each orbit, up to 72 limb scans are recorded. In March 2004, operations were suspended following problems with the interferometer slide mechanism. Operations were resumed in January 2005 with a 35% duty cycle and reduced spectral resolution (0.0625 cm^{-1}; apodized 0.089 cm^{-1}). By December 2007 a duty cycle of 100% had again been reached.

There are two MIPAS data products available for the comparisons. The MIPAS IMK-IAA (Institut für Meteorologie und Klimaforschung–Instituto de Astrofísica de Andalucía) data used here are vertical profiles of NO$_2$ and NO$_x$ (i.e. the sum of NO$_2$ and NO), which were retrieved with the dedicated scientific IMK-IAA data processor (von Clarmann et al., 2003a,b) from spectra recorded in the standard

observation mode in the period February to March 2004. Retrieval strategies considering non-local thermodynamic equilibrium (non-LTE) effects, error budget and altitude resolution for the species under investigation are reported in Funke et al. (2005). Here, we use data versions $NO\_9.0$ and $NO_2\_9.0$, which include several retrieval improvements, such as: i) the use of log(VMR) instead of VMR in the retrieval vector, ii) revised non-LTE parameters for NO_2, and iii) jointly-fitted VMR horizontal gradients at constant longitudes and latitudes. For NO retrievals, a revised set of microwindows is applied, which allows NO to be measured down to altitudes of about 15 km. The estimated precision, in terms of the quadratic sum of all random errors, is better than 1 ppbv for NO, at an altitude resolution of 4 to 7 km. The accuracy, derived by quadratically adding the errors due to uncertainties in spectroscopic data, temperature, non-LTE related parameters, and horizontal gradients to the measurement noise error, varies between 0.6 and 1.8 ppbv. The precision, accuracy and altitude resolution of the NO_2 retrieval are estimated to be 0.2 to 0.3 ppbv, 0.3 to 1.5 ppbv and 3.5 to 6.5 km, respectively. At the VMR peak height, the estimated accuracy is 5 to 10% for NO_2 and 10 to 20% for NO.

The second data product is the MIPAS ESA operational product (v4.62). The Level-1b processing of the data, including processing from raw data to calibrated phase-corrected and geolocated radiance spectra, is performed by ESA (Kleinert et al., 2007). For the high-resolution mission, ESA has processed pressure, temperature and the six key species H_2O, O_3, HNO_3, CH_4, N_2O and NO_2. The algorithm used for the Level 2 analysis is based on the optimized retrieval model (Raspollini et al., 2006; Ridolfi et al., 2000).

3.1.3 OSIRIS on Odin

OSIRIS, launched in February 2001, is currently in orbit on the Odin satellite (Llewellyn et al., 2004). It is in a circular, sun-synchronous, near-terminator orbit (18:00 local time ascending node) at an altitude of 600 km. OSIRIS measures sunlight scattered from the Earth's limb between 280 and 800 nm at a resolution of 1 nm and for tangent heights between 7 and 70 km.

A comprehensive description of the NO_2 retrieval algorithm is provided in Haley et al. (2004), with the most recent improvements given in Haley and Brohede (2007). In summary, NO_2 profiles are retrieved by first performing a spectral fit on OSIRIS radiances between 435 and 451 nm. The slant column densities (SCDs) derived from this fit are then inverted to number density profiles from 10 to 46 km, at a vertical resolution of about 2 km using the optimal estimation technique (Rodgers, 2000). Version 2.3/2.4 OSIRIS NO_2 has been extensively validated against satellite occultation instruments (after mapping the OSIRIS profiles from their solar zenith angle to 90°) (Brohede et al., 2007a). These comparisons were recently repeated with the most recent NO_2 product, version 3.0 (Haley and Brohede, 2007), and

it is this version that is used in the comparisons here (available from http://osirus.usask.ca/). The validation studies concluded that the OSIRIS random/systematic uncertainties are 16/22% from 15 to 25 km, 6/16% from 25 to 35 km and 9/31% from 35 to 40 km.

3.2 SPIRALE balloon measurements in the Arctic

SPIRALE (SPectroscopie Infra-Rouge d'Absorption par Lasers Embarqués) is a balloon-borne instrument operated by the Laboratoire de Physique et Chimie de l'Environnement (LPCE) (Centre National de la Recherche Scientifique (CNRS)-Université d'Orléans) and routinely used at all latitudes, in particular as part of European satellite validation campaigns (e.g. Odin and Envisat). This instrument is an absorption spectrometer with six tunable diode lasers and has been previously described in detail by Moreau et al. (2005). In brief, it can perform simultaneous in situ measurements of about ten different chemical species from about 10 to 35 km height, with a high sampling frequency of about 1 Hz, thus enabling a vertical resolution of a few meters depending on the ascent rate of the balloon. The diode lasers emit in the mid-infrared spectral region (from 3 to 8 μm) with beams injected into a multipass Heriott cell located under the gondola and largely exposed to ambient air. The cell (3.5-m long) is deployed during the ascent when pressure is lower than 300 hPa. The multiple reflections obtained between the two cell mirrors give a total optical path of 430.78 m.

Species concentrations are retrieved from direct infrared absorption, by fitting experimental spectra with spectra calculated using the HITRAN 2004 database (Rothman et al., 2005). Specifically, the ro-vibrational lines at 1598.50626 and 1598.82167 cm^{-1} were used for NO_2. Measurements of pressure (provided by two calibrated and temperature-regulated capacitance manometers) and temperature (obtained from two probes made of resistive platinum wire) aboard the gondola allow the species concentrations to be converted to VMR. Uncertainties in these parameters have been found to be negligible with respect to the other uncertainties discussed below. The global uncertainties in the VMRs have been assessed by taking into account the random errors and the systematic errors, and combining them as the square root of their quadratic sum. The two important sources of random errors are the fluctuations of the laser background emission signal and the signal-to-noise ratio. These error sources are the main contributions for NO_2, giving a total uncertainty for the flight used in this work of 50% at the lowest altitude (23.64 km) where it was detectable (>20 pptv), rapidly decreasing to 20% at 23.83 km (with a VMR of 32 pptv), and even to 6% above 24.28 km height. Between 17.00 and 23.60 km height, NO_2 was undetectable (<20 pptv, with uncertainties of about 50 to 200%). With respect to these errors, systematic errors in spectroscopic data (essentially molecular line strength and pressure broadening coefficients) are considered to be negligible.

The measurements were performed near Kiruna, Sweden (67.6° N and 21.55° E) (see Fig. 5).

3.3 UV-VIS balloon and ground-based instruments.

Vertical profiles of NO$_2$ from three UV-VIS instruments have been used in this study. They were retrieved from ground-based measurements by a SAOZ (Système d'Analyse par Observation Zénitale) spectrometer from CNRS, deployed in Vanscoy, Canada and by a DOAS system from Belgisch Instituut voor Ruimte-Aëronomie–Institut d'Aéronomie Spatiale de Belgique (IASB/BIRA) in Harestua, Norway. Additionally, there were NO$_2$ profiles obtained during flights of a SAOZ balloon instrument in France and Niger.

The SAOZ instrument is a UV-VIS spectrometer existing in two configurations: a ground-based version for the measurement of O$_3$ and NO$_2$ columns at sunrise and sunset by looking at sunlight scattered at zenith (Pommereau and Goutail, 1988a,b), and a balloon version for the measurement of the same species by solar occultation during the ascent of the balloon and at twilight from float altitude (Pommereau and Piquard, 1994). The ground-based instrument, part of the Network for the Detection of Atmospheric Composition Change (NDACC), has been compared several times to other UV-VIS systems (Vandaele et al., 2005, and references therein). There are about 20 ground-based SAOZ instruments deployed at latitudes from Antarctica to the Arctic; data from these instruments have been used since 1988 for the validation of O$_3$ and NO$_2$ column satellite measurements by TOMS, GOME, SCIAMACHY and OMI (e.g. Lambert et al., 1999, 2001), whilst the profiles from the balloon version have been also used for the validation of profiles measured by SAGE II, HALOE, POAM II and III, ILAS II, MIPAS and GOMOS (e.g. Irie et al., 2002; Wetzel et al., 2007).

The ground-based SAOZ data used in the present work are from a SAOZ deployed in Vanscoy (Canada, 52.02° N, 107.03° W) during the MANTRA (Middle Atmosphere Nitrogen TRend Assessment) campaign (Strong et al., 2005) in September 2004, from which profiles have been retrieved by the optimal estimation technique (Melo et al., 2005). The SAOZ balloon data are from one midlatitude flight at Aire-sur-l'Adour, France (43.71° N, 0.25° W) in May 2005 and from three tropical flights in Niamey, Niger (13.48° N, 2.15° E) in August 2006. The other ground-based instrument used in this study is the IASB-BIRA DOAS spectrometer, also part of NDACC, operating permanently at Harestua, Norway (60° N, 11° E) (Roscoe et al., 1999) (see Fig. 5). It has been validated during several NDACC comparison campaigns (Vandaele et al., 2005, and references therein).

The retrieval of NO$_2$ profiles from ground-based UV-VIS measurements is based on the dependence of the mean scattering height on solar zenith angle (Preston et al., 1997). The fitting window used for NO$_2$ is 425 to 450 nm. The IASB-BIRA NO$_2$ profiling algorithm is described in detail in Hendrick et al. (2004). In brief, it employs the optimal estima-
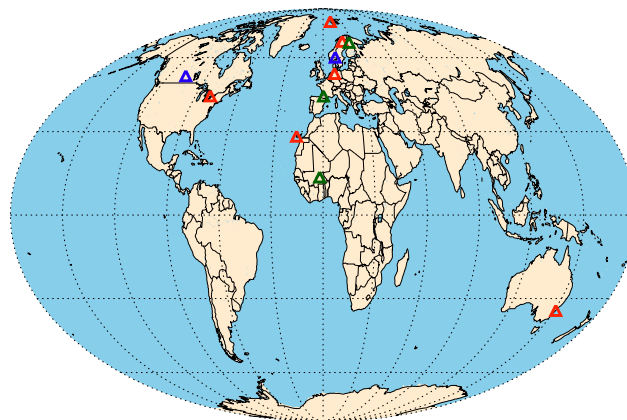

Fig. 5. Locations of the ground-based and balloon instruments used in the comparisons. From the north, FTIRs in red: Ny-Ålesund, Kiruna, Bremen, Toronto, Izaña, Wollongong, UV-VIS in blue: Harestua, Vanscoy and balloon launches in green: Kiruna, Aire-sur-l'Adour, Niamey.

tion method (Rodgers, 2000) and the forward model consists of the radiative transfer model UVspec/DISORT (Mayer and Kylling, 2005; Hendrick et al., 2007) coupled to the IASB-BIRA stacked box photochemical model PSCBOX (Hendrick et al., 2004). The inclusion of a photochemical model in the retrieval algorithm allows the effect of the rapid variation of the NO$_2$ concentration along the light path to be reproduced. It also makes profile retrieval possible at any solar zenith angle. Estimations of the error budget and information content are given in Hendrick et al. (2004). In the ground-based DOAS NO$_2$ observations at Harestua there are about 2.5 independent pieces of information and the vertical resolution is 8 to 10 km at best. In order to reduce the smoothing error associated with the difference in vertical resolution between ground-based and ACE profiles in the comparisons, ACE-FTS and MAESTRO profiles are degraded to the vertical resolution of the ground-based retrievals. This is done by convolving the ACE profiles with the ground-based DOAS averaging kernels (Hendrick et al., 2004).

3.4 Ground-based Fourier transform infrared spectrometers

In addition to the vertical profile and the UV-VIS partial column comparisons, ACE-FTS NO and NO$_2$ measurements have been compared with partial columns retrieved from solar absorption spectra recorded by ground-based Fourier Transform Infrared Spectrometers (FTIRs). NO was provided by five and NO$_2$ by six stations that are part of NDACC. These instruments make regular measurements of a suite of tropospheric and stratospheric species.

Table 1 lists the stations that participated, their locations and the coincidence criteria used. Toronto and Wollongong

Table 1. List of the FTIR stations that provided data for the analyses (Sect. 5.3 and Sect. 6.3). The latitude and longitude of each station are provided, together with the altitude above sea level in meters (m.a.s.l.). The coincidence criteria used in this study are indicated for each station in column 4. References describing the stations, measurements and analyses are given in column 5.

Station	Coordinates	Alt. [m.a.s.l.]	Coincidence criteria	Reference
Ny Ålesund, Svalbard	78.9° N, 11.9° E	20	±24 h, 1000 km	Notholt et al. (1997)
Kiruna, Sweden	67.8° N, 20.4° E	419	±12 h, 500 km	Blumenstock et al. (2006)
Bremen, Germany	53.1° N, 8.9° E	27	±24 h, 1000 km	Buchwitz et al. (2007)
Toronto, Canada	43.7° N, 79.4° W	174	±48 h, 1000 km	Wiacek et al. (2007)
Izaña, Canary Islands	28.3° N, 16.5° W	2367	±24 h, 1000 km	Schneider et al. (2005)
Wollongong, Australia	34.5° S, 150.9° E	30	±24 h, 1000 km	Paton-Walsh et al. (2005)

use Bomem DA8 FTIRs with resolutions of $0.004\,cm^{-1}$ and optical path differences of 250 cm, whereas the other stations use Bruker FTIRs (Ny Ålesund and Kiruna: 120 HR, Bremen: 125 HR and Izaña: 120 M until end of 2004, then 125 HR). All Bruker instruments have a resolution of $0.004\,cm^{-1}$, but those shown here normally use $0.005\,cm^{-1}$ for better signal-to-noise ratio. More information about the instruments, the retrieval methodologies and the measurements made at each of these sites can be found in the references provided in Table 1. The participating stations cover latitudes from 34.5° S to 78.9° N, and provide measurements from the subtropics to the polar regions in the Northern Hemisphere (see Fig. 5). There is only one station for which we have measurements in the Southern Hemisphere. Days for which coincident FTIR data were available for comparison with ACE are as follows:

– Ny Ålesund: NO_2: 23 and 28 September 2004, 14 and 16 March 2005, 26 September 2005; NO: 14 and 16 March 2005.

– Kiruna: NO_2: 27 and 29 October 2004, 25 January 2005, 1, 2 and 7 February 2005, 18, 19, 23 and 25 May 2005, 5 February 2006, 20 March 2006, 18 May 2006; NO: 27 and 29 October 2004, 7 February 2005, 18, 19 and 25 May 2005, 10 November 2005, 5 February 2006, 18 May 2006.

– Bremen: NO_2: 2 and 3 September 2004, 24 March 2005, 13 February 2006, 8, 9 and 12 May 2006, 3, 25, 26 and 27 July 2006, 28 November 2006.

– Toronto: NO_2: 23 and 29 July 2004, 2 June 2005, 1 and 2 September 2005, 3 and 5 May 2006, 31 August 2006; NO: 23 and 29 July 2004, 29 July 2005, 3 May 2006, 29 July 2006, 31 August 2006.

– Izaña: NO_2: 5 and 30 April 2005, 1, 2 and 30 August 2005 and 20 October 2005; NO: 3 August 2004, 5 and 30 April 2005, 1, 2 and 30 August 2005.

– Wollongong: NO_2: 1 March 2005, 3 November 2005, 20 and 21 August 2006, 31 October 2006 and 1 Novem-

ber 2006; NO: 3 and 4 October 2004, 1 March 2005, 19 April 2005, 20 and 21 August 2006, 31 October 2006 and 1 November 2006.

The FTIR measurements require clear-sky conditions and take measurements all year round during daylight. Only cloud-free measurements are included in the comparisons.

The data used here were analyzed using either the SFIT2 retrieval code (Pougatchev and Rinsland, 1995; Pougatchev et al., 1995; Rinsland et al., 1998) or PROFFIT92 (Hase, 2000). Both algorithms employ the optimal estimation method (Rodgers, 2000) to retrieve vertical profiles from a statistical weighting between a priori information and the high-resolution spectral measurements. The retrieval codes have been compared and it was found that the differences were less than ∼1% (Hase et al., 2004). Averaging kernels calculated as part of this analysis quantify the information content of the retrievals, and can be used to smooth the ACE profiles, which have higher vertical resolution.

For NO_2, there are typically 0.1 to 2 Degrees Of Freedom for Signal (DOFS, equal to the trace of the averaging kernel matrix) and for NO about one DOFS is found in the altitude range coincident with ACE-FTS measurements and about half a DOFS greater for the total columns.

Given this coarse vertical resolution, we compare partial columns rather than profiles. All sites used spectroscopic data from HITRAN 2004, with the exception of Kiruna and Izaña (HITRAN 1996 for NO_2 and HITRAN 2001 for NO). Comparisons of FTIR retrievals using HITRAN 1996 and 2004 showed that NO_2 total and partial columns are about 2% lower when using HITRAN 1996.

Other information required for the retrievals, such as a priori profiles and covariances, treatment of instrument lineshape, and atmospheric temperature and pressure are optimized for each site as appropriate for the local conditions.

4 Validation approach

4.1 Comparison methodology

The comparisons shown in this work use ACE data from 21 February 2004 (the start of the ACE Science Operations phase) through to 28 March 2007. The coincidence criteria needed to search for correlative measurements were determined by considering temporal and spatial variability. The statistical significance of the results for the satellite comparisons was also considered. Ground-based and balloon measurements were considered coincident with the ACE measurements when they were within 1000 km and 24 h of each other. This resulted in cases, notably for balloon comparisons, where only one ACE coincidence profile was available. The value that was used in searching for coincidences is the location for each ACE occultation, which is defined as the latitude, longitude and time of the tangent point at 30 km (calculated geometrically). We do not expect a seasonal bias with solar occultation instruments, therefore seasonal dependencies were not studied here.

Because NO$_2$ and NO are short-lived species, a chemical box model (described in Sect. 4.2) was used for all but the solar occultation comparisons and the MIPAS-IMK/IAA NO$_x$ comparisons, to correct for the time difference in satellite comparisons. For the ground-based, aircraft and balloon measurements, box model scaling was applied when the measurements were not taken at the same solar zenith angle.

For the balloon measurements, profiles obtained within 36 h and 1000 km of ACE were used. For the FTIR comparisons, measurements that occurred within 24 h and 1000 km of ACE occultations were compared, with the exception of Kiruna where tighter criteria (12 h and 500 km) were used. These relaxed criteria were necessary to obtain a reasonable number of ACE coincidences for each station (between 5 and 72). In cases where several FTIR measurements from a site were available for one ACE occultation or vice versa, all pairs were considered.

Table 1 lists the FTIR stations and Table 2 summarizes all other correlative data sets, comparison periods, temporal and spatial coincidence criteria, and number of coincidences.

The satellite VMR profiles and the SAOZ-balloon VMR profiles all have vertical resolutions that are similar to those of the ACE instruments, and so no averaging kernel smoothing was applied to these data. These correlative profiles were linearly interpolated on to the 1-km ACE-FTS or the 0.5-km MAESTRO altitude grid. The balloon-borne SPIRALE VMR profile was obtained at significantly higher vertical resolution than the ACE instruments, and so was convolved with a triangular function having full width at the base equal to 3 km and centered at the tangent heights of each occultation for ACE-FTS and with a Gaussian function having full width at half maximum equal to 1.7 km for MAESTRO. This approach simulates the smoothing effect of the limited resolution of the ACE instruments, as discussed by Dupuy

et al. (2008). The resulting smoothed profiles were then interpolated onto the 1-km grid for ACE-FTS and the 0.5-km grid for MAESTRO. Finally, for the comparisons with the ground-based FTIR and UV-VIS measurements, which have significantly lower vertical resolution, the ACE profiles were smoothed by the appropriate FTIR or UV-VIS averaging kernels to account for the different vertical sensitivities of the two measurement techniques. The method of Rodgers and Connor (2003) was followed and Eq. (4) from their paper was applied, using the a priori profile and the averaging kernel matrix of the FTIR and the UV-VIS instruments (see Sect. 5.3). Partial columns over specified altitude ranges were then calculated for the ACE instruments and the FTIRs or the UV-VIS instruments and used in the comparisons. Additionally, the UV-VIS profiles were compared to the smoothed profiles from the ACE instruments.

Pairs of vertical VMR profiles from ACE (both FTS and MAESTRO) and each validation experiment (referred to as VAL in text and figures below) were identified using the appropriate temporal and spatial coincidence criteria. The results of the vertical profile comparisons will be shown below, with some modifications for the GOMOS comparisons (Sect. 5.1.3), the single profile comparisons (SPIRALE and SAOZ; Sect. 5.2) and the FTIR and UV-VIS partial column comparisons (Sects. 5.3 and 5.4).

(a) The mean profile of the ensemble for ACE and the mean profile for VAL are plotted as solid lines with the standard deviations on each of these two profiles, $\pm 1\sigma$, as dotted lines, in panel (a) of the comparison figures discussed below. The uncertainty in the mean is calculated as $\sigma(z)/\sqrt{N(z)}$ (where $N(z)$ is the number of points used to calculate the mean at a particular altitude) and is included as error bars on the lines in panel (a). Note: in some cases, these error bars, as well as those in panels (b) and (c) (see below) may be small and difficult to distinguish.

(b) The mean profile of the absolute differences, ACE–VAL is plotted as a solid line in panel (b) of the comparison figures below, and the standard deviation in the distribution of this mean difference, $\pm 1\sigma$ as dotted lines. The term absolute here refers to differences of the compared VMR values and not to absolute values in the mathematical sense. The differences are calculated for each pair of profiles at each altitude, and then averaged to obtain the mean absolute difference at altitude z:

$$\Delta_{abs}(z) = \frac{1}{N(z)} \sum_{i=1}^{N(z)} [\mathrm{ACE}_i(z) - \mathrm{VAL}_i(z)] \tag{1}$$

where $N(z)$ is the number of coincidences at z, $\mathrm{ACE}_i(z)$ is the ACE (FTS or MAESTRO) VMR at z for the ith coincident pair, and $\mathrm{VAL}_i(z)$ is the corresponding VMR for the validation instrument. Error bars are also included in these figures. For the statistical comparisons involving multiple coincidence pairs (the satellite and UV-VIS profile comparisons), these error bars represent the uncertainty in the mean.

Table 2. Summary of the correlative data sets for the instruments used in the statistical and individual profile comparisons with ACE-FTS and MAESTRO NO$_2$ and ACE-FTS NO. All values are for NO$_2$ comparisons unless noted for NO or NO$_x$, SR is sunrise and SS is sunset.

Instrument (retrieval version)	Comparison period	Comparison location	Vertical range and resolution	Coincidence criteria	Number of coincidences
HALOE (version 19)	2004/07/04– 2005/08/15	66° N, 60° N & 49° S	20–50 km[a] at 2 km	±2 h, 500 km	36
SAGE II (version 6.2)	2004/08/09– 2005/05/04	65° N, 21° N & 14° S	20–50 km at 2 km	±2 h, 500 km	148 SR / 17 SS[b] 126[c]
SAGE III (version 3.0)	2004/02/22– 2005/12/05	59° S – 82° N	20–50 km at 1 km	±2 h, 500 km	776
POAM III (version 4.0)	2004/03/16– 2005/11/27	85° S – 69° N	20–46 km at 1 km	±2 h, 500 km	295
SCIAMACHY solar occs (version 2.5)	2004/03/21– 2007/03/28	49° N – 69° N	16–40 km at 3–5 km	±2 h, 500 km	372[b] 377[c]
SCIAMACHY nadir (version 2.0)	2004/02/21– 2007/02/26	85° S – 85° N	total column	same day 200 km	4457[b] 4366[c]
GOMOS (IPF 5.00)	2004/04/06– 2005/12/08	72° S – 80° N	14–50 km at 2–3 km	±12 h, 500 km	6285
MIPAS ESA (ESA v4.62)	2004/02/21– 2004/03/26	20° N – 85° N	25–46 km at 3 km	±6 h, 300 km	84
OSIRIS (version 3.0)	2004/02/21– 2006/12/31	82° S – 82° N	12–43 km at 2 km	±2 h, 500 km	543[b] 524[c]
MIPAS IMK-IAA[d] (version 9.0)	2004/02/22– 2004/03/25	20° N– 85° N	12–70 km at 3.5–6.5 km	±18 h, 1000 km	493
SPIRALE	2006/01/20	67.6° N, 21.55° E	15–26 km at several m	13 h, 413 km	1
SAOZ (balloon)	2005/05/07 & 2006/08/07 – 2006/08/19	13.48° N, 2.15° E 43.71° N, 0.25° W	13–28 km at 1 km	+12 d, 1000 km	4
UV-VIS Harestua (DOAS)	2004/03/22– 2005/09/01	60.20° N, 12.80° E	13–37 km at 8–10 km	same day 750 km	13 SR / 15 SS[b] 6 SR / 11 SS[c]
SAOZ (ground-based)	2004/09/01– 2004/09/06	52.02° N, 107.03° W	15–37 km at 5 km	±24 h, 1000 km	5

[a] Value given for NO$_2$ comparisons. For the ACE-FTS comparison with NO, 20 to 108 km was used.
[b] Number of coincidences for ACE-FTS.
[c] Number of coincidences for MAESTRO.
[d] Comparisons with NO$_x$ from ACE-FTS only.

(c) Panel (c) of the comparison figures presents the mean profile of the relative differences. This mean relative difference is defined, as a percentage, using:

$$\Delta_{\mathrm{rel}}(z) = 100\% \times \frac{1}{N(z)} \sum_{i=1}^{N(z)} \frac{\mathrm{ACE}_i(z) - \mathrm{VAL}_i(z)}{\mathrm{MEAN}_i(z)} \quad (2)$$

where $\mathrm{MEAN}_i(z) = [\mathrm{ACE}_i(z) + \mathrm{VAL}_i(z)]/2$ is the mean of the two coincident profiles at z for the ith coincident pair.

(d) The relative standard deviations on each of the ACE and VAL mean profiles calculated in step (a) are given in panel (d), with the number of coincident pairs given as a function of altitude on the right-hand y-axis for the statistical comparisons.

For single profile comparisons (SPIRALE, SAOZ), error bars represent the combined random error for all panels. The

ACE-FTS data products include only statistical fitting errors, while MAESTRO provides an estimate of relative uncertainties (as described in Sect. 2). No systematic errors are available, therefore the error bars for the single profile comparisons are very small. They cannot be compared directly with the total errors of the single profile instruments.

4.2 Diurnal mapping using a chemical box model

In Fig. 6, we present a typical example of the modelled temporal evolution of the NO$_2$ concentration in the equatorial region together with the ACE-FTS and GOMOS local solar time at six different altitudes using the photochemical box model described by Prather (1997) and McLinden et al. (2000). This highlights an obstacle faced in the validation of species that experience diurnal variations when there are

mismatches between the local time of the primary measurement and that of the correlative measurement. Since diurnal gradients are generally largest through sunrise and sunset, this is even more problematic for comparisons involving solar occultation instruments such as ACE-FTS and MAESTRO. The approach adopted in this paper is to simply scale, or map, the profile from the local time, t_1, of one instrument to the local time, t_2, of another instrument. The diurnal scaling factors, s_t, were computed in a photochemical box model as follows:

$$s_t(z) = \frac{\text{VMR}_{\text{model}}(t_2, z)}{\text{VMR}_{\text{model}}(t_1, z)}, \tag{3}$$

where $\text{VMR}_{\text{model}}$ is the modelled VMR and z represents the vertical co-ordinate (altitude, pressure or potential temperature). Then the VMR at local time, t_2, can be calculated from the VMR at local time t_1 using

$$\text{VMR}(t_2, z) = s_t(z) \times \text{VMR}(t_1, z). \tag{4}$$

This approach was successfully applied in the validation of OSIRIS NO₂ observations, in which diurnal scaling factor look-up tables, based on climatological ozone and temperature, were employed to enable comparisons with solar occultation instruments (Brohede et al., 2007a). A recent improvement is the calculation of scaling factors for each profile, using simultaneous observations of ozone, temperature, and pressure to help constrain the diurnal cycle (Brohede et al., 2007b). Similar approaches have been used elsewhere (Bracher et al., 2005b).

Following this method, diurnal scaling factors have been pre-calculated for each ACE occultation using the University of California at Irvine (UCI) photochemical box model (Prather, 1997; McLinden et al., 2000). Each simulation is constrained with the ACE-FTS version 2.2 retrieved temperature, pressure, and ozone (with updates). Other model input fields include NO$_y$ and N₂O from a three-dimensional model (Olsen et al., 2001), Cl$_y$ and Br$_y$ from tracer-tracer correlations with N₂O (Salawitch, personal communication, 2004), and background aerosol surface area from SAGE II (climatology data). Photochemical rate data was taken from Sander et al. (2003) and a surface albedo of 0.2 is assumed. Uncertainties introduced into the diurnally shifted profile are expected to be small, generally less than 10% in the middle stratosphere and 20% in the lower/upper stratosphere (Brohede et al., 2007b).

Beyond the local time issue, there is the more subtle problem of the so-called diurnal effect (Newchurch et al., 1996; McLinden et al., 2006). The diurnal effect arises when a range of solar zenith angles are sampled along the line-of-sight and systematic errors in species that experience diurnal variations (such as NO and NO₂) may result. The sign and magnitude of the error are governed by the gradients of the species through the effective range in solar zenith angle sampled (roughly 85 to 95° for solar occultations) (McLinden et al., 2006). For solar occultation measurements below 20
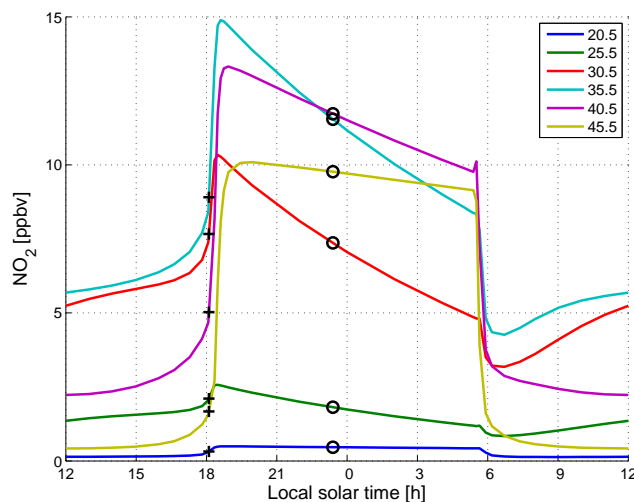

Fig. 6. Modelled time evolution of the NO₂ concentration at different altitudes in the equatorial region (ACE sunset for orbit 3491: 9.0° N, 64.6° E; GOMOS: 7.7° N, 60.6° E). Crosses and circles refer to ACE and GOMOS local solar times, respectively.

to 25 km, NO₂ will be biased high by up to 50% and NO will be biased low by as much as a factor of 2 to 4 if the diurnal effect is not accounted for in the retrieval, as is the case for the ACE instruments. The diurnal effect has a much smaller impact above about 25 km due to a near complete cancellation of the near (SZAs greater than 90°) and far (SZAs less than 90°) side biases.

A straightforward, yet representative method of estimating these so-called diurnal effect errors for occultation has been developed by McLinden (2008)[2]. In some comparisons, the diurnal effect has been forward modelled and a correction has been applied to the ACE measurements. For comparisons with OSIRIS (a limb-scatter instrument, which is subject to its own, analogous diurnal effect errors) an analogous correction has been applied (McLinden et al., 2006; Brohede et al., 2007a). Note that for comparisons with most other solar occultation instuments, no correction is necessary as the effect will manifest equally. The exception to this is HALOE, which is corrected for the diurnal effect (Gordley et al., 1996).

---

[2]McLinden, C. A.: Diurnal effects in solar occultation observations: error estimate and application to ACE-OSIRIS NO₂ comparisons, in preparation, 2008.
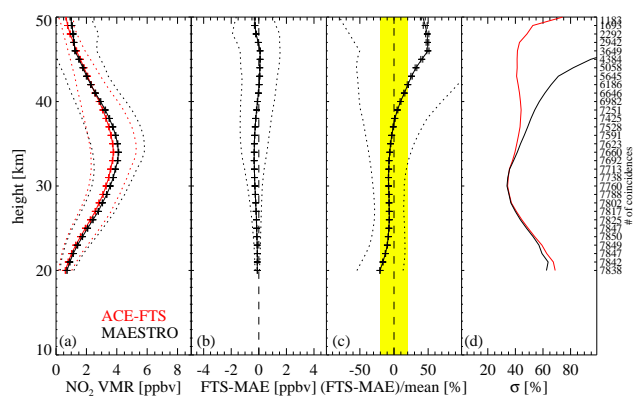
Fig. 7. (a) Mean profiles for all measurements by ACE-FTS (solid red) and MAESTRO (solid black) from 21 February 2004 to 31 December 2006. Dotted lines are the profiles of standard deviations (σ) of the distributions, while error bars (often too small to be seen) represent the uncertainty in the mean ($\sigma/\sqrt{N}$). **(b)** Mean absolute differences between ACE-FTS and MAESTRO (solid). Dotted lines represent the standard deviation of the distribution of the differences while error bars represent the uncertainty in the mean difference. **(c)** Mean percent differences (solid) between ACE-FTS and MAESTRO relative to the mean of the two instruments, for all coincidences. Dotted lines represent the standard deviation of the distribution of the differences while error bars represent the uncertainty in the mean difference. The range from ±20% is highlighted in yellow. **(d)** Standard deviations of the distributions (σ) relative to the mean VMR of each instrument at each altitude, for all coincident events, for ACE-FTS (red) and MAESTRO (black). The number of the coincidences is indicated on the right-hand y-axis.
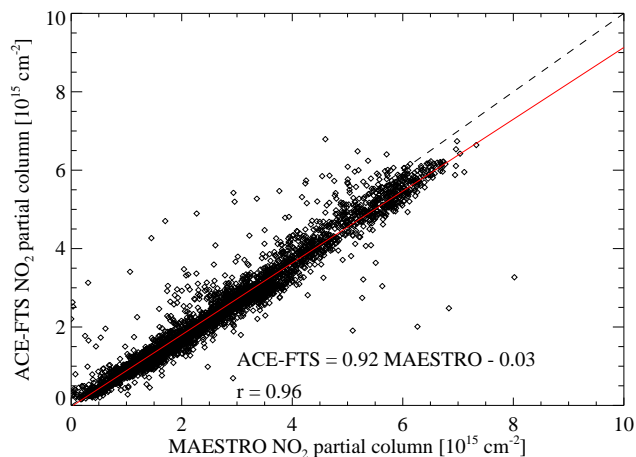
Fig. 8. Scatter plot of the ACE-FTS and the MAESTRO NO₂ partial columns (14.5 to 46.5 km). Data shown is used for the SCIA-MACHY nadir comparisons (Sect. 5.1.6). The solid red line is the linear least-squares fit to the data, with the slope, intercept, and correlation coefficient given in the figure. The dashed black line shows the one-to-one linear relationship for comparison.
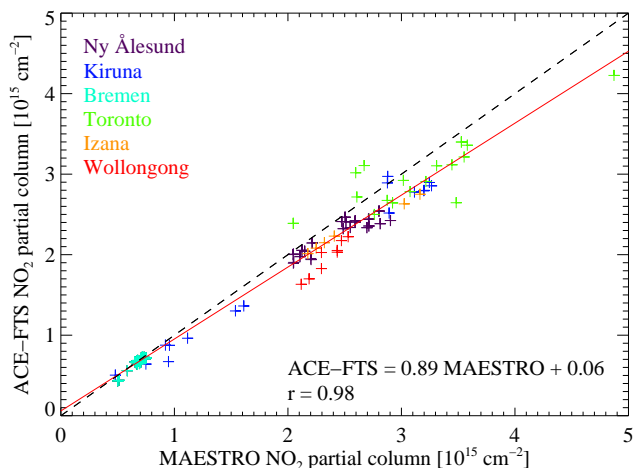
Fig. 9. Scatter plot of the ACE-FTS and MAESTRO NO₂ partial columns (data shown is used in the FTIR comparisons in Sect. 5.3) at the times of the FTIR comparisons. The red line is the linear least-squares fit to the data, with the slope, intercept, and correlation coefficient given in the figure. The dashed black line shows the one-to-one line relationship for comparison. The colours indicate the NDACC stations for which coincident measurements exist. The partial columns were calculated over different altitude ranges for each station (see Table 3). ACE-FTS and MAESTRO VMRs have been photochemically corrected to the times of the ground-based measurements.

5 Results for the NO₂ comparisons

5.1 Satellites

5.1.1 ACE-FTS and MAESTRO NO₂

Because they share a single suntracker and have aligned fields-of-view, ACE-FTS and MAESTRO measure the same air mass at the same time and place. Comparisons of NO₂ measurements from these two instruments have been done previously by Kerzenmacher et al. (2005) for ACE-FTS version 1.0 and preliminary MAESTRO data, for which agreement of 40% was found with a very small data set, and by Kar et al. (2007) for one year of the current data sets. Kar et al. (2007) found good agreement (within 10 to 15% from 15 to 40 km) for sunrise measurements and similar agreement for the sunset measurements (within 10 to 15% from 22 to 35 km). In Fig. 7, a comparison of all MAESTRO and ACE-FTS NO₂ measurements is shown (from 21 February 2004 to 31 December 2006). It can be seen that the differences are in very good agreement with Kar et al. (2007): the ACE-FTS and MAESTRO measurements agree to within 10% from 23 to 40 km. Up to 35 km, ACE-FTS measures less NO₂ than MAESTRO. MAESTRO VMRs are lower at higher altitudes, with differences reaching values of 50% at 45 km.

There are some altitudes (38 to 41 km and 47 to 50 km) where the absolute differences are negative but the relative differences are positive. This is most obvious near 47

to 50 km, where the mean absolute differences are around −0.2 ppbv, but mean relative differences are greater than 40%. The absolute differences at 50 km have a mean difference of −0.2 ppbv, but most of the points lie above 0 ppbv. So the large negative differences are skewing the result. The median does give +0.2 ppbv. Relative differences at 50 km have a mean of 41.2% and a median of 41.3%, so the mean relative difference is probably more meaningful than the mean absolute difference. But this carries with it the caveat that the mixing ratios at this altitude are very small, so even large percent differences are not very significant in terms of the actual measurements. Examination of the ACE-FTS and MAESTRO data at 50 km shows that the negative absolute differences come from the many large MAESTRO VMRs caused by scatter in the data.

From the NO$_2$ profiles, partial columns can be calculated for both ACE-FTS and MAESTRO. These have been calculated over the range 14.5 to 46.5 km, used for the SCIAMACHY nadir comparisons in Sect. 5.1.6, and for different height ranges shown in Table 3 for all the FTIR comparisons in Sect. 5.3. Figures 8 and 9 show the scatter plots of the partial columns of the ACE-FTS and MAESTRO used for these comparisons. They indicate that there is very good agreement, with MAESTRO providing larger column amounts than the ACE-FTS. Overall there is a very good correlation ($r \sim 0.97$) with the intercept near zero and the slope ~ 0.91 in both scatter comparisons.

It should be noted that the MAESTRO measurements are known to have occasional timing errors of up to one second with respect to the ACE-FTS measurements. Since the MAESTRO retrievals use the tangent heights retrieved for ACE-FTS and these are imported as a tangent height versus time table, this can lead to an offset of up to a few kilometers in the MAESTRO tangent heights, resulting in VMR profiles that can be smaller or larger than those retrieved from ACE-FTS or the comparison instrument (Manney et al., 2007). This problem affects approximately 6% of the v1.2 MAESTRO profiles. It is possible to screen out most of these outliers on a statistical basis, but that has not been done in this comparison. The inclusion of these data in the analysis is probably responsible for much of the excess variance in the MAESTRO data as compared to that of similar data sets (e.g. SAGE III). Additionally, because of the shape of the NO$_2$ distribution, the effect is larger at high altitudes and the positive deviations contribute more on average than the negative ones. As a result, the problem also has an impact on the bias between MAESTRO and other data sets. This issue is still under investigation and has not yet been resolved.

5.1.2 NO$_2$ from solar occultation instruments: HALOE, SAGE II, SAGE III, POAM III and SCIAMACHY

In this section, NO$_2$ measurements from ACE-FTS and MAESTRO are compared with solar occultation observations from HALOE, SAGE II, SAGE III, POAM III and
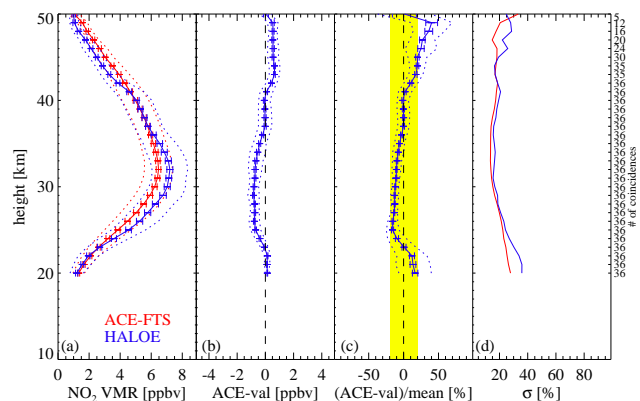

Fig. 10. **(a)** Mean profiles for all measurements by ACE-FTS (solid red) and HALOE (solid blue). Dotted lines are the profiles of standard deviations (σ) of the distributions, while error bars (often too small to be seen) represent the uncertainty in the mean ($\sigma/\sqrt{N}$). **(b)** Mean differences (solid) between ACE-FTS and HALOE for all coincidences. Dotted lines represent the standard deviation of the distribution of the differences while error bars represent the uncertainty in the mean difference. **(c)** Mean percent differences (solid) between ACE-FTS and HALOE relative to the mean of the two instruments, for all coincidences. Dotted lines represent the standard deviation of the distribution of the differences while error bars represent the uncertainty in the mean difference. The range ±20% is highlighted in yellow. **(d)** Standard deviations of the distributions (σ) relative to the mean NO$_2$ VMR at each altitude, for all coincident events, for ACE-FTS (red) and HALOE (blue). The number of the coincidences is indicated on the right-hand y-axis.

SCIAMACHY. The comparisons of MAESTRO data with POAM III and SAGE III were done by Kar et al. (2007) and will not be repeated here. Instead, a short summary of their results will be given.

The comparisons with HALOE, SAGE II, SAGE III and POAM III were carried out separately for sunrise and sunset events. Only in the case of SAGE II were the sunrise/sunset differences significantly larger than the average differences themselves. Thus, comparisons shown below combine sunrise and sunset data for HALOE, SAGE III and POAM III, but separate these data for SAGE II. For the MAESTRO comparison the combined sunrise/sunset dataset is shown. SCIAMACHY observes only sunset events, therefore the comparison is limited to sunset.

For the HALOE, SAGE II, SAGE III and POAM III comparisons, the coincidence criteria were chosen so that the ACE measurements are within 500 km and 2 h of the correlative observation. Thus, differences due to diurnal variations in NO$_2$ should be minimized. Comparisons with HALOE occurred primarily in the northern polar region summer, and with SAGE II primarily in the Northern Hemisphere spring. A large number of coincidences with POAM III and SAGE III occurred in the northern polar vortex season, where the measurements could exhibit substantial variability. The
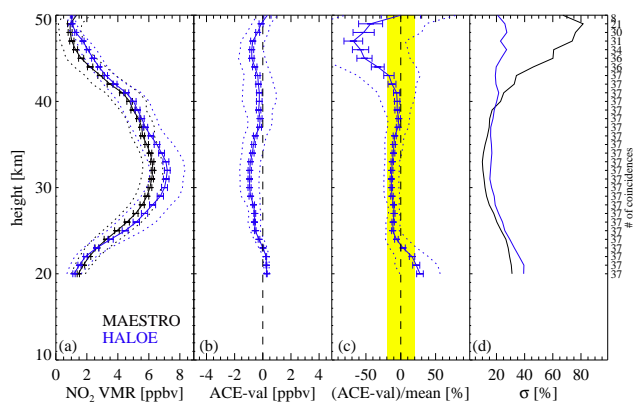
Fig. 11. Same as Fig. 10 but for MAESTRO (black) and HALOE (blue).

Fig. 13. Same as Fig. 10, but for MAESTRO (black) and SAGE II (blue). Sunrise and sunset observations were combined.
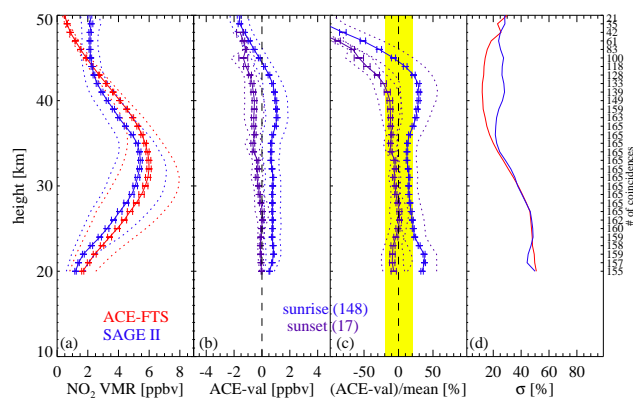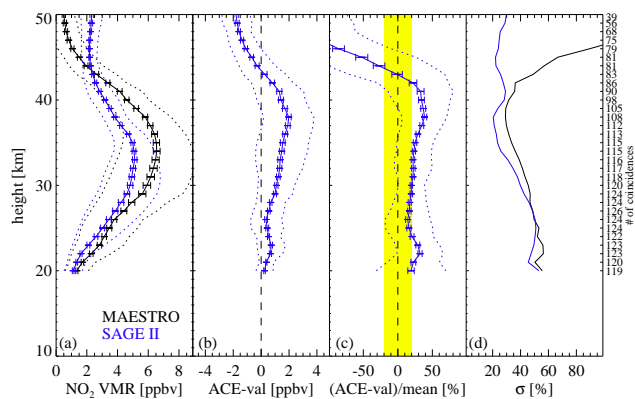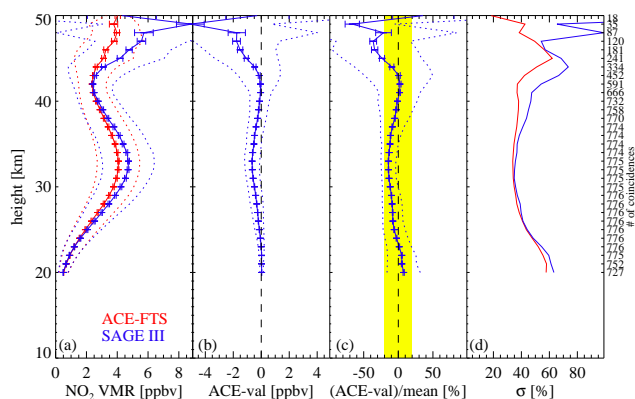

Fig. 12. Same as Fig. 10, but for ACE-FTS and SAGE II. The results for sunrise–sunrise (blue) and sunset–sunset (purple) comparisons are presented separately in the difference plots.

Fig. 14. Same as Fig. 10 but for ACE-FTS and SAGE III.

SCIAMACHY comparisons are all in northern midlatitudes.

Figures 10 to 17 show the results of the statistical comparisons between the ACE instruments and HALOE, SAGE II, SAGE III, POAM III and SCIAMACHY. For the results of the comparison of MAESTRO with SAGE III and POAM III, the reader is referred to Fig. 8a and b and Fig. 9a and b of Kar et al. (2007), respectively, and the summary plot in Sect. 7 of this paper.

Over the altitude range investigated, all instruments show that NO₂ has a smooth VMR profile with a broad peak between 30 and 35 km. Profile-to-profile variations, as measured by the standard deviations of the distributions, are generally similar in the ACE-FTS data set to those measured by the other instruments. A notable difference is that ACE-FTS variations are significantly smaller than SAGE II from 40 to 45 km (Fig. 12d) and than SAGE III above 45 km (Fig. 14d). MAESTRO shows generally larger variability than ACE-FTS, especially above 35 km. As noted above, the standard deviations for ACE-FTS and MAESTRO shown in panels (d)

are significantly larger in the POAM III and SAGE III comparisons, consistent with the fact that these coincidences are predominantly at high latitudes during the vortex season.

Differences of ACE-FTS with respect to HALOE are within about ±15% from 20 to 45 km, with a suggestion of an ACE-FTS low bias of about 10 to 15% from 24 to 36 km. A positive bias relative to HALOE increases above 40 km to a maximum of 40% at 49 km (Fig. 10). MAESTRO shows similar differences, relative to HALOE: there is agreement to within about ±15% from 22 to 42 km, with a suggestion of a MAESTRO low bias of about 10 to 15% from 24 to 41 km. There is, however, a negative bias above 45 km of up to 55% for MAESTRO, and a similar but more pronounced high bias than that of ACE-FTS below 22 km (Fig. 11). This could be a feature of the HALOE data.

Differences of ACE-FTS above 40 km, with respect to SAGE II, are in the opposite direction, with ACE-FTS lower than SAGE II by more than 50% from 47 to 50 km. For sunrise comparisons, ACE-FTS NO₂ is higher than SAGE II by 12 to 38% from 20 to 43 km. ACE-FTS sunsets agree with
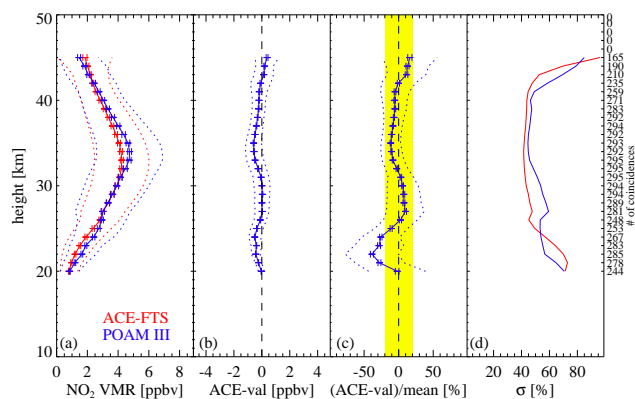
Fig. 15. Same as Fig. 10 but for ACE-FTS and POAM III.

Fig. 16. Same as Fig. 10 but for ACE-FTS and SCIAMACHY occultations.

Fig. 17. Same as Fig. 10 but for MAESTRO (black) and SCIA-MACHY occultations (blue).

SAGE II sunset events to within 13% from 20 to 42 km, with a low bias throughout most of this altitude range (Fig. 12). Since none of the other comparisons suggest a large ACE-FTS positive bias, nor a significant ACE-FTS sunrise/sunset bias, we conclude that this is an artifact of the SAGE II sunrise/sunset bias (Randall et al., 2005b). Differences of MAESTRO with respect to SAGE II are plotted for sunset and sunrise occultations together (Fig. 13). It can be seen that these differences are very similar to the ACE-FTS sunrise comparisons. From 20 to 35 km, MAESTRO is higher than SAGE II by 15 to 30%. MAESTRO is much lower than SAGE II above 42 km.

ACE-FTS NO_2 is lower than SAGE III NO_2 above 43 km, consistent with the SAGE II comparisons at these altitudes, but in the opposite direction to the HALOE comparisons. From 20 to 44 km, ACE-FTS agrees with SAGE III to within 14%, with a low bias from 24 to 40 km (Fig. 14). MAESTRO shows good agreement with SAGE III (within ±16%) in the range 25 to 40 km (Fig. 8a of Kar et al., 2007). The VMRs reported by MAESTRO are consistently lower than those of SAGE III above approximately 27 km, with maximum differences of up to −16% around 36 km.

Differences between ACE-FTS and POAM III are within 13% from 25 to 44 km, with negative values approaching 40% below 25 km (Fig. 15). Results for MAESTRO are similar below 25 km, with a low bias compared to POAM III (of about −25% at 23 km). Above 25 km, the MAESTRO–POAM III differences remain mostly within ±20% and decrease with increasing altitude, with mean values of +12% at 27 km to about −24% around 40 km (Fig. 9a of Kar et al., 2007). Unlike all the other solar occultation instruments considered in this study, HALOE NO_2 has been corrected for the diurnal effect. This may explain the larger ACE VMRs relative to HALOE below 25 km because of retrieval errors due to concentration gradients along the scattering/absorption paths (see Sect. 4.2).
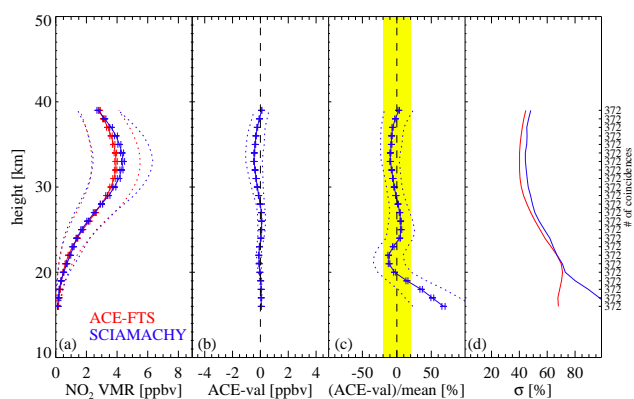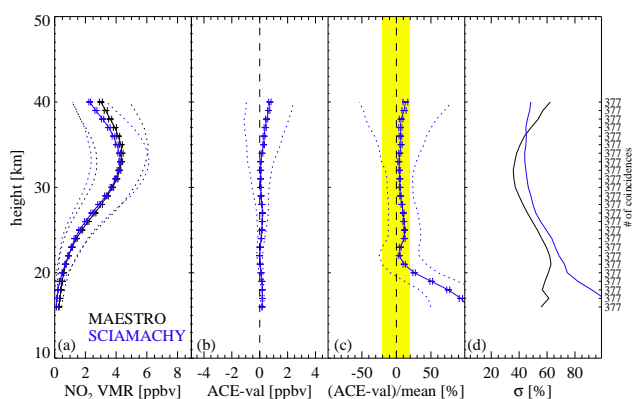
For SCIAMACHY comparisons, 372 coincidences were found for ACE-FTS and 377 for MAESTRO because only ACE data that extended from at least 16 to 39 km were used. Only ACE sunset data were used. In this case, the ACE data were interpolated onto the SCIAMACHY 1-km grid. The SCIAMACHY retrieval gives concentrations in number density, and has no pressure and temperature measurements. Therefore, the coincident ACE-FTS temperature and pressure profiles were used to calculate the VMR values from the SCIAMACHY profiles.

Figures 16 and 17 show the results of the comparison between SCIAMACHY and the ACE instruments. Below 20 km, ACE-FTS is higher than SCIAMACHY. From 20 to 39 km, the agreement is within 12% with a positive bias between 22 and 25 km and a negative bias elsewhere. The results are comparable to the comparisons with POAM III, only with smaller discrepancies. MAESTRO measures higher NO_2 than SCIAMACHY everywhere. The agreement is within 12% between 20 km and 40 km. Below
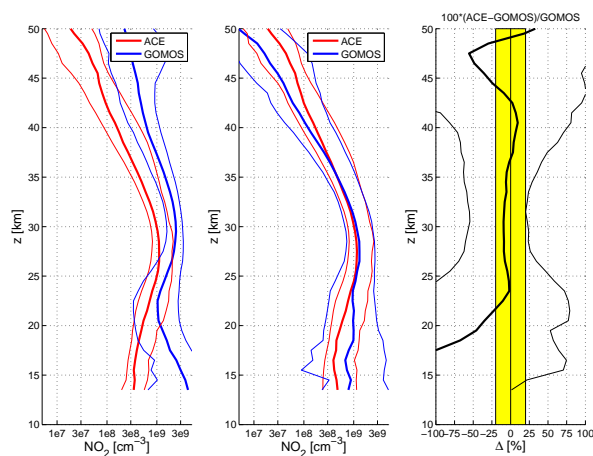
Fig. 18. Left: Uncorrected ACE-FTS and GOMOS weighted median profiles (thick lines) with the 16th and 84th percentiles (thin lines). Middle: Diurnal scaling has been taken into account. Right: Weighted median of the differences (Δ) between ACE-FTS and GOMOS. Note: the relative median difference is calculated with respect to the GOMOS median profile.

20 km, at low VMRs in the stratosphere, the differences grow to more than 100% at 16 km.

Although there are inconsistencies in the solar occultation comparisons, taken together, and considering previous validation of the correlative measurements, they suggest that the ACE-FTS and the MAESTRO NO_2 measurements are accurate to within 15% or better in the altitude range from 20 to at least 40 km, with SAGE II being the exception. Comparisons among the correlative measurements themselves, as well as between the correlative measurements ACE-FTS and MAESTRO, lead to inconclusive results for altitudes above about 40 km.

5.1.3 GOMOS stellar occultation NO_2 measurements

For the GOMOS comparison, 6865 profiles, of which 1812 are GOMOS dark limb events (at local night), were used with a time window of 12 h and a distance of 500 km, which is approximately the effective optical path length at the 30-km tangent altitude.

Weighted medians were used for the ACE-FTS comparisons instead of means for the reasons described by Dupuy et al. (2008). Briefly, when comparing a large number of vertical profiles for two experiments, there might be altitudes missing, leading to a variable statistical significance of the data, and there might be outliers that severely contaminate the data set. The dispersion of the data can then be estimated by taking the difference of the 84th and 16th percentiles of this distribution, which corresponds to the standard deviations, σ, in the analysis of a Gaussian distribution.

A second difficulty arises with the co-location criterion. By shrinking the co-location window in time and space, the

number of events decreases and the result of the comparison is hardly statistically significant. On the other hand, increasing the window may introduce systematic biases due to spatio-temporal NO_2 inhomogeneities.

In the left panel of Fig. 18, we present the weighted median (with the 16th and 84th percentiles) NO_2 number density profiles for GOMOS and ACE-FTS, which were calculated from the VMR profiles. These data consist of 6865 co-located occultations and are not corrected for the diurnal NO_2 evolution. The GOMOS densities are larger due to a large number of GOMOS dark limb occultations, for which NO_2 is not photolyzed. The dispersion of the GOMOS data is wider than that of the ACE-FTS data due to the variable precision for different stars, to the variable local solar time and also to the much smaller signal-to-noise ratio obtained by the stellar occultation method.

In the middle panel of Fig. 18, we present the same comparison data set corrected for the diurnal variation with the box model described in Sect. 4.2. Clearly, much better agreement is observed and both weighted medians are within the dispersion of the other instrument. It is interesting that both experiments (mainly seen in the ACE-FTS profile) report a decreased negative slope of NO_2 in their median profiles above 40 km. Large NO_2 enhancements in the polar winter mesosphere have previously been reported by several authors and have been attributed to NO production by solar proton or by energetic electron precipitation (e.g. Hauchecorne et al., 2007; Randall et al., 2005a, and references therein). Strong descent of air occurring in the polar regions, can transport large quantities of NO from the upper mesosphere-lower thermosphere to the lower mesosphere or upper stratosphere, thus increasing NO_2 concentrations.

In the right panel of Fig. 18, we show the weighted median difference profile between ACE-FTS and GOMOS. These are given relative to the GOMOS data set (unlike all the other satellite comparisons shown in this paper). It can be seen that between 23 and 43 km there is an agreement to within 10%, being positive between 37 and 42 km, and above 49 km. The generally negative bias of ACE-FTS increases to approximately 55% at 47 km and to more than 100% below 18 km.

It is important to realize that even if the photodiurnal correction is essential to compare a stellar and a solar occultation instrument, it is of limited accuracy. Indeed, it is clear that the true local solar occultation time is crucial to compute the correction factor (see Fig. 6). This may be quite sensitive to the geometry of the occultation through the altitude dependence and even with respect to atmospheric refraction. Also, the GOMOS line-of-sight direction should be taken into account as well as the extended Sun angular diameter in the ACE-FTS retrievals. The diurnal effect should be evident in the GOMOS-ACE comparisons but may be swamped by other, larger systematic errors.

5.1.4 MIPAS ESA NO$_2$

For MIPAS, correlative data were only available for a two-month period in early 2004 for northern mid- and high latitudes, and the coincidence criteria were chosen to be 300 km and 6 h to have a sufficient number of coincidences for the statistics of the comparison. MIPAS ESA data v4.62 are compared in the period from 21 February 2004 to 26 March 2004. During the first five months of the ACE mission, only sunsets were measured because of problems with spacecraft pointing at sunrise. Therefore the latitude coverage for this comparison is limited to between 20° N and 85° N. The comparison has been done including all the matching pairs of measurements available in the overlap period. Only MIPAS ESA profiles associated with a successful pressure/temperature and target species retrievals have been considered.

Wetzel et al. (2007) studied Arctic daytime sunset profiles (ACE-FTS data version 2.2) around 75° N, which were compared to MIPAS ESA daytime observations. There the three-dimensional chemical transport model KASIMA (Karlsruhe Simulation model of the Middle Atmosphere; Kouker et al., 1999) was used to photochemically correct the MIPAS ESA profiles to the time of the ACE-FTS profiles. They used co-location criteria of 1 h and 300 km, leading to 12 coincidences. The time period was 4 February to 26 March 2004. They found an overall good agreement (−5.8%) with a small negative bias of MIPAS below 32 km reaching 40% at the lowest altitudes. Note that this comparison time period included part of the science commissioning prior to the ACE Science Operations phase that started on 21 February 2004.

In the study presented here, we have 84 coincidences in the period 21 February to 26 March 2004. Panel (a) in Fig. 19 shows the average profiles of ACE-FTS in red, ACE-FTS (photochemically corrected to the MIPAS times) in black and the MIPAS ESA profiles in blue. The absolute differences in panel (b) have combined error bars (mainly from MIPAS). It can be seen that the differences are small when the error bars are taken into account. In panel (c) it can be seen that there is good agreement to within 20% below 32 km, with a small negative bias for the ACE-FTS for the photochemically corrected data. Above 32 km, the differences are not small anymore: the negative bias increases to 75% at 45 km, but the error bars also become larger.

There are uncertainties above 35 to 40 km in the comparison of ACE-FTS with MIPAS ESA, which might be related to the fact that the ESA retrieval rejects negative values. These are particularly important if the retrieved VMRs are close to the noise error (with high noise errors because of the low temperatures encountered during the measurements for the comparisons presented here).
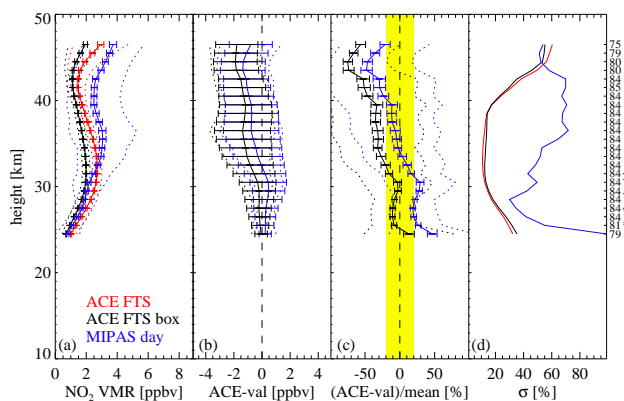

Fig. 19. Same as Fig. 10 but for ACE-FTS and MIPAS ESA. In addition to the ACE-FTS box model corrected data (ACE-FTS box, black), the uncorrected data is plotted (ACE-FTS, red). Note: here the error bars in panel **(b)** are the combined random errors.

5.1.5 OSIRIS NO$_2$

For OSIRIS, the coincidence criteria used are 500 km and 2 h. Local ACE sunset measurements are compared to OSIRIS evening observations. Too few coincidences are found at sunrise/morning to make a relevant statistical analysis. Only profiles that are both inside or both outside the polar vortex are used. This is done by studying potential vorticity fields from the European Centre for Medium-range Weather Forecast (ECMWF). The conversion of OSIRIS data from number density to VMR is done using ECMWF temperature and pressure at OSIRIS measurement locations. Only OSIRIS data with measurement response above 0.5 are used. OSIRIS profiles are interpolated onto the ACE-FTS and MAESTRO altitude grids. ACE data with reported errors above 100% are rejected. OSIRIS data flagged for bad pointing are removed. OSIRIS profiles are scaled to the solar zenith angle of ACE (i.e. 90°) using box model data for local OSIRIS conditions. Only profiles for which the magnitude of the scaling is less than 100% are used. In addition to solar occultation diurnal effects, an ACE-OSIRIS comparison must contend with limb-scatter diurnal effects (McLinden et al., 2006), although these are generally smaller and vary depending on OSIRIS viewing geometry. Model calculations have been performed using the VECTOR radiative transfer model (McLinden et al., 2002; Haley and Brohede, 2007) to quantify diurnal effect errors in each coincident OSIRIS and ACE profile; these were then applied to the individual profiles. The largest portion of the correction lies usually in the ACE data. Retrieval errors due to concentration gradients along the scattering/absorption paths (due to varying local times/solar zenith angles) are only important below 25 km, because usually biases in the near field are compensated for opposite biases in the far field. This is, however, not the case below 25 km, where the signal is becoming saturated and
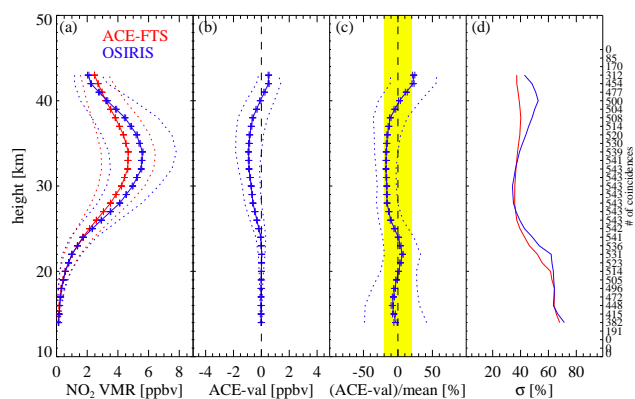
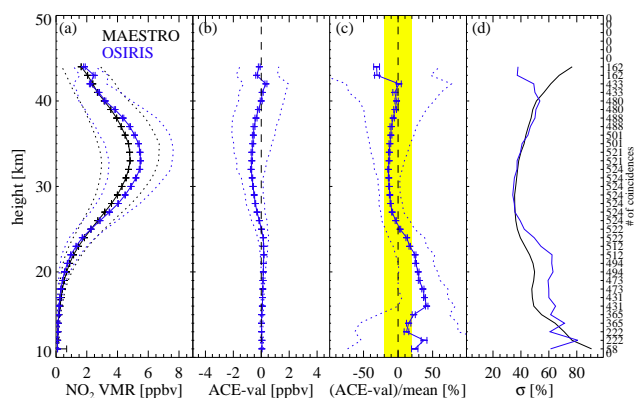**Fig. 20.** Same as Fig. 10 but for ACE-FTS and OSIRIS.

Fig. 21. Same as Fig. 10 but for MAESTRO and OSIRIS.

is henceforth weighted toward the near side. After applying all this filtering, 543 sunset coincidences remained for ACE-FTS and 524 sunset coincidences remained for MAE-STRO. Most coincidences occur in February and March 2004 to 2006 between 30° N and 90° N. The few results from other latitudes and seasons are not very different. The results from ACE-FTS and MAESTRO comparisons are generally similar.

Figure 20 shows the ACE-FTS–OSIRIS comparison and Fig. 21 the MAESTRO–OSIRIS comparison. OSIRIS VMRs are higher at the NO₂ peak by about 0.9 ppbv or 17% for ACE-FTS and by about 0.7 ppbv or 14% for MAE-STRO. The results for MAESTRO and ACE-FTS are similar here due to sampling biases in the OSIRIS comparisons due to Odin/OSIRIS viewing constraints. Below the peak, the agreement is very good down to 15 km where there appear to be issues with the MAESTRO data. The good agreement below 25 km (especially for ACE-FTS) indicates that the diurnal effect correction is working appropriately.

The random difference (1σ) is around 20% just below the peak and increases towards lower and higher altitudes

(Fig. 21c). The random differences are larger for MAESTRO comparisons at the upper edge of the altitude range.

5.1.6 SCIAMACHY NO₂ total columns from nadir measurements

For the nadir comparisons, all SCIAMACHY measurements within 200 km of the ACE occultation measurements taken on the same day were averaged into one value for the comparisons. This leads to about 8000 coincidences. Profiles that did not extend to sufficiently low altitudes and profiles for which the diurnal correction could not be calculated were excluded. There were also missing MAESTRO profiles that could not be taken into account for the comparisons.

To correct for photochemistry, the SCIAMACHY NO₂ vertical column is multiplied with photochemical correction factors derived with the photochemical model described earlier (see Sect. 4.2), integrated over the stratosphere and interpolated linearly on the times of the overpass. Then these diurnally scaled SCIAMACHY vertical column densities were compared to the corrected ACE-FTS and MAE-STRO partial columns. Figure 22 shows the comparisons of ACE-FTS and MAESTRO NO₂ partial columns and SCIA-MACHY NO₂ total columns. They show very good correlations, r=0.94 and 0.91, respectively, with both ACE partial columns are in general smaller than the SCIAMACHY total columns (as expected). The diurnal effect was quantified by forward modelling the expected error for each ACE-SCIAMACHY coincidence and then applied as a correction to the partial column of the ACE instruments. Typically the diurnal effect led to an overestimate in the ACE partial column by about 12%.

As mentioned above, it is expected that SCIAMACHY total columns are larger than ACE partial columns. The differences seen are of the order of the expected tropospheric contribution of about 0.5×10^{15} molec/cm^2 with some scatter introduced either by polluted scenes, which have not been removed fully, or the photochemical correction, which is expected to introduce a significant uncertainty when the time difference is large. Interestingly, the correlation between SCIAMACHY columns and ACE-FTS columns is more compact although the measurement principle (UV-VIS absorption spectroscopy) is very similar to the one used by MAESTRO. The main conclusion from this comparison is that the overall consistency of the two ACE NO₂ products with SCIAMACHY nadir columns is very high with no indication of systematic latitudinal/SZA biases larger than the intrinsic uncertainties of the comparison (based on further examination of the data, not shown). The photochemical correction on the SCIAMACHY data, however, is relatively large in many cases and introduces a significant uncertainty in the comparison.
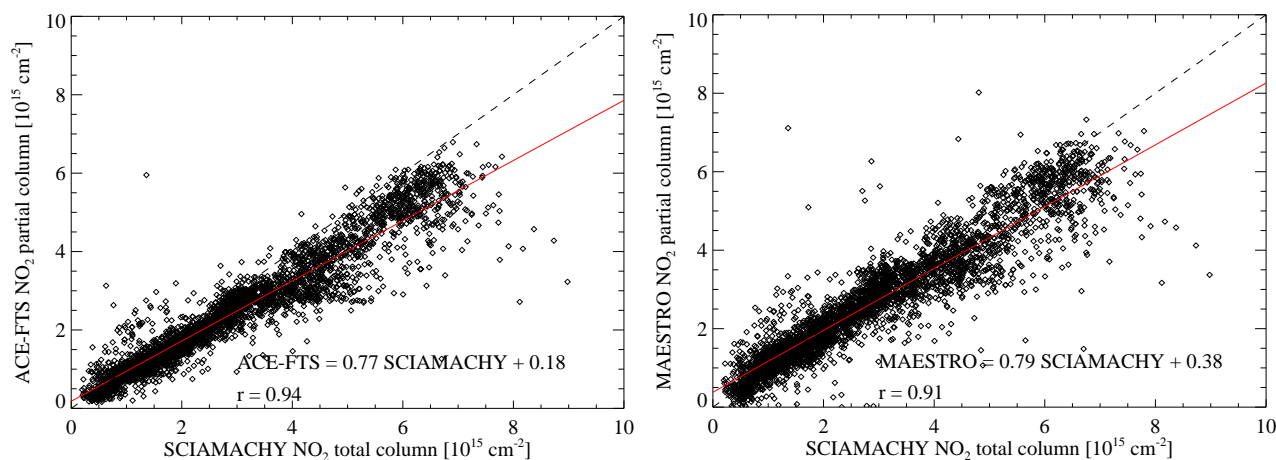
Fig. 22. Scatter plot of the ACE-FTS (left) and the MAESTRO (right) NO$_2$ partial columns (calculated between 14.5 to 46.5 km) and the SCIAMACHY NO$_2$ nadir total columns. In both figures the red lines are the least-squares linear fit to the data, with the slope, intercept, and correlation coefficient given in the figures. The dashed black lines show the one-to-one line relationship for comparison.

5.2 Comparisons with balloon measurements

5.2.1 SPIRALE NO$_2$ measurements near Kiruna

The SPIRALE NO$_2$ measurement was made on 20 January 2006 between 17:46 UT and 19:47 UT, with a vertical profile obtained during ascent between 17.0 and 27.2 km. The measurement position remained rather constant, with the balloon mean location of 67.6±0.2° N and 21.55±0.20° E. The comparison is made with ACE occultation sr13151, which occurred 13 h later (on 21 January 2006 at 08:00 UT) and was located at 64.28° N, 21.56° E, i.e. 413 km away from the SPIRALE position. Using the MIMOSA (Modèle Isentropique de transport Mésoéchelle de l'Ozone Stratosphérique par Advection) contour advection model (Hauchecorne et al., 2002), potential vorticity maps in the region of both measurements have been calculated each hour between 17:00 UT on 20 January and 08:00 UT on 21 January on isentropic surfaces, every 50 K from 400 K to 800 K (corresponding to 16 to 30 km height). From these potential vorticity fields, it can be deduced that the SPIRALE and ACE profiles were located in similar air masses in the well-established polar vortex for the whole range of altitudes sounded by SPIRALE. The dynamical situation was very stable with potential vorticity agreement better than 10%, which gives a geophysical situation suitable for direct comparisons.

Since SPIRALE measurements were performed at night (when the NO$_2$ VMR is a maximum) and ACE measurements were performed at twilight (when there is a strong decrease of NO$_2$), the diurnal variations of NO$_2$ had to be taken into account. Appropriate coefficients deduced from the photochemical model described in Sect. 4.2 have been applied to the ACE NO$_2$ measurements.
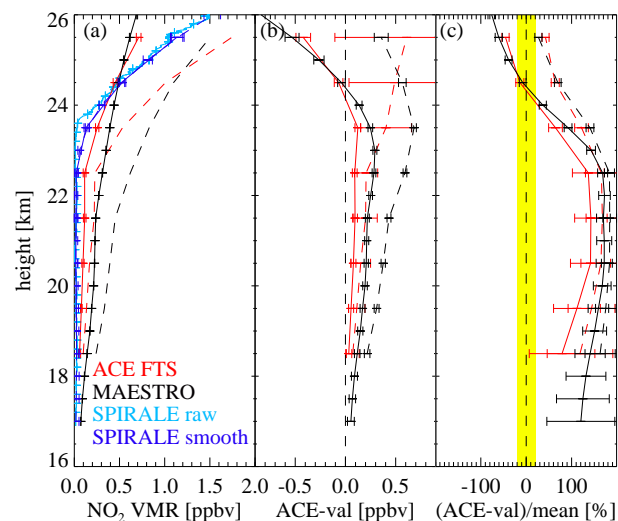

Fig. 23. (a) NO$_2$ profiles obtained by SPIRALE on 20 January 2006 (in turquoise (raw) and blue (smoothed)), sunrise occultation 13151 on 21 January 2006: ACE-FTS (in red) and MAESTRO (in black), ACE corrected by using a photochemical model (dashed lines). **(b)** Absolute differences between the ACE instruments and SPIRALE (smooth) and the photochemically corrected profiles (dashed). **(c)** Relative differences between SPIRALE data and ACE uncorrected (solid) and corrected data (dashed). The region ±20% is highlighted in yellow. Error bars represent the combined random error for panels (b) and (c).

In Fig. 23, between 17 and 23.6 km height, SPIRALE measurements show the expected denoxification (removal of NO$_x$) with NO$_2$ concentrations close to zero (accounting for error bars) in agreement with a vertical profile (not shown) simulated by the REPROBUS (REactive Processes Ruling
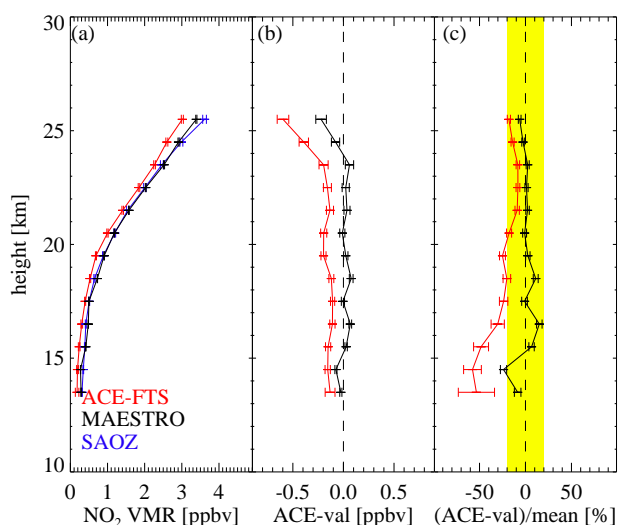
Fig. 24. (a) NO$_2$ profiles obtained by SAOZ at Aire-sur-l'Adour on 7 May 2005 (blue), sunrise occultation 9317 on 6 May 2005: ACE-FTS (red) and MAESTRO (black). (b) Absolute differences between SAOZ and the ACE instruments. (c) Relative differences between SAOZ and the ACE instruments. The region ±20% is highlighted in yellow. Error bars represent the combined random error for panels (b) and (c).
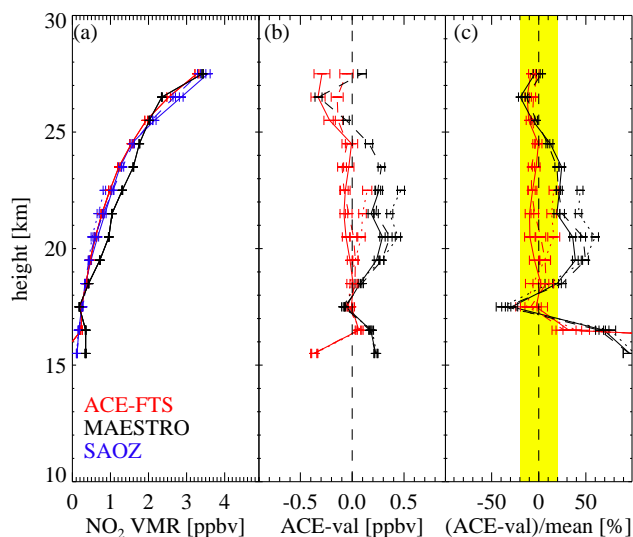

Fig. 25. (a) NO$_2$ profiles obtained by SAOZ at Niamey, Niger on 7 (dotted blue), 10 (solid blue) and 19 August 2006 (dashed blue); ACE occultation sunset 16076 on 7 August 2006, ACE-FTS in red and MAESTRO in black. (b) Absolute differences between SAOZ and the ACE instruments. (c) Relative differences between SAOZ and the ACE instruments. The region ±20% is highlighted in yellow. Error bars represent the combined random error for panels (b) and (c).

the Ozone BUdget in the Stratosphere) Chemical Transport Model (CTM) (Lefèvre et al., 1998) for these polar winter

conditions. This result clearly differs from the ACE-FTS and MAESTRO observations (with or without photochemical corrections), which show significant amounts of stratospheric NO$_2$ in the lower stratosphere. Such NO$_2$ enhancements are also present in the vertical profiles previously obtained at polar latitudes by balloon-borne instruments using remote-sensing techniques (e.g. Payan et al., 1999; Rivière et al., 2002) in contradiction with our current knowledge of polar chemistry. As demonstrated by Berthet et al. (2007), such non-zero values can be attributed to effects of NO$_2$ local inhomogeneities present at higher altitudes along the lines-of-sight of these instruments and mainly resulting from perturbed dynamical situations. In such cases, the validity of the spatial homogeneity hypothesis inherent in remote-sensing methods can be ruled out, consequently affecting the retrievals of the lower part of the vertical profile. In the ACE observation case, the vortex appears to be vertically distorted, as shown by the MIMOSA potential vorticity fields between 800 and 950 K, which are above the vertical levels corresponding to the SPIRALE measurements. Some of the ACE lines-of-sight appear to cross the vortex edge, thus sounding both denoxified air masses in the inner part of the vortex (as shown by SPIRALE inside the vortex) and NO$_2$-richer air in the outer part of the vortex. Above 23.6 km, NO$_2$ concentrations measured by SPIRALE sharply increase and the disagreement between both instruments is reduced to less than 50%. Note that the REPROBUS CTM simulates a profile with a similar gradient above 23.6 km (Berthet et al., 2007).

5.2.2 SAOZ balloon measurements of NO$_2$ from Aire-sur-l'Adour and Niamey

The SAOZ balloon profiles available for comparison with ACE-FTS and MAESTRO are those from one flight from Aire-sur-l'Adour in France (43.7° N, 0.2° W) and three from Niamey, Niger (13.4° N, 2.1° E). Two profiles are available for each flight: during the ascent of the balloon in the late afternoon and during sunset occultation from float altitude. The latter is more precise so it is used in the comparisons. Figure 24 shows the comparisons for the flight from Aire-sur-l'Adour launched on 7 May 2005 at 18:00 UT. There is a coincident ACE sunrise (sr 9317) profile on 6 May 2005 at 05:00 UT, which is at a distance of about 700 km and 37 h earlier. It can be seen that despite of the large time difference there is very good agreement between all three instruments. In this case, MAESTRO agrees better than ACE-FTS (generally to within 20%), whereas ACE-FTS shows a low bias from 57% at 14.5 km to 8% at 22.5 km. There is no difference between the SAOZ float occultation measurements and the ascent profiles (not shown).

The closest flight in the tropics took place at Niamey, Niger on 7 August 2006 at 18:00 UT, for which there was a sunset occultation (ss16076) at 18:51 UT, at a distance of about 850 km. However, because of the 22 km float altitude
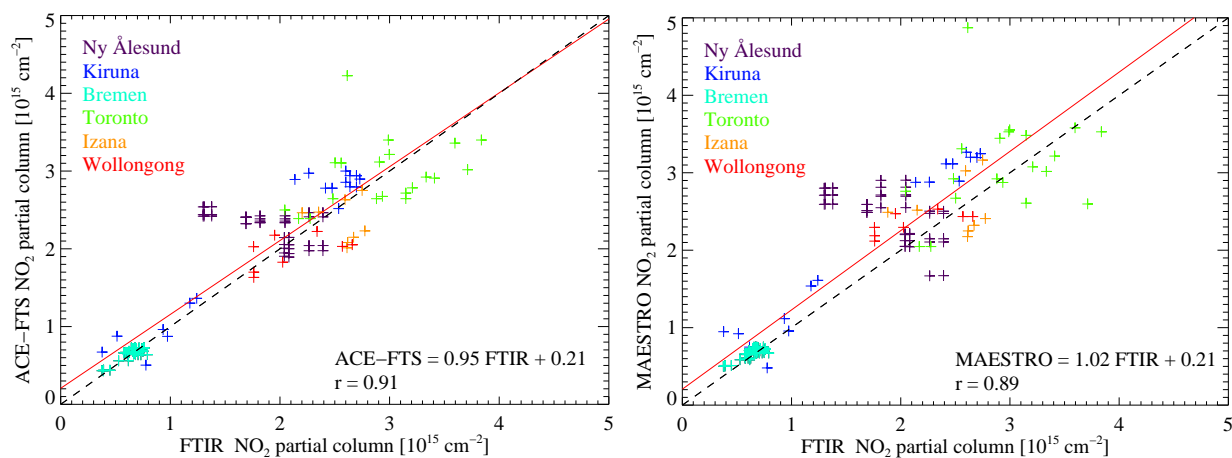
Fig. 26. Scatter plots of the ACE-FTS (left) and the MAESTRO (right) and ground-based FTIR NO$_2$ partial columns. For both panels the red lines are the linear least-squares fit to the data, with the slope, intercept, and correlation coefficient given in the figures. The black lines show the one-to-one linear relationship for comparison.

of this flight, which was dedicated to the study of NO$_x$ production by lightning near a thunderstorm, the profiles only extend from 16 to 21 km. Because the measurements are very consistent within this altitude range with those of two other flights performed on 10 and 19 August up to 28 km and because NO$_2$ is not expected to vary in the stratosphere in the tropics, the data from the two later flights were also used in the comparison although not co-located with ACE. Figure 25 shows the profiles of the three flights together with those of ACE-FTS and MAESTRO. It can be seen that the variability of the SAOZ NO$_2$ is indeed very small: sunset NO$_2$ profiles are very close together. They compare very well with the profiles from the ACE instruments. The agreement with ACE-FTS is better than 20% above 16 km with a slight negative bias. The MAESTRO NO$_2$ VMR is larger than both the SAOZ and ACE-FTS VMRs between ~18.5 and 25 km, and agrees with the three SAOZ profiles to within 20% above 22 km. Below 17 km the data are less reliable, because of the large variation of NO$_2$ in the upper troposphere and the tropical tropopause layer caused by lightning.

5.3 Ground-based FTIR NO$_2$

For the validation of ACE NO$_2$ by ground-based FTIRs, data are available from six stations: Ny Ålesund, Kiruna, Bremen, Toronto, Izaña and Wollongong (see Table 1). For each station, the ACE-FTS profiles were interpolated onto the FTIR retrieval grid and extended below the lowest retrieved altitude using the FTIR a priori VMR values. This combined profile was smoothed using the FTIR averaging kernels and a priori profile, as described in Sect. 4.1, to minimize the smoothing error (Rodgers and Connor, 2003). For the calculation of partial columns, atmospheric densities were needed; the density derived from the pressure and temperature profiles used in the FTIR retrievals was used for both the ground-based and the ACE measurements. The lower limit of the altitude range of the partial columns at each station was determined by the ACE-FTS altitudes and the upper limit was determined by the sensitivity of the FTIR measurements, which was required to be 0.5 or greater. The sensitivity of the FTIR measurements was calculated using the sum of the elements of the columns of the averaging kernel matrix that was not normalized with the a priori profile. This results in a sensitivity with respect to altitude (Vigouroux et al., 2007). This sensitivity indicates the contribution to the retrieval from the measurement. Thus a sensitivity greater than 0.5 means that at that altitude more than half of the information is being gained from the measurement itself and less than half remains from the a priori VMR profile.

Table 3 lists the microwindows used at the participating sites, and the altitude ranges where the sensitivity for the FTIR measurements were greater than 0.5 and for which ACE data were available. The partial columns for NO$_2$ at the different locations were calculated for these altitude ranges. As can be seen, the altitude ranges over which the partial columns were calculated vary from station to station. For Kiruna and Izaña, the profiles were scaled a priori profiles and therefore there were no averaging kernels for NO$_2$ and DOFS were not calculated. Averaging kernel smoothing could not be applied for these two stations. Therefore partial columns of unsmoothed ACE profiles were compared with partial columns from Kiruna and Izaña. The DOFS for the other stations are indicated in Table 3. It can be seen that the Bremen result has 0.1 DOFS, because the altitude range with sensitivity >0.5 is very small (from 19.6 to 24.4 km). The Wollongong result has 0.6 DOFS, which is due to large water vapour concentration in the atmosphere and therefore low signal-to-noise ratio. The ACE data were adjusted to match the local times of the FTIR stations using the photochemical box model (see Sect. 4.2).

In Table 3, it can be seen that the agreement between the ground-based stations and the ACE instruments is good:

Table 3. Results of the NO$_2$ partial column comparisons of ACE-FTS and MAESTRO with the ground-based FTIRs. The microwindow(s) used in the retrievals are listed in column 2. For each ACE / FTIR pair, the number of coincidences, the vertical range used to calculate the partial columns and the corresponding degrees of freedom for signal (DOFS) are given in columns 3 to 5. The mean difference and 1σ standard deviation of the mean are indicated in columns 6 and 7 for ACE-FTS and MAESTRO, respectively. The retrieval code (with version number) and the spectroscopic database used by the FTIRs are given in the footnotes.

FTIR station[a]	Microwindow(s)[b,c] [cm^{-1}]	# of pairs	Range [km]	DOFS	Mean diff. ± std dev. [%] ACE-FTS	MAESTRO
Ny Ålesund	2914.5900–2914.7070	45	14.8–39.2	1.0	+20.5±25.4	+25.6±29.1
Kiruna[d]	2888.2500–2888.3200	21	19.5–34.2	–	+11.1±20.6	+22.0±26.1
	2893.2806–2893.3610					
	2911.6610–2911.7194					
	2914.6000–2914.7000					
Bremen	2914.5900–2914.7070	72	19.6–24.4	0.1	+2.8± 7.5	+5.4± 8.2
Toronto	2914.5900–2914.7070	20	15.6–39.6	2.1	+1.1±17.4	+5.0±20.4
Izaña[d]	2888.2500–2888.3200	10	19.5–52.8	–	−9.3±15.1	+1.4±18.5
	2893.2806–2893.3610					
	2911.6610–2911.7194					
	2914.6000–2914.7000					
Wollongong	2914.5500–2914.8000	13	23.0–37.0	0.6	−6.3±14.2	+12.0±13.2
Total		181			+7.3±19.6	+12.8±22.1

[a] Retrieval codes: PROFFIT92 is used for Kiruna and Izaña with the solar model of Hase et al. (2006).
   SFIT2 is used for Ny Ålesund (v3.92a), Bremen (v3.92a), Toronto (v3.82β3) and Wollongong (v3.92).
[b] Spectroscopic linelist: HITRAN 1996 for Kiruna and Izaña. All other stations use HITRAN 2004.
[c] Multiple microwindows are fitted simultaneously during the retrieval process for some stations.
[d] Izaña and Kiruna profiles are scaled, i.e. no DOFS were calculated.

within approximately 20% for all but a few cases, and generally better than this. For ACE-FTS, the mean differences lie between 20.5% with σ=25.4% for Ny Ålesund and –9.3% with σ=15.1% for Izaña. The MAESTRO differences are between 25.6% with σ=29.1% for Ny Ålesund and 1.4% with σ=18.5% for Izaña. The mean relative difference is positive in the MAESTRO comparisons, and positive for all but two stations in the ACE-FTS comparisons. This suggests that the ACE-FTS and MAESTRO partial columns have a small positive bias. Good correlation between ACE and the FTIR partial columns is seen in the scatter plots of the data from all stations. Figure 26 shows a tight correlation, with a correlation coefficient, r, defined as

$$r = \frac{\text{covariance of ACE and VAL}}{\sigma_{\text{ACE}}\sigma_{\text{VAL}}} \quad (5)$$

where σ_{ACE} = standard deviation of ACE and σ_{VAL} = standard deviation of VAL. The correlation, r, is 0.91 for ACE-FTS and 0.89 for MAESTRO. The line fitted to the ACE-FTS versus FTIR data has slope 0.95, indicating good agreement, and intercept 0.21×10^{15} molec/cm^2 and that for MAESTRO versus FTIR, slope 1.02 and intercept 0.21×10^{15} molec/cm^2. The largest standard deviations in Table 3 are found for the high-latitude stations. For Kiruna, 8 out of 12 days of available measurements are during the strong vortex winter of 2005, but these data do not show more scatter than Ny Ålesund, which has only two available measurement days

during the same period. There also do not appear to be significant gradients in NO and NO$_2$ across the vortex edge for the corresponding ACE-FTS measurements. Therefore we do not think that the larger scatter at the northern high latitude stations is due to the polar vortex.

5.4 Ground-based UV-VIS NO$_2$

For the ground-based UV-VIS comparisons, we have data from Harestua, Norway (60.2° N, 12.8° E) and Vanscoy, Canada (52.02° N, 107.03° W) for profiles and column comparisons.

5.4.1 Ground-based NO$_2$ profiles and partial columns at Harestua

Both ACE-FTS and MAESTRO NO$_2$ profiles have been compared to height-resolved data retrieved from ground-based zenith-sky UV-VIS observations. For the comparison at Harestua, the maximum distance between the station and the ACE NO$_2$ measurements was 750 km. The measurements by ACE and the ground-based observations were required to be on the same day. Ground-based profiles are converted to the solar zenith angle corresponding to the ACE-FTS and MAESTRO NO$_2$ measurements using the stacked box photochemical model PSCBOX (Hendrick et al., 2004) included in the profiling algorithm. Photochemical conditions are therefore similar for both ACE and ground-

Table 4. Same as Table 3, but for the NO partial column comparisons between ACE-FTS and the ground-based FTIRs.

FTIR station[a]	Microwindow(s)[b,c] [cm^{-1}]	# of pairs	Range [km]	DOFS	Mean diff. ± std dev. [%]
Ny Ålesund	1899.8017–1900.1981	50	24.4–41.3	0.9	−67.5±17.4
Kiruna	1900.0278–1900.1220 1929.0100–1929.0400	18	19.5–44.8	1.6	−39.7±15.4
Toronto	1899.8800–1900.1500	11	25.1–47.9	1.0	−25.7±32.0
Izaña	1900.0278–1900.1220 1929.0100–1929.0400	9	22.1–44.8	1.3	−20.6±31.8
Wollongong	1900.0000–1900.1000 1900.4900–1900.5400 1903.0500–1903.2000 1928.5400–1928.7000	19	23.0–43.0	0.7	−14.5±16.1
Total		107			−46.7±29.6

[a] Retrieval codes: PROFFIT92 is used for Kiruna and Izaña with the solar model of Hase et al. (2006). SFIT2 is used for Ny Ålesund (v3.92a), Toronto (v3.82β3) and Wollongong (v3.92).

[b] Spectroscopic linelist: HITRAN 2001 for Kiruna and Izaña. All other stations use HITRAN 2004.

[c] Multiple microwindows are fitted simultaneously during the retrieval process for some stations.

based UV-VIS profiles. The ACE data from both ACE-FTS and MAESTRO were smoothed with the averaging kernels from the ground-based instrument. After applying these criteria, the following numbers of coincident events have been selected for comparison for the 2004 to 2005 period: 13 sunrises (May and September) and 15 sunsets (March and July) for ACE-FTS and six sunrises (September) and 11 sunsets (March and July) for MAESTRO.

Figure 27 shows the comparison results for all the sunrise profiles and Fig. 28 for the sunset profiles. Below 32 to 35 km, ACE-FTS reports more NO$_2$ than the ground-based instrument with a maximum difference of 23% at 23 km for sunrise and 25% at 25 km for sunset. Qualitatively, similar results are obtained with MAESTRO. However, the positive bias with MAESTRO is larger than for ACE-FTS with a maximum value of about 33% at about 22 km. At sunrise, the observed differences are just outside the variability of both ground-based and MAESTRO profiles.

In order to minimize the effect of the vertical smoothing associated with the ground-based measurements on the comparison (Hendrick et al., 2004, 2007), NO$_2$ partial columns from 17 to 35 km are also compared. This roughly corresponds to the common altitude range where ACE-FTS, MAESTRO, and the ground-based UV-VIS measurements are significantly sensitive to the vertical distribution of NO$_2$. Partial column comparison results are presented in Fig. 29.

The ACE-FTS results are higher than the UV-VIS results by 15% at sunrise and 14% at sunset. This corresponds to absolute difference values of 0.4 and 0.5×10^{15} molec/cm^2,
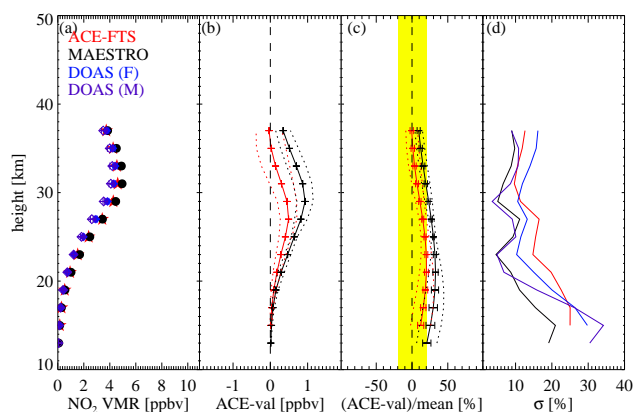

Fig. 27. **(a)** Mean smoothed ACE-FTS (red stars), MAESTRO (black circles) and ground-based UV-VIS NO$_2$ sunrise profiles at Harestua for 2004 to 2005: filled blue diamonds indicate the mean UV-VIS profile for the comparison with ACE-FTS (DOAS (F)), open purple diamonds indicate the mean UV-VIS profile for the MAESTRO comparison (DOAS (M)). **(b)** Absolute differences. **(c)** Relative differences. The ±20% region is highlighted in yellow. **(d)** Standard deviations of the distributions, 1σ, relative to the mean NO$_2$ VMR at each altitude, for all coincident events, for ACE-FTS (red), MAESTRO (black) and UV-VIS (blue and purple). The number of coincidences is 13 (11 at 15 km) for ACE-FTS and 6 for MAESTRO at all levels. The error bars represent the uncertainty in the mean.
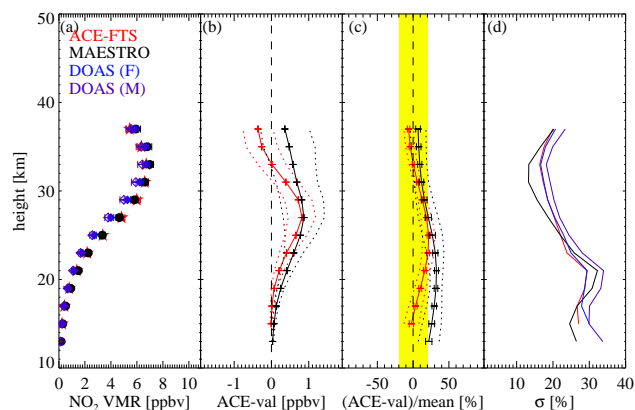
Fig. 28. Same as Fig. 27 but for sunset profiles. The number of coincidences is 15 (12 at 15 km) for ACE-FTS and 11 for MAESTRO at all levels.
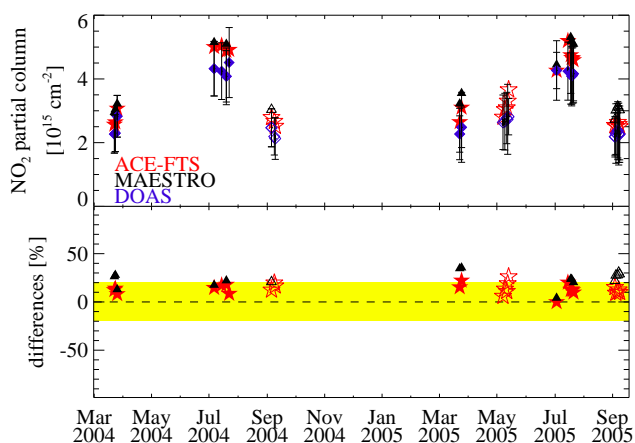

Fig. 29. Comparison of NO$_2$ partial columns from 17 to 35 km from ACE-FTS (red stars), MAESTRO (black triangles) and the ground-based UV-VIS (blue diamonds) at Harestua for 2004 and 2005. Sunrises are indicated with open and sunsets with filled symbols. The relative differences with respect to the mean appear in the lower panel. The ±20% region is indicated in yellow. The error bars on the ground-based UV-VIS columns are estimated from the total retrieval errors on the retrieved ground-based profiles (Hendrick et al., 2004, 2007).

Fig. 30. (a) Mean ACE-FTS (red stars), MAESTRO (black circles) and ground-based UV-VIS NO$_2$ profiles (blue diamonds) at Vanscoy for September 2004. (b) Absolute differences and (c) relative differences are shown. (d) Standard deviations of the distributions, 1σ, relative to the mean NO$_2$ VMR at each altitude, for all coincident events, for ACE-FTS (red), MAESTRO (black) and UV-VIS (blue). The ±20% region is indicated in yellow. The number of coincidences is 5 for all levels.
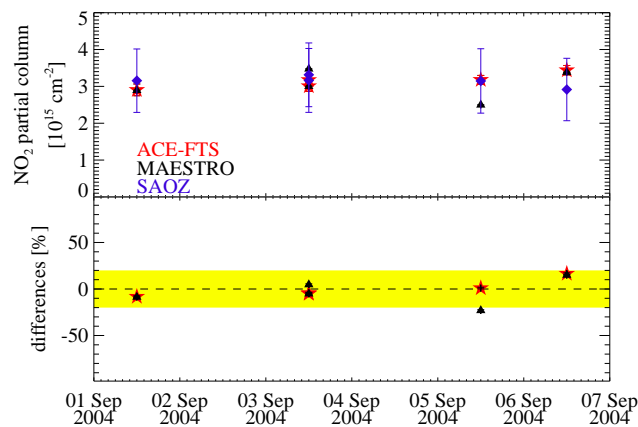

Fig. 31. Comparison of NO$_2$ partial columns (between 10 and 45 km calculated from the ACE-FTS (red stars), MAESTRO (black triangles), and ground-based UV-VIS (blue diamonds) NO$_2$ profiles at Vanscoy for 1 to 6 September 2004. The relative differences appear in the lower panel. The ±20% region is highlighted in yellow. The error bars on the ground-based UV-VIS columns are estimated from the total retrieval errors on the retrieved ground-based profiles (Hendrick et al., 2004, 2007).

respectively. However, these differences are not significant since ACE-FTS partial columns are always within the error bars associated with the ground-based partial columns. As expected from the profile comparison, a larger difference is obtained with MAESTRO: 30% on average at sunrise and 26% at sunset, which corresponds to absolute difference values of 0.7 and 0.8×10^{15} molec/cm^2, respectively. For some of the coincident events, these differences are significant since the MAESTRO partial column values are outside the

error bars associated with the ground-based columns. Because the ACE data set does not report systematic errors, a combined error bar could not be calculated, however we expect the differences to be within the combined error bars. The partial column comparison results from the DOAS system at Harestua (60.2° N), (14 to 15% for ACE-FTS and 26 to 30%

for MAESTRO), show similar magnitudes to those from the FTIR measurements at Kiruna (67.8° N), (11% for ACE-FTS and 22% for MAESTRO for the smaller columns).

5.4.2 Ground-based MANTRA SAOZ NO$_2$ profiles and partial columns at Vanscoy

For the SAOZ profile comparisons, the method described for Harestua in Sect. 5.4.1 has been applied, but sunrises and sunsets have not been distinguished, because only five co-incidences were available. In order to convert the SAOZ profiles into VMRs, pressure and temperature profiles from ACE-FTS were used. The profiles from the ACE instruments were smoothed with the SAOZ averaging kernels. No diurnal scaling needed to be applied because the measurement took place at the same solar zenith angles. It can be seen in Fig. 30 that the profiles agree very well, for ACE-FTS typically, i.e. on average, to within 15% (maximum +35%), and for MAESTRO typically to within 10% (maximum +25%) from 12 to 43 km as shown in Table 5. The partial columns calculated from 10 to 45 km also show a very good agreement (within retrieval errors): only one MAESTRO partial column that is not within 20% of the SAOZ partial column (Fig. 31).

This result was anticipated because the measurements were calculated during the MANTRA campaign, which took place at midlatitudes in late summer, a time of minimal dynamical variability, i.e. ideal conditions for validation studies (Wunch et al., 2005).

6 Results for the NO and NO$_x$ comparisons

In this section, the comparisons available for NO will be shown. Data from only two satellite instruments were available for comparison: HALOE and MIPAS IMK-IAA. The MIPAS comparisons were done for NO$_x$ rather than NO or NO$_2$ because of the difficulty of correcting for diurnal variations under perturbed (NO$_x$ descent) conditions. The only other datasets available for NO comparisons are the ground-based FTIR measurements from the NDACC sites Ny Ålesund, Kiruna, Toronto, Izaña and Wollongong.

6.1 MIPAS IMK-IAA comparison of NO and NO$_x$

The observational period under investigation includes the extraordinary 2004 Arctic winter, which was characterized by enormous amounts of NO$_x$ transported downwards from the upper atmosphere inside the polar vortex (e.g. López-Puertas et al., 2005; Randall et al., 2005a) raising stratospheric NO$_x$ abundances by more than 1 ppm in February/March. These unusual atmospheric conditions make it difficult to combine this comparison with the others undertaken during this validation exercise. For the comparison, we used as coincidence criteria a maximum time difference of 18 h and a maximum spatial mismatch of 1000 km with a maximum potential vorticity difference of 30%. MIPAS version 9.0 NO$_2$ observa-
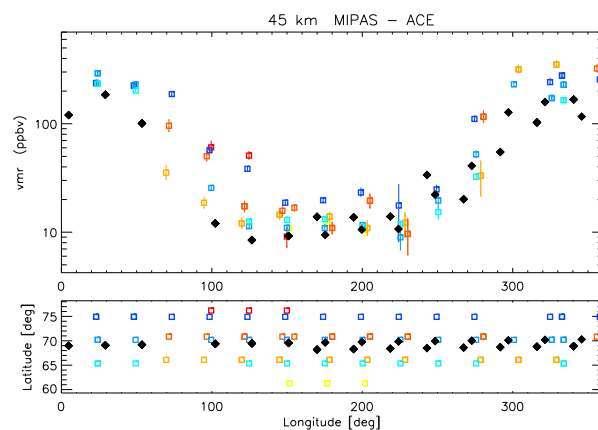

Fig. 32. Longitudinal distributions of ACE-FTS and MIPAS IMK-IAA NO$_x$ abundances measured on 18 March 2004 at VMR peak height (top) and respective geographic locations of the measurements (bottom). The error bars indicate random errors. Black diamonds: ACE-FTS, open squares: MIPAS (color coding: yellow, orange, red: daytime measurements; green, blue: nighttime measurements).
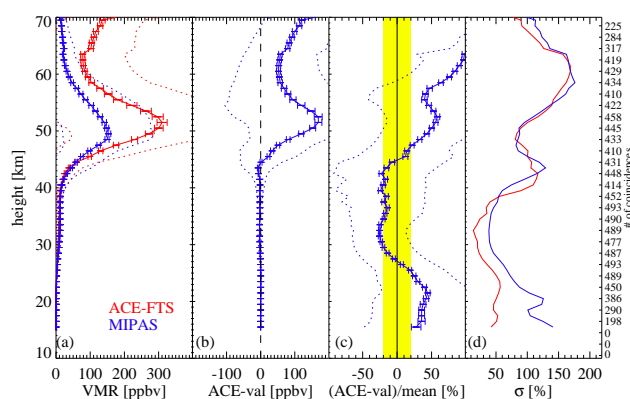

Fig. 33. Same as Fig. 10, for MIPAS IMK-IAA NO$_2$ night and ACE-FTS NO$_x$ (February–March 2004, all days merged). Coincidence criteria: distance 1000 km, time 18 h, potential vorticity difference 30%, MIPAS solar zenith angle >96°.

tions close to high-latitude (75 to 80° N) ACE occultations are available for 22, 28 February and 4, 12 March 2004. Furthermore, on 18 and 25 March, MIPAS observations of both NO$_x$ species could be compared to ACE-FTS measurements taken around 69° N and 56° N, respectively. Since a chemical transport model that could properly account for NO$_x$ descent during polar winter was not available, a photochemical correction to account for the diurnal cycling of the NO$_x$ species could not be applied here. Thus, only MIPAS nighttime NO$_2$ measurements were compared to ACE-FTS NO$_x$ (the sum of the NO$_2$ and NO products) for observations until 12 March 2004, assuming that NO$_x$ is in the form of NO$_2$ at

Table 5. Results of the NO$_2$ partial column comparisons of ACE-FTS and MAESTRO with the ground-based UV-VIS instruments and with SCIAMACHY nadir measurements. The spectral window used in the retrievals is listed in column 2. For each ACE / UV-VIS pair, the number of coincidences, the vertical range used to calculate the partial columns and the corresponding degrees of freedom for signal (DOFS) are given in columns 3 to 5. The mean difference and 1σ standard deviation of the mean are indicated in columns 6 and 7 for ACE-FTS and MAESTRO, respectively.

Instrument	Spectral window [nm]	# of pairs	Range [km]	DOFS	Mean diff. ± std dev. [%] ACE-FTS	MAESTRO
DOAS[a] (ACE sunrise)	425–450	13/6[c]	17–35	2.5	+15.2± 6.4	+30.3± 5.2
(ACE sunset)		15 / 11[c]	17–35		+14.4± 6.1	+26.0±11.4
SAOZ[b]	406–526	5	10–45	0.93	+0.4±10.4	−2.6±13.9
SCIAMACHY nadir	425–450	4457/4366[c]	14.5–46.5	1	−17.1±22.5	−5.9±28.0

[a] Ground-based UV-VIS measurements from Harestua, Norway.
[b] Ground-based UV-VIS measurements from Vanscoy, Canada.
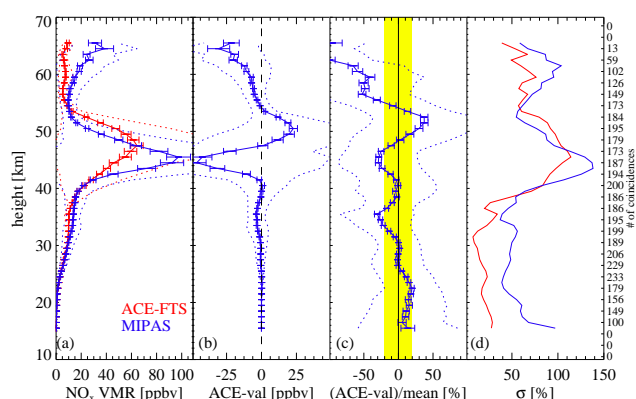[c] Number of coincidences with ACE-FTS and MAESTRO, respectively.

Fig. 34. Same as Fig. 10, for MIPAS IMK-IAA NO$_x$ and ACE-FTS NO$_x$ (18 and 25 March 2004 merged). Coincidence criteria: distance 1000 km, time 18 h, potential vorticity difference 30%, with all MIPAS solar zenith angles.

Fig. 35. Same as Fig. 10, for MIPAS IMK-IAA NO$_x$ and ACE NO$_x$, (25 March 2004; mainly midlatitude conditions). Coincidence criteria: distance 1000 km, time 18 h, potential vorticity difference 10%, with all MIPAS solar zenith angles.

night. For 18 and 25 March, daytime and nighttime MIPAS observations of total NO$_x$ (NO+NO$_2$) could be compared to ACE-FTS occultations. The ability of both instruments to capture the spatial distribution of NO$_x$ in a consistent manner is shown in Fig. 32.

In Fig. 33, we show the results of the comparison of MIPAS nighttime NO$_2$ with ACE-FTS NO$_x$. Similar results for the comparison of MIPAS and ACE-FTS NO$_x$ measurements (18 and 25 March 2004) are shown in Fig. 34. A pronounced NO$_x$ enhancement of several 100 ppbv due to polar winter descent at altitudes around 45 to 50 km is visible in both MIPAS and ACE-FTS observations. In general, excellent qualitative agreement is seen for MIPAS and ACE-FTS observations of descended NO$_x$-enriched air masses, which is further corroborated by the high consistency of observed spatial distributions of NO$_x$ (Fig. 32). The extreme spatial variabil-
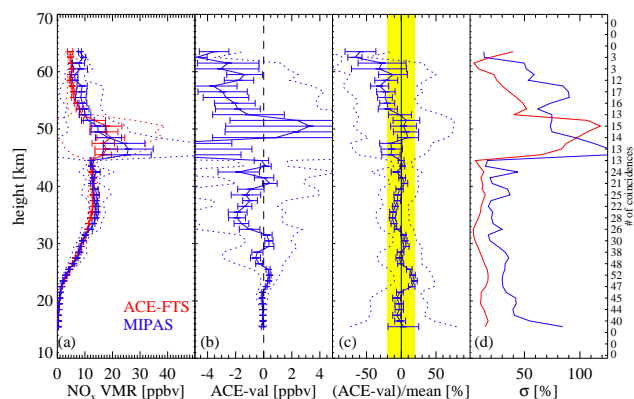
ity of measured NO$_x$ abundances at the VMR peak height is the most likely cause of deviations of the peak magnitude between MIPAS and ACE-FTS of the order of 50%. Above the VMR peak height of between 40 and 50 km, NO starts to contribute to nighttime NO$_x$, which explains higher values of ACE-FTS NO$_x$ when compared to MIPAS nighttime NO$_2$ only (see Fig. 33). On 25 March, ACE-FTS was mainly sampling air masses outside the polar vortex at latitudes around 55° N, which allows for a comparison to MIPAS under unperturbed conditions. For this particular day, the ACE-FTS and MIPAS NO$_x$ measurements agree within 20% except at altitudes above 52 km, where the maximum difference is 30% up to 60 km (Fig. 35). A detailed inspection of the spatial distribution of MIPAS NO$_x$ measurements at this particular altitude showed that MIPAS, contrary to ACE-FTS, was sampling NO$_x$-enriched vortex air masses at longitudes around 130° W (Fig. 32).
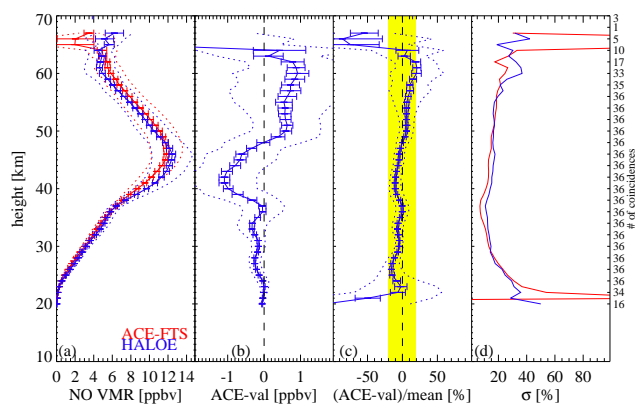
Fig. 36. Same as Fig. 10 but for HALOE NO.

Fig. 37. Same as Fig. 36 but for the height range 90 to 108 km and with logarithmic abscissae for panel **(a)** and **(d)**. One of the standard deviation curves in panel (a) is discontinuous because of the logarithmic axis.

6.2 HALOE NO

For NO, the HALOE and ACE-FTS data sets were searched for coincident measurements, defined as occurring within 2 h and 500 km. A total of 36 coincidences were found; five of these corresponded to satellite sunrise occultations in both instruments, while the other 31 corresponded to satellite sunset occultations in both instruments. The sunset coincidences occurred from 4 to 10 July 2004 (29 coincidences, average latitude 66° N) and 15 August 2005 (two coincidences, average latitude 49° S); the sunrise coincidences occurred on 6 and 7 September 2004 (five coincidences, average latitude 60° N). Thus the majority of the comparisons correspond to polar summer conditions in the Northern Hemisphere. Because only five coincidences corresponded to satellite sunrise occultations, the results below do not distinguish between sunrise-sunrise and sunset-sunset comparisons; thus no information is gained regarding possible sunrise/sunset biases in the ACE-FTS measurements.

Figures 36 and 37 show the average NO profiles measured by ACE-FTS and HALOE for all coincidences. Only measurements where the reported error for ACE-FTS and HALOE was less than 100% are included in the results presented. Because VMRs vary strongly over the altitude range of the retrievals, the profiles are shown on a linear scale from 20 to 70 km, and on a log scale from 90 to 110 km. Both instruments show very similar profile shapes, with a stratospheric VMR peak near 45 km, and generally increasing VMRs above 65 km. ACE-FTS VMRs are biased slightly low compared to HALOE below about 48 km, and slightly high from 50 to 64 km. There are gaps in the curves between 70 and 90 km (not shown) because there were fewer than three coincident measurements where both instruments reported errors less than 100%. In this altitude range, the NO densities (not shown) are one to two orders of magnitude lower than below 65 km or above 90 km, so the retrievals are much more difficult. When both instruments do
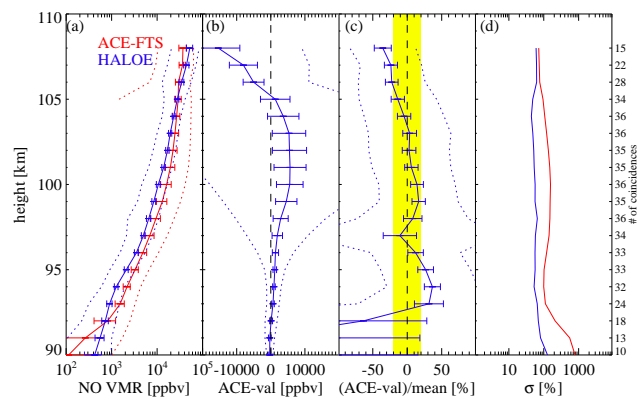
have data, the differences above 65 km are often significantly larger than at the lower altitudes. Dotted lines in panels (a) of the figures represent the standard deviations of the distribution of profiles measured by each instrument. Qualitatively, it is clear that both instruments measure similar variability below 60 km as seen in Fig. 36d. Above this altitude, profiles from both instruments show substantially more variability, but not necessarily of the same magnitude.

Variability is quantified more clearly in panels (d) of Figs. 36 and 37, which show the standard deviations of the distributions relative to the mean VMRs, again separately for the low- and high-altitude cases. Below 65 km, there is very good agreement between ACE-FTS and HALOE, with both instruments showing slightly increasing standard deviations above about 35 km, and more steeply increasing standard deviations below 35 km. The standard deviations shown here reflect both instrument precision and geophysical variability in the measurements. Above 64 km (only shown from 90 km), there is substantial disagreement between the ACE-FTS and HALOE standard deviations, with ACE-FTS showing higher variability. It is possible that these standard deviation differences are due to different geophysical conditions sampled by the instruments, but this should not be a large effect given the relatively tight coincidence criteria employed here. In addition, geophysical variability would not be expected to result in a bias in one instrument compared to the other, since it is unlikely that one instrument would always sample geophysical conditions that were biased in the same way with respect to the conditions sampled by the other instrument. We thus speculate that the precision of the ACE-FTS measurements is generally worse than that of HALOE above 64 km.

Panels (c) of Figs. 36 and 37 show the percent differences between the instruments. As noted above, measurements from ACE-FTS are biased slightly low compared to
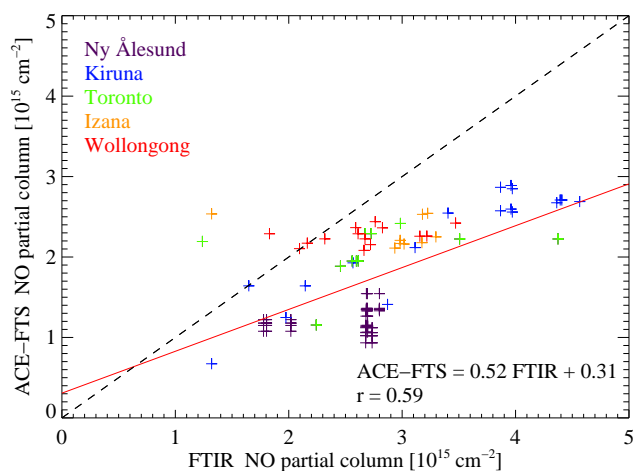
Fig. 38. Scatter plot of the ACE-FTS and ground-based FTIR NO partial columns. The red line is the linear least-squares fit to the data, with the slope, intercept, and correlation coefficient given in the figure. The black line shows the one-to-one line relationship for comparison.

HALOE below 48 km, with differences generally within ~10 to 15%. From 49 to 64 km, ACE-FTS measurements are biased slightly high compared to HALOE, with differences increasing to 21% at 60 km. To summarize, the overall agreement below 60 km is excellent, with differences within 20% and typically ±8% from 22 to 60 km. The comparisons between 64 and 90 km show very large and variable differences (not shown). Note, however, that the error bars, which represent the uncertainty in the mean difference, often cross zero. Thus, for much of the altitude range between 64 and 100 km, the statistical differences are not significant. Part of the problem here is that so few of the measurements are predicted to have errors smaller than 100%. Overall, there is a suggestion that the ACE-FTS NO measurements are biased low with respect to HALOE above 64 km but below 90 km, but this should be considered a tentative conclusion.

6.3 Ground-based NO from FTIRs

For the validation of ACE-FTS NO, data were available from all the FTIR stations used for the NO_2 comparisons (see Table 1) except for Bremen. The same analysis has been applied here as in Sect. 5.3. Table 4 shows the ranges where the sensitivity for the FTIR measurements were greater than 0.5 and for which ACE-FTS data were available. The partial columns were calculated over altitude ranges between approximately 20 and 45 km. The DOFS are indicated in Table 4. Kiruna and Izaña are showing DOFS larger than one: 1.6 and 1.3, respectively, while the DOFS of the three other stations are ~1. For the NO comparisons, averaging kernels for Kiruna and Izaña were available so that all coincident ACE-FTS profiles could be smoothed using the method de-

scribed in Sect. 5.3. Then the ACE-FTS data were adjusted to match the local times of the FTIR stations using the photochemical box model.

Table 4 lists the mean relative differences between ACE-FTS and the ground-based FTIR partial columns. The agreement is not very good: there is a consistent low bias in the ACE-FTS partial columns, ranging from −14.5% for Wollongong to −67.5% for Ny Ålesund). The average difference for all stations is −47% with σ=30%.

One possible explanation for this discrepancy is that at high latitudes during winter and spring there can be high levels of NO in the upper atmosphere that contribute to the FTIR stratospheric partial columns, but not to the ACE-FTS partial columns, as the retrieval grid and the model atmospheres of the ground-based stations extend only to 100 km (Wiacek et al., 2006). This affects Kiruna and Ny Ålesund the most, which have the largest bias compared with the other stations. We also expect a low bias for the ACE-FTS, because of the diurnal effect, of about 10%, which is not enough to account for the large differences observed.

A weak correlation between ACE-FTS and the FTIR partial columns is seen in the scatter plot of the data from all stations. Figure 38 shows a correlation coefficient, r=0.59, while the line fitted to the ACE-FTS versus FTIR data has slope 0.52 and intercept 0.31×10^{15} molec/cm^2. The small slope indicates that the smoothed ACE-FTS partial columns do not vary sufficiently, i.e. it looks as if they are relatively constant.

7 Summary and conclusions

An assessment of the quality of the ACE-FTS version 2.2 NO_2 and NO and MAESTRO version 1.2 NO_2 data has been presented in this paper. NO_2 and NO are two of the 14 baseline species for the ACE mission. Version 2.2 ACE-FTS VMR profiles are retrieved from solar occultation measurements for NO between 15 and 110 km and for NO_2 between 13 and 58 km at a vertical resolution of about 3 to 4 km. Version 1.2 MAESTRO data are retrieved from solar occultation measurements in the wavelength range 420 to 545 nm with a resolution of 1 to 2 km.

ACE NO_2 profiles from the first three years of the mission have been compared with coincident measurements made by the HALOE, SAGE II, SAGE III, POAM III, SCIAMACHY (solar occultations), GOMOS, OSIRIS and MIPAS satellite instruments, individual balloon flights of SPIRALE and SAOZ, and ground-based UV-VIS spectrometers (retrieved profiles). MAESTRO comparisons with SAGE III and POAM III were previously performed by Kar et al. (2007). No MAESTRO comparisons with GOMOS and MIPAS were available for this study. ACE-FTS NO profiles have been compared with HALOE. For MIPAS, a composite of NO and NO_2, NO_x, has been compared with ACE-FTS, because a photochemical model accounting for polar

Table 6. Summary of results of the NO$_2$ statistical profile comparisons between ACE-FTS, MAESTRO and the correlative measurements. For cases when the sunrise (SR) and sunset (SS) comparisons were performed separately, this is shown in column 1. The number of coincidences is given in column 2. Columns 3 to 7: for ACE-FTS, altitude range for valid results, absolute (typical, column 4; maximum, column 5) and relative (typical, column 6; maximum, column 7) differences in this range. Columns 8 to 12: same information for MAESTRO.

Instrument (data product)	# of pairs	ACE-FTS Range [km]	Absolute diff.: [ppbv] typical	max.	Relative diff.: [%] typical	max.	MAESTRO Range [km]	Absolute diff.: [ppbv] typical	max.	Relative diff.: [%] typical	max.
HALOE	36	23–40	−0.70	−0.85	−10%	−15.8%	22–43	−0.49	−0.94	−10%	−17.0%
		41–50	+0.55	+0.65	+20%	+40.0%	43–50	−0.42	−0.79	−45%	−68.1%
SAGE II (SR/SR)[a]	148	20–43	+0.80	+1.10	+22%	+37.7%	20–42	+1.06	+1.98	+25%	+38.7%
(SS/SS)	17	20–40	−0.27	−0.66	−6%	−12.6%	—	—	—	—	—
SAGE III[b]	776/712[c]	20–44	−0.28	−0.65	−8%	−14.3%	25–40	−0.35	−0.64	−9%	−15.8%
POAM III[b]	295/180[c]	20–24	−0.30	−0.50	−25%	−38.6%	20–24	−0.30	−0.51	−14%	−24.8%
		25–44	±0.20	−0.59	±6%	+12.8%	25–40	−0.27	−0.43	±8%	−22.7%
SCIAMACHY	372	20–39	−0.15	−0.46	±4%	−11.9%	21–40	+0.21	+0.73	+8%	+13.0%
GOMOS	6865	23–43	n/a	n/a	±10%	−10.0%	—	—	—	—	—
MIPAS	84	24–32	−0.24	−0.57	−8%	−15.5%	—	—	—	—	—
(ESA)		32–47	−1.40	−1.90	−45%	−7.8%	—	—	—	—	—
MIPAS (IMK-IAA)	493	28–44	−3.00	−10.00	−20%	−25.5%	—	—	—	—	—
OSIRIS	543/524[c]	14–24	~0	−0.04	±6%	−8.2%	12–24	+0.15	+0.32	+25%	+38.5%
		25–40	−0.60	−0.92	−13%	−17.3%	25–42	−0.60	−0.91	−14%	−16.7%
DOAS[d] (ACE SR)	13/6[c]	15–37	+0.20	+0.49	+13%	+23.0%	13–37	+0.45	+0.93	+28%	+39.9%
(ACE SS)	15/11[c]	15–37	±0.30	+0.82	+13%	+24.9%	13–37	+0.47	+0.87	+25%	+39.7%
SAOZ[e]	5	12–29	−0.04	−0.07	−11%	−28.2%	12–33	−0.05	−0.09	−6%	−19.8%
		29–43	+0.80	+1.10	+19%	+34.6%	33–43	+0.66	+0.71	+18%	+24.7%

[a] SR/SR for comparisons with ACE-FTS only. For the comparisons with MAESTRO, no separation was made.

[b] For comparisons of MAESTRO with POAM III and SAGE III, results are taken from Kar et al. (2007).

[c] Number of profile pairs for ACE-FTS and MAESTRO, respectively.

[d] Ground-based UV-VIS measurements from Harestua, Norway.

[e] Ground-based UV-VIS measurements from Vanscoy, Canada.

NO$_x$ descent was not available. In addition, ACE NO$_2$ partial columns have been compared with measurements by six ground-based FTIRs. For the comparison of ACE-FTS NO partial columns, five FTIR stations provided data. In the case of the lower vertical resolution UV-VIS and FTIR comparisons, the ACE VMR profiles were smoothed by the appropriate averaging kernels, while the high-resolution SPIRALE profile was smoothed with a triangular function to match the ACE-FTS resolution and a Gaussian function to match the MAESTRO resolution. For the UV-VIS, ground-based FTIR, balloon and four satellite (GOMOS, OSIRIS, MIPAS ESA NO$_2$, SCIAMACHY nadir) comparisons, a photochemical box model was employed in order to correct NO$_2$ and NO to the same local time.

The results of the statistical and individual vertical profile comparisons of NO$_2$ for MAESTRO and ACE-FTS are summarized in Table 6. Typical values are calculated using average values. When the averages are close to zero and hence not so typical, averages of all negative error values and all positive error values are calculated and the maxi-

mum difference is given. Figures 39 and 40 show all absolute and relative differences. For the ACE-FTS comparisons, the mean absolute differences are all within ±1 ppbv between 13 and 40 km (and well within ±0.5 ppbv below 20 km), with the exception of MIPAS ESA product, for which the difference is more negative above 33 km. Looking at the mean relative differences for ACE-FTS and MAESTRO, nearly all of the satellite measurements agree to within about 20% between 25 and 40 km, again with the exception of MIPAS ESA and SAGE II. MAESTRO reports larger VMR values than ACE-FTS in the lower and middle stratosphere (see Fig. 7).

The maximum NO$_2$ VMR occurs between 30 and 35 km; the agreement in this region is good. Below about 25 km, it can be seen that the diurnal effect has not been fully corrected and ACE-FTS has a low bias relative to POAM III at about 23 km, which is also present in other studies (e.g. Brohede et al., 2007a). Above 40 km, there is a suggestion of a slight low bias in the ACE-FTS data, although the results are not consistent for all comparisons. For MAESTRO, the mean absolute differences are within ±1 ppbv between
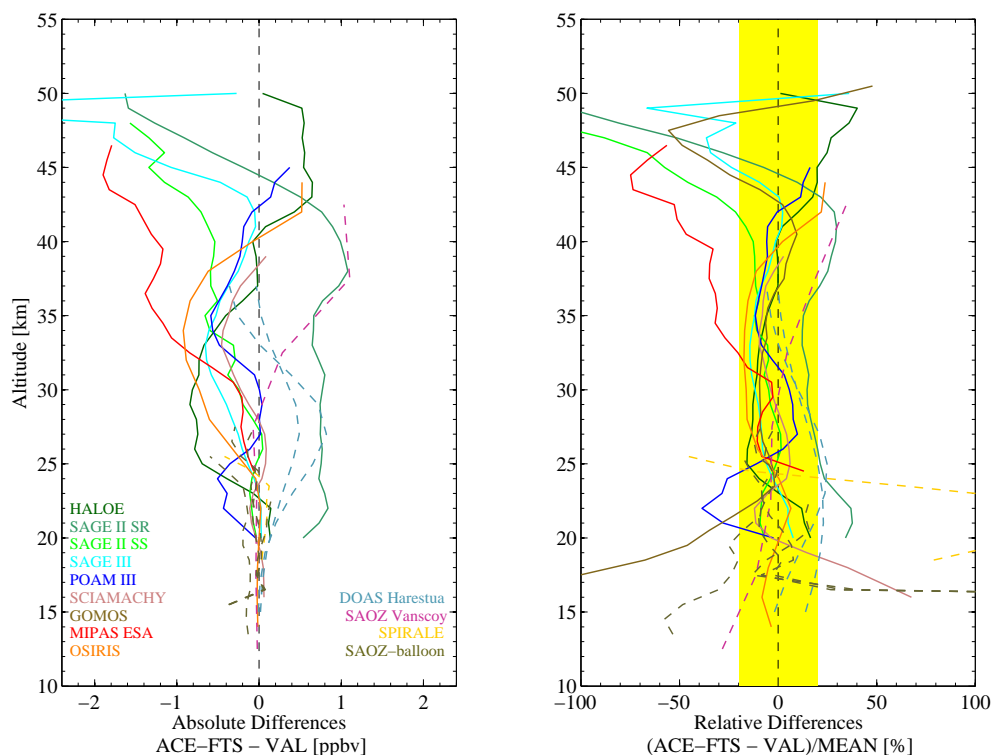
Fig. 39. Summary plot for all the comparisons with ACE-FTS NO$_2$. Left panel: Profiles of the mean absolute differences. Right panel: Profiles of the mean relative differences. In both panels, satellite comparisons are indicated by solid lines and other profile comparisons are indicated by dashed lines. Highlighted in yellow are the ±20% relative differences. Note that for SAGE II the results are separated into sunrise and sunset profiles. GOMOS is only present in the right hand panel, because no VMRs are available (number densities were used).

13 and 40 km (with the exception of the comparisons with SAGE II) and within ±0.5 ppbv below 20 km. The mean relative differences for MAESTRO are all within 20% between 25 and 40 km, with the exception of the Harestua UV-VIS data and the SAGE II data.

It can be seen from the statistical comparisons in Figs. 39 and 40 that there is a systematic low bias between 25 and 35 km for both ACE-FTS and MAESTRO when SAGE II, POAM III, SCIAMACHY for MAESTRO and the ground-based profile results are ignored. The shape of the bias is the same in the HALOE, SAGE III, POAM III, SCIAMACHY and OSIRIS comparisons. Only SAGE II shows different results among the solar occultation measurements, but this instrument is generally considered less accurate than SAGE III, with SAGE II sunset measurements known to be much better than the sunrise ones.

Since the random errors for the ACE instruments are very small, combined random errors are dominated by those of the comparison instruments. The combined random errors for the ACE instruments with OSIRIS and MIPAS ESA were compared to the standard deviation of the relative differences of the ACE instruments with OSIRIS and MIPAS ESA. The combined random errors of the ACE instruments with OSIRIS were found to be around 6 to 19% compared to the standard deviation in the relative differences of 15 to 55% and with MIPAS ESA, the combined random errors were 50 to 70% compared to the standard deviation of 30 to 78%.

Comparisons were also made with single profiles obtained from three balloon flights, and are included in Figs. 39 and 40. Of these, the comparison with the in situ SPIRALE measurement shows the biggest difference, with both ACE instruments showing a high bias. A likely explanation is that the assumption of spatial homogeneity of the stratospheric layers crossed by the lines-of-sight of the satellite instruments is not valid in case of a perturbed dynamical situation such as that experienced in the high latitude winter. The SAOZ balloon comparisons are good to within 20% for the Aire-sur-l'Adour–MAESTRO comparisons, but differences vary between 5% and 50% for ACE-FTS. Even though the SAOZ balloon profiles from Niamey were taken over a longer time span, they all agree to within 20% with the ACE-FTS measurements. MAESTRO and SAOZ balloon measurements agree to within 50%. Below ~17 km the agreement is not as good. This is probably due to the fact that the measurements took place during strong convective activity that extended up to 17 km and possibly generated NO$_x$ due to lightning. The ground-based UV-VIS profile comparisons with data from Harestua agree to within 25% (ACE-
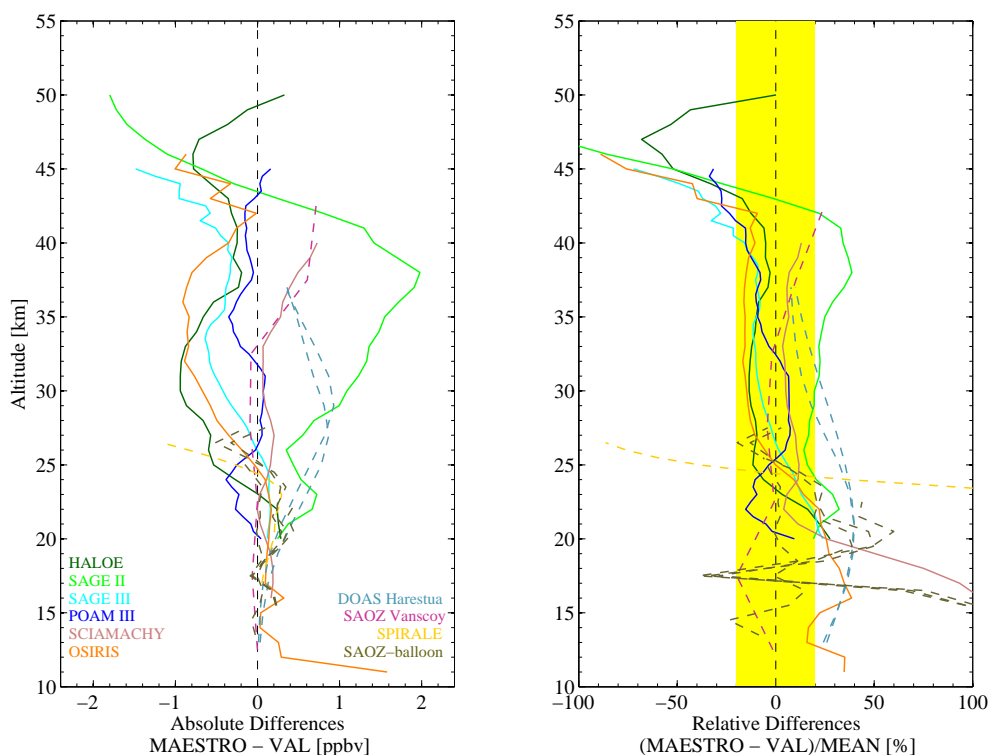
Fig. 40. Same as Fig. 39 but for MAESTRO. The SAGE III and POAM III results are taken from Kar et al. (2007). For SAGE II, results from the combined sunrise and sunset comparisons are shown.

FTS) and 40% (MAESTRO), and for Vanscoy to within 35% (ACE-FTS) and 25% (MAESTRO).

The SCIAMACHY nadir total columns of NO$_2$ showed good correlations with the partial columns of the ACE instruments: $r=0.94$ for ACE-FTS and $r=0.91$ for MAESTRO. The slopes are 0.77 (ACE-FTS) and 0.79 (MAESTRO) and the intercepts are 0.18×10^{15} molec/cm^2 (ACE-FTS) and 0.38×10^{15} molec/cm^2 (MAESTRO). The observed differences are of the order expected for the tropospheric NO$_2$, which is included in the SCIAMACHY columns but not in ACE partial columns.

The last set of comparisons with NO$_2$ was done with partial columns measured by the ground-based FTIRs. Agreement here is good: the mean relative differences are within $\pm12\%$ for five of the six stations for comparisons with ACE-FTS and for four stations for comparisons with MAESTRO. The MAESTRO mean differences are all positive, indicating that there is a high bias whereas for ACE-FTS this mean relative difference does not show a bias. A good correlation ($r=0.91$) is observed between the ACE-FTS and FTIR partial columns, with a slope of 0.95 and an intercept of 0.21×10^{15} molec/cm^2. Good correlation ($r=0.89$) is also observed between the MAESTRO and FTIR partial columns, with a slope of 1.02 and an intercept of 0.21×10^{15} molec/cm^2.

There are fewer comparisons available to assess the quality of the ACE-FTS NO VMRs. Tables 4 and 7 show summaries for the results for the NO and NO$_x$ comparisons of ACE-FTS with ground-based instruments and satellites. It can be seen that the satellite comparison with HALOE shows a very good agreement, typically $\pm8\%$ (and within 20.6%) between 22 and 64 km, and typically $+10\%$ (and within 36%) from 93 to 105 km. There is a small low bias in the ACE-FTS NO measurements below 50 km and a high bias above. The comparisons with MIPAS IMK-IAA NO$_x$ show typical relative differences of $\pm10\%$ (maximum -30.8%) from 15 to 42 km, and -20% (maximum -52.5%) from 42 to 60 km. Given the high variability at the time when coincidences were available this agreement is very good.

For the comparisons of ACE-FTS NO with partial columns measured by the ground-based FTIRs the agreement is not as good. The mean relative differences are all negative, having values between -14.5% and -67.5%, and increasing (becoming more negative) from South to North. This indicates a low bias in the ACE-FTS partial columns relative to the FTIRs. The correlation is poor ($r=0.59$) between the ACE-FTS and FTIR NO partial columns, with a slope of 0.52 and an intercept of 0.31×10^{15} molec/cm^2 on the line fitted to the data.

Table 7. Summary of results of the NO and NO$_x$ statistical comparisons between ACE-FTS and the correlative measurements. The number of coincidences is given in column 2. Columns 3 to 7: altitude range for valid results, absolute (typical value, column 4; maximum value, column 5) and relative (typical, column 6; maximum, column 7) differences in this range.

Instrument (data product)	# of pairs	Range [km]	Absolute diff.: [ppbv]		Relative diff.: [%]	
			typical	max.	typical	max.
MIPAS NO$_x$ (IMK-IAA)	493	15–42	−1	−3.7	±10 %	−30.8%
		42–60	±15	−46.4	−20 %	−52.5 %
HALOE	36	22–64	±0.6	−1.1	±8 %	+20.6%
		93–105	+3100	+5640	+10 %	+36.0 %

In summary, it has been found that the ACE-FTS version 2.2 NO$_2$ and NO and the MAESTRO version 1.2 NO$_2$ are generally consistent with other satellite data. The ACE-FTS and MAESTRO NO$_2$ VMRs agree with the other satellite data sets (with the exception of MIPAS ESA (for ACE-FTS) and SAGE II (for ACE- FTS (sunrise) and MAESTRO)) to within about 20% between 25 and 40 km, and show a negative bias between 23 and 40 km of about 10%. In comparisons with HALOE, ACE-FTS NO VMRs typically agree to ±8% for 22 to 64 km (maximum 21%) and to +10% for 93 to 105 km (maximum 36%). Partial column comparisons for NO$_2$ show that there is quite good agreement between the ACE instruments and the FTIRs, with a mean difference of +7.3% for ACE-FTS and +12.8% for MAESTRO.

References

Abrams, M. C., Chang, A. Y., Gunson, M. R., Abbas, M. M., Goldman, A., Irion, F. W., Michelsen, H. A., Newchurch, M. J., Rinsland, C. P., Stiller, G. P., and Zander, R.: On the assessment and uncertainty of atmospheric trace gas burden measurements with high resolution infrared solar occultation spectra from space by the ATMOS experiment, Geophys. Res. Lett., 23, 2337–2340, doi:10.1029/96GL01794, 1996.

Ackermann, M. and Muller, C.: Stratospheric Nitrogen Dioxide from Infrared Absorption Spectra, Nature, 240, 300–301, 1972.

Amekudzi, L. K., Sinnhuber, B.-M., Sheode, N. V., Meyer, J., Rozanov, A., Lamsal, L. N., Bovensmann, H., and Burrows, J. P.: Retrieval of stratospheric NO$_3$ vertical profiles from sciamachy lunar occultation measurement over the Antarctic, J. Geophys. Res., 110, D20304, doi:10.1029/2004JD005748, 2005.

Amekudzi, L. K., Bramstedt, K., Bracher, A., Rozanov, A., Bovensmann, H., and Burrows, J. P.: SCIAMACHY solar and lunar occultation: validation of ozone, NO$_2$ and NO$_3$ profiles, in: Proc. of Atmospheric Chemistry Validation (ACVE-3) December 2006, SP-642, ESA Publication Division, ESTEC, Noordwijk, The Netherlands, http://www.sciamachy.org/validation/documentation/proceedings_ACVE-3/amekudzi.pdf, 2007.

Bernath, P. F.: Atmospheric chemistry experiment (ACE): Analytical chemistry from orbit, Trend. Anal. Chem., 25, 647–654, 2006.

Bernath, P. F., McElroy, C. T., Abrams, M. C., Boone, C. D., Butler, M., Camy-Peyret, C., Carleer, M., Clerbaux, C., Coheur, P.-F., Colin, R., DeCola, P., De Mazière, M., Drummond, J. R., Dufour, D., Evans, W. F. J., Fast, H., Fussen, D., Gilbert, K., Jennings, D. E., Llewellyn, E. J., Lowe, R. P., Mahieu, E., McConnell, J. C., McHugh, M., McLeod, S. D., Michaud, R., Midwinter, C., Nassar, R., Nichitiu, F., Nowlan, C., Rinsland, C. P., Rochon, Y. J., Rowlands, N., Semeniuk, K., Simon, P., Skelton, R., Sloan, J. J., Soucy, M.-A., Strong, K., Tremblay, P., Turnbull, D., Walker, K. A., Walkty, I., Wardle, D. A., Wehrle, V., Zander, R., and Zou, J.: Atmospheric Chemistry Experiment (ACE): Mission overview, Geophys. Res. Lett., 32, L15S01, doi:10.1029/2005GL022386, 2005.

Berthet, G., Renard, J.-B., Catoire, V., Chartier, M., Robert, C., Huret, N., Coquelet, F., Bourgeois, Q., Rivière, E. D., Barret, B., Lefèvre, F., and Hauchecorne, A.: Remote-sensing measurements in the polar vortex: Comparison to in situ observations and implications for the simultaneous retrievals and analysis of the NO$_2$ and OClO species, J. Geophys. Res., 112, D21310, doi:10.1029/2007JD008699, 2007.

Blumenstock, T., Kopp, G., Hase, F., Hochschild, G., Mikuteit, S., Raffalski, U., and Ruhnke, R.: Observation of unusual chlorine activation by ground-based infrared and microwave spectroscopy in the late Arctic winter 2000/01, Atmos. Chem. Phys., 6, 897–905, 2006, http://www.atmos-chem-phys.net/6/897/2006/.

Boone, C. D., Nassar, R., Walker, K. A., Rochon, Y., McLeod, S. D., Rinsland, C. P., and Bernath, P. F.: Retrievals for the Atmospheric Chemistry Experiment Fourier-transform spectrometer, Appl. Optics, 44, 7218–7231, 2005.

Bovensmann, H., Burrows, J. P., Buchwitz, M., Frerick, J., Noël, S., Rozanov, V. V., Chance, K. V., and Goede, A. P. H.: SCIAMACHY: Mission Objectives and Measurement Modes, J. Atmos. Sci., 56, 127–150, 1999.

Bracher, A., Bovensmann, H., Bramstedt, K., Burrows, J., von Clarmann, T., Eichmann, K.-U., Fischer, H., Funke, B., Gil-López, S., Glatthor, N., Grabowski, U., Höpfner, M., Kaufmann, M., Kellmann, S., Kiefer, M., Koukouli, M., Linden, A., López-Puertas, M., Tsidu, G. M., Milz, M., Noel, S., Rohen, G., Rozanov, A., Rozanov, V., von Savigny, C., Sinnhuber, M., Skupin, J., Steck, T., Stiller, G., Wang, D.-Y., Weber, M., and Wuttke, M.: Cross comparisons of O$_3$ and NO$_2$ measured by the atmospheric ENVISAT instruments GOMOS, MIPAS, and SCIAMACHY, Adv. Space Res., 36, 855–867, 2005.

Bracher A., Sinnhuber M., Rozanov A., and Burrows J.P.: Using a photochemical model for the validation of NO$_2$ satellite measurements at different solar zenith angles, Atmos. Chem. Phys., 5, 393–408, 2005, http://www.atmos-chem-phys.net/5/393/2005/.

Bramstedt, K., Amekudzi, L. K., Bracher, A., Rozanov, A., Bovensmann, H., and Burrows, J. P.: SCIAMACHY solar occultation: Ozone and NO$_2$ profiles from 2002–2006, in: Proc. of Envisat Symposium 2007, SP-636, ESA Publication Division, ESTEC, Noordwijk, The Netherlands, http://www.sciamachy.org/validation/documentation/proceedings_ES2007/463231br.pdf, 2007.

Brewer, A. W., McElroy, C. T., and Kerr, J. B.: Nitrogen dioxide concentrations in the atmosphere, Nature, 246, 129–133, doi:10.1038/246129a0, 1973.

Brohede, S. M., Haley, C. S., McLinden, C. A., Sioris, C. E., Murtagh, D. P., Petelina, S. V., Llewellyn, E. J., Bazureau, A., Goutail, F., Randall, C. E., Lumpe, J. D., Taha, G., Thomasson, L. W., and Gordley, L. L.: Validation of Odin/OSIRIS stratospheric NO$_2$ profiles, J. Geophys. Res., 112, D07310, doi:10.1029/2006JD007586, 2007a.

Brohede, S. M., McLinden, C. A., Berthet, G., Haley, C. S., Murtagh, D., and Sioris, C. E.: A stratospheric NO$_2$ climatology from Odin/OSIRIS limb-scatter measurements, Can. J. Phys., 85, 1253–1274, doi:10.1139/P07-141, 2007b.

Buchwitz, M., Schneising, O., Burrows, J. P., Bovensmann, H., Reuter, M., and Notholt, J.: First direct observation of the atmospheric CO$_2$ year-to-year increase from space, Atmos. Chem. Phys., 7, 4249–4256, 2007, http://www.atmos-chem-phys.net/7/4249/2007/.

Burkhardt, E. G., Lambert, C. A., and Patel, C. K. N.: Stratospheric nitric oxide: Measurements during daytime and sunset, Science, 188, 1111–1113, 1975.

Burrows, J. P., Dehn, A., Deters, B., Himmelmann, S., Richter, A., Voigt, S., and Orphal, J.: Atmospheric remote-sensing reference data from GOME: 1. Temperature-dependent absorption cross-sections of NO$_2$ in the 231–794 nm range, J. Quant. Spectrosc. Ra., 60, 1025–1031, 1998.

Burrows, J. P., Weber, M., Buchwitz, M., Rozanov, V., Ladstätter-Weißenmayer, A., Richter, A., Debeek, R., Hoogen, R., Bramstedt, K., Eichmann, K.-U., Eisinger, M., and Perner, D.: The Global Ozone Monitoring Experiment (GOME): Mission Concept and First Scientific Results, J. Atmos. Sci., 56, 151–175, 1999.

Callies, J., Corpaccioli, E., Eisinger, M., Lefebvre, A., Munro, R., Perez-Albinana, A., Ricciarelli, B., Calamai, L., Gironi, G., Veratti, R., Otter, G., Eschen, M., and van Riel, L.: GOME-2 ozone instrument onboard the European METOP satellites, in: Weather and Environmental Satellites, vol. 5549 of Proc. SPIE Int. Soc. Opt. Eng., 60–70, doi:10.1117/12.557860,

http://spiedigitallibrary.aip.org/getpdf/servlet/GetPDFServlet?
filetype=pdf\&id=PSISDG005549000001000060000001\
&idtype=cvips\&prog=normal, 2004.

Chahine, M. T.: Inverse problems in radiative transfer: determination of atmospheric parameters, J. Atmos. Sci., 27, 960–967, 1970.

Chu, W. P. and McCormick, M. P.: Inversion of stratospheric aerosol and gaseous constituents from spacecraft solar extinction data in the 0.38–1.0 μm wavelength region, Appl. Optics, 18, 1404–1413, 1979.

Chu, W. P. and McCormick, M. P.: SAGE observations of stratospheric nitrogen dioxide, J. Geophys. Res., 91, 5465–5476, 1986.

Dessler, A. E.: The Chemistry and Physics of Stratospheric Ozone, Academic Press, London, 2000.

Drummond, J. R., Houghton, J. T., Peskett, G. D., Rodgers, C. D., Wale, M. J., Whitney, J., and Williamson, E. J.: The Stratospheric and Mesospheric Sounder on Nimbus 7, Phil. Trans. R. Soc. Lond. A, 296, 219–241, 1980.

Dupuy, E., Walker, K. A., Kar, J., Boone, C. D., McElroy, C. T., Bernath, P. F., Drummond, J. R., Skelton, R., McLeod, S. D., Hughes, R. C., Nowlan, C. R., Dufour, D. G., Zou, J., Nichitiu, F., Strong, K., Baron, P., Bevilacqua, R. M., Blumenstock, T., Bodeker, G. E., Borsdorff, T., Bourassa, A. E., Bovensmann, H., Boyd, I. S., Bracher, A., Brogniez, C., Burrows, J. P., Catoire, V., Ceccherini, S., Chabrillat, S., Christensen, T., Coffey, M. T., Cortesi, U., Davies, J., Clercq, C. D., Degenstein, D. A., De Mazière, M., Demoulin, P., Dodion, J., Firanski, B., Fischer, H., Forbes, G., Froidevaux, L., Fussen, D., Gerard, P., Godin-Beekman, S., Goutail, F., Granville, J., Griffith, D., Haley, C. S., Hannigan, J. W., Höpfner, M., Jin, J. J., Jones, A., Jones, N. B., Jucks, K., Kagawa, A., Kasai, Y., Kerzenmacher, T. E., Kleinböhl, A., Klekociuk, A. R., Kramer, I., Küllmann, H., Kuttippurath, J., Kyrölä, E., Lambert, J.-C., Livesey, N. J., Llewellyn, E. J., Lloyd, N. D., Mahieu, E., Manney, G. L., Marshall, B. T., McConnell, J. C., McCormick, M. P., McDermid, I. S., McHugh, M., McLinden, C. A., Mellqvist, J., Mizutani, K., Murayama, Y., Murtagh, D. P., Oelhaf, H., Parrish, A., Petelina, S. V., Piccolo, C., Pommereau, J.-P., Randall, C. E., Robert, C., Roth, Schneider, M., Senten, C., Steck, T., Strandberg, A., Strawbridge, K. B., Sussmann, R., Swart, D. P. J., Tarasick, D. W., Taylor, J. R., Tétard, C., Thomason, L. W., Thompson, A. M., Tully, M. B., Urban, J., Vanhellemont, F., von Clarmann, T., von der Gathen, P., von Savigny, C., Waters, J. W., Witte, J. C., Wolff, M., and Zawodny, J. M.: Validation of ozone measurements from the Atmospheric Chemistry Experiment (ACE), Atmos. Chem. Phys. Discuss., 8, 2513–2656, 2008, http://www.atmos-chem-phys-discuss.net/8/2513/2008/.

Fischer, H. and Oelhaf, H.: Remote sensing of vertical profiles of atmospheric trace constituents with MIPAS limb-emission spectrometers, Appl. Optics, 35, 2787–2796, 1996.

Fischer, H., Birk, M., Blom, C., Carli, B., Carlotti, M., von Clarmann, T., Delbouille, L., Dudhia, A., Ehhalt, D., Endemann, M., Flaud, J.-M., Gessner, R., Kleinert, A., Koopmann, R., Langen, J., López-Puertas, M., Mosner, P., Nett, H., Oelhaf, H., Perron, G., Remedios, J., Ridolfi, M., Stiller, G., and Zander, R.: MIPAS: an instrument for atmospheric and climate research, Atmos. Chem. Phys., 8, 2151–2188, 2008, http://www.atmos-chem-phys.net/8/2151/2008/.

Fontanella, J.-C., Girard, A., Gramont, L., and Louisnard, N.: Vertical Distribution of NO, NO_2, and HNO_3 as Derived from Stratospheric Absorption Infrared Spectra, Appl. Optics, 14, 825–839, 1975.

Fraser, A., Goutail, F., Strong, K., Bernath, P. F., Boone, C., Daffer, W. H., Drummond, J. R., Dufour, D. G., Kerzenmacher, T. E., Manney, G. L., McElroy, C. T., Midwinter, C., McLinden, C. A., Nichitiu, F., Nowlan, C. R., Walker, J., Walker, K. A., Wu, H., and Zou, J.: Intercomparison of UV-visible measurements of ozone and NO_2 during the Canadian Arctic ACE validation campaigns: 2004–2006, Atmos. Chem. Phys., 8, 1763–1788, 2008, http://www.atmos-chem-phys.net/8/1763/2008/.

Fu, D., Mittermeier, R., Sung, K., Bernath, P. F., Walker, K. A., Boone, C. D., Strong, K., Fast, H., Fogal, P., Loewen, P., and Mikhailov, O.: Simultaneous atmospheric measurements using two Fourier transform infrared spectrometers at the Polar Environment Atmospheric Research Laboratory (PEARL) during spring 2006, Atmos. Chem. Phys. Discuss., 8, 5305–5358, 2008, http://www.atmos-chem-phys-discuss.net/8/5305/2008/.

Funke, B., López-Puertas, M., von Clarmann, T., Stiller, G. P., Fischer, H., Glatthor, N., Grabowski, U., Höpfner, M., Kellmann, S., Kiefer, M., Linden, A., Mengistu Tsidu, G., Milz, M., Steck, T., and Wang, D. Y.: Retrieval of stratospheric NO_x from 5.3 and 6.2 μm nonlocal thermodynamic equilibrium emissions measured by Michelson Interferometer for Passive Atmospheric Sounding (MIPAS) on Envisat, J. Geophys. Res., 110, D09302, doi:10.1029/2004JD005225, 2005.

Gille, J. C., Bailey, P. L., and Russell III, J. M.: Temperature and Composition Measurements from the l.r.i.r. and l.i.m.s. Experiments on Nimbus 6 and 7, Phil. Trans. R. Soc. Lond. A, 296, 205–218, 1980.

Glaccum, W., Lucke, R. L., Bevilacqua, R. M., Shettle, E. P., Hornstein, J. S., Chen, D. T., Lumpe, J. D., Krigman, S. S., Debrestian, D. J., Fromm, M. D., Dalaudier, F., Chassefière, E., Deniel, C., Randall, C. E., Rusch, D. W., Olivero, J. J., Brogniez, C., Lenoble, J., and Kremer, R.: The Polar Ozone and Aerosol Measurement instrument, J. Geophys. Res., 101, 14 479–14 488, doi:10.1029/96JD00576, 1996.

Gordley, L. L., Russell III, J. M., Mickley, L. J., Frederick, J. E., Park, J. H., Stone, K. A., Beaver, G. M., McInerney, J. M., Deaver, L. E., Toon, G. C., Murcray, F. J., Blatherwick, R. D., Gunson, M. R., Abbatt, J. P. D., Mauldin III, R. L., Mount, G. H., Sen, B., and Blavier, J.-F.: Validation of nitric oxide and nitrogen dioxide measurements made by the Halogen Occultation Experiment for UARS platform, J. Geophys. Res., 101, 10 241–10 266, 1996.

Gottwald, M., Bovensmann, H., Lichtenberg, G., Noel, S., von Bargen, A., Slijkhuis, S., Piters, A., Hoogeveen, R., von Savigny, C., Buchwitz, M., Kokhanovsky, A., Richter, A., Rozanov, A., Holzer-Popp, T., Bramstedt, K., Lambert, J.-C., Skupin, J., Wittrock, F., Schrijver, H., and Burrows, J. P.: SCIAMACHY, monitoring the changing Earth's atmosphere, published by DLR, http://atmos.caf.dlr.de/projects/scops/sciamachy_book/sciamachy_book.html, 2006.

Gunson, M. R., Abbas, M. M., Abrams, M. C., Allen, M., Brown, L. R., Brown, T. L., Chang, A. Y., Goldman, A., Irion, F. W., Lowes, L. L., Mahieu, E., Manney, G. L., Michelsen, H. A., Newchurch, M. J., Rinsland, C. P., Salawitch, R. J., Stiller, G. P., Toon, G. C., Yung, Y. L., and Zander, R.: The Atmospheric Trace Molecule Spectroscopy (ATMOS) experiment: Deployment on the ATLAS

Space Shuttle missions, Geophys. Res. Lett., 23, 2333–2336, 1996.

Haley, C. S. and Brohede, S.: Status of the Odin/OSIRIS Stratospheric O$_3$ and NO$_2$ Data Products, Can. J. Phys., 85, doi:10.1139/P07-114, 2007.

Haley, C. S., Brohede, S. M., Sioris, C. E., Griffioen, E., Murtagh, D. P., McDade, I. C., Eriksson, P., Llewellyn, E. J., Bazureau, A., and Goutail, F.: Retrieval of stratospheric O$_3$ and NO$_2$ profiles from Odin Optical Spectrograph and Infrared Imager System (OSIRIS) limb-scattered sunlight measurements, J. Geophys. Res., 109(D16), doi:10.1029/2004JD004588, 2004.

Hase, F.: Inversion von Spurengasprofilen aus hochaufgelösten bodengebundenen FTIR-Messungen in Absorption, in: Wissenschaftliche Berichte, no. 6512 in FZK Report, Forschungszentrum Karlsruhe, ISSN 0947–8620, 2000.

Hase, F., Hannigan, J. W., Coffey, M. T., A., G., Höpfner, M., Jones, N. B., Rinsland, C. P., and Wood, S. W.: Intercomparison of retrieval codes used for the analysis of high-resolution, ground-based FTIR measurements, J. Quant. Spectrosc. Ra., 87, 25–52, 2004.

Hase, F., Demoulin, P., Sauval, A., Toon, G., Bernath, P., Goldman, A., Hannigan, J., and Rinsland, C.: An empirical line-by-line model for the infrared solar transmittance spectrum from 700 to 5000 cm^{-1}, J, Quant. Spectros. Ra., 102, 450–463, doi:10.1016/j.jqsrt.2006.02.026, 2006.

Hauchecorne, A., Godin, S., Marchand, M., Heese, B., and Souprayen, C.: Quantification of the transport of chemical constituents from the polar vortex to midlatitudes in the lower stratosphere using the high-resolution advection model MIMOSA and effective diffusivity, J. Geophys. Res., 107, 8289, doi:10.1029/2001JD000491, 2002.

Hauchecorne, A., Bertaux, J.-L., Dalaudier, F., Russell III, J. M., Mlynczakand, M. G., Kyrölä, E., and Fussen, D.: Large increase of NO$_2$ in the north polar mesosphere in January–February 2004: Evidence of a dynamical origin from GOMOS/ENVISAT and SABER/TIMED data, Geophys. Res. Lett., 34(L03), 810, doi:10.1029/2006GL027628, 2007.

Hendrick, F., Barret, B., van Roozendael, M., Boesch, H., Butz, A., De Mazière, M., Goutail, F., Hermans, C., Lambert, J.-C., Pfeilsticker, K., and Pommereau, J.-P.: Retrieval of nitrogen dioxide stratospheric profiles from ground-based zenith-sky UV-visible observations: Validation of the technique through correlative comparisons, Atmos. Chem. Phys., 4, 2091–2106, 2004, http://www.atmos-chem-phys.net/4/2091/2004/.

Hendrick, F., Granville, J., Lambert, J.-C., and van Roozendael, M.: Validation of SCIAMACHY OL3.0 NO$_2$ Profiles and Columns Using Ground-Based DOAS Profiling, in: Proceedings of the Third Workshop on the Atmospheric Chemistry Validation of Envisat (ACVE-3), ESA-ESRIN, Frascati, Italy, http://www.sciamachy.org/validation/documentation/proceedings_ACVE-3/hendrick.pdf, ESA SP-642, 2007.

Irie, H., Kondo, Y., Koike, M., Danilin, M. Y., Camy-Peyret, C., Payan, S., Pommereau, J. P., Goutail, F., Oelhaf, H., Wetzel, G., Toon, G. C., Sen, B., Bevilacqua, R. M., Russell III, J. M., Renard, J. B., Kanzawa, H., Nakajima, H., Yokota, T., Sugita, T., and Sasano, Y.: Validation of NO$_2$ and HNO$_3$ measurements from the Improved Limb Atmospheric Spectrometer (ILAS) with the version 5.20 retrieval algorithm, J. Geophys. Res., 107, 8206, doi:10.1029/2001JD001304, 2002.

Kar, J., McElroy, C. T., Drummond, J. R., Zou, J., Nichitiu, F., Walker, K. A., Randall, C. E., Nowlan, C. R., Dufour, D. G., Boone, C. D., Bernath, P. F., Trepte, C. R., Thomason, L. W., and McLinden, C.: Initial Comparison of Ozone and NO$_2$ profiles from ACE-MAESTRO with Balloon and Satellite Data, J. Geophys. Res., 112(D16), 301, doi:10.1029/2006JD008242, 2007.

Kerzenmacher, T., Walker, K. A., Strong, K., Berman, R., Bernath, P. F., Boone, C. D., Drummond, J. R., Fast, H., Fraser, A., MacQuarrie, K., Midwinter, C., Sung, K., McElroy, C. T., Mittermeier, R. L., Walker, J., and Wu, H.: Measurements of O$_3$, NO$_2$ and Temperature during the 2004 Canadian Arctic ACE Validation Campaign, Geophys. Res. Lett., 32, L16S07, doi:10.1029/2005GL023032, 2005.

Kleinert, A., Aubertin, G., Perron, G., Birk, M., Wagner, G., Hase, F., Nett, H., and Poulin, R.: MIPAS Level 1B algorithms overview: operational processing and characterization, Atmos. Chem. Phys., 7, 1395–1406, 2007, http://www.atmos-chem-phys.net/7/1395/2007/.

Kouker, W., Langbein, I., Reddmann, T., and Ruhnke, R.: The Karlsruhe simulation model of the middle atmosphere (KASIMA), version 2, Tech. Rep. 6278, Forschungszentrum Karlsruhe, 1999.

Kyrölä, E., Tamminen, J., Leppelmeier, G. W., Sofieva, V., Hassinen, S., Bertaux, J.-L., Hauchecorne, A., Dalaudier, F., Cot, C., Korablev, O., Hembise, O., Barrot, G., Mangin, A., Théodore, B., Guirlet, M., Etanchaud, F., Snoeij, P., Koopman, R., Saavedra, L., Fraisse, R., Fussen, D., and Vanhellemont, F.: GOMOS on Envisat: An overview, Adv. Space Res., 33, 1020–1028, doi:10.1016/S0273-1177(03)00590-8, 2004.

Lambert, J., Van Roozendael, M., Simon, P., Pommereau, J., Goutail, F., Gleason, J., Andersen, S., Arlander, D., Buivan, N., Claude, H., De La Noe, J., De Mazière, M., Dorokhov, V., Eriksen, P., Green, A., Karlsen Tornqvist, K., Kastadt Hoiskar, B., Kyro, E., Leveau, J., Merienne, M., Milinevsky, G., Roscoe, H., Sarkissian, A., Shanklin, J., Staehelin, J., Wahlstrom Tellefsen, C., and Vaughan, G.: Combined characterization of GOME and TOMS total ozone measurements from space using ground-based observations from the NDSC, Adv. Space Res., 26, 1931–1940, 2001.

Lambert, J.-C., Roozendael, M. V., Mazière, M. D., Simon, P. C., Pommereau, J.-P., Goutail, F., Sarkissian, A., and Gleason, J. F.: Investigation of to pole-to pole performances of space-borne atmospheric chemistry sensors with ground-based networks, J. Atmos. Sci., 56, 176–193, 1999.

Lefèvre, F., Figarol, F., Carslaw, K., and Peter, T.: The 1997 Arctic ozone depletion quantified from three-dimensional model simulations, Geophys. Res. Lett., 25, 2425–2428, 1998.

Levelt, P. F., van den Oord, G. H. J., Dobber, M. R., Mlkki, A., Visser, H., de Vries, J., Stammes, P., Lundell, J. O. V., and Saari, H.: The Ozone Monitoring Instrument, IEEE Trans. Geosci. Remote Sens., 44, 1093–1101, 2006.

Llewellyn, E. J., Lloyd, N. D., Degenstein, D. A., Gattinger, R. L., Petelina, S. V., Bourassa, A. E., Wiensz, J. T., Ivanov, E. V., McDade, I. C., Solheim, B. H., McConnell, J. C., Haley, C. S., von Savigny, C., Sioris, C. E., McLinden, C. A., Griffioen, E., Kaminski, J., Evans, W. F. J., Puckrin, E., Strong, K., Wehrle, V., Hum, R. H., Kendall, D. J. W., Matsushita, J., Murtagh, D. P., Brohede, S., Stegman, J., Witt, G., Barnes, G., Payne, W. F., Piché, L., Smith, K., Warshaw, G., Deslauniers, D.-L., Marchand, P., Richardson, E. H., King, R. A., Wevers, I., McCreath,

W., Kyrölä, E., Oikarinen, L., Leppelmeier, G. W., Auvinen, H., Mégie, G., Hauchecorne, A., Lefèvre, F., de La Nöe, J., Ricaud, P., Frisk, U., Sjoberg, F., von Scheele, F., and Nordh, L.: The OSIRIS instrument on the Odin spacecraft, Can. J. Phys., 82, 411–422, 2004.

López-Puertas, M., Funke, B., Gil-López, S., von Clarmann, T., Stiller, G. P., Höpfner, M., Kellmann, S., Fischer, H., and Jackman, C. H.: Observation of NO_x Enhancement and Ozone Depletion in the Northern and Southern Hemispheres after the October-November 2003 Solar Proton Events, J. Geophys. Res., 110, A09S43, doi:10.1029/2005JA011050, 2005.

Lucke, R. L., Korwan, D. R., Bevilacqua, R. M., Hornstein, J. S., Shettle, E. P., Chen, D. T., Daehler, M., Lumpe, J. D., Fromm, M. D., Debrestian, D., Neff, B., Squire, M., König-Langlo, G., and Davies, J.: The Polar Ozone and Aerosol Measurement (POAM) III instrument and early validation results, J. Geophys. Res., 104, 18 785–18 800, doi:10.1029/1999JD900235, 1999.

Manney, G. L., Michelsen, H. A., Santee, M. L., Gunson, M. R., Irion, F. W., Roche, A. E., and Livesey, N. J.: Polar vortex dynamics during spring and fall diagnosed using trace gas observations from the Atmospheric Trace Molecule Spectroscopy instrument, J. Geophys. Res., 104, 18 841–18 469, doi:10.1029/1999JD900317, 1999.

Manney, G. L., Daffer, W. H., Zawodny, J. M., Bernath, P. F., Hoppel, K. W., Walker, K. A., Knosp, B. W., Boone, C. D., E., R. E., L., S. M., L., H. V., S., P., R., J. D., L., D., T., M. C., A., M. C., Drummond, J. R., Pumphrey, H. C., Lambert, A., Schwartz, M. J., Froidevaux, L., McLeod, S. D., Takacs, L. L., Suarez, M. J., R., T. C., Cuddy, D. C., Livesey, N. J., Harwood, R. S., and Waters, J. W.: Solar occultation satellite data and derived meteorological products: sampling issues and comparisons with Aura MLS, J. Geophys. Res., 112, D24S50, doi:10.1029/2007JD008709, 2007.

Mauldin, L. E. I., Zaun, N. H., McCormick, M. P., Guy, J. H., and Vaughn, W. R.: Stratospheric Aerosol and Gas Experiment II instruments: A functional description, Opt. Eng., 24, 307–312, 1985.

Mayer, B. and Kylling, A.: Technical note: The libRadtran software package for radiative transfer calculations – description and examples of use, Atmos. Chem. Phys., 5, 1855–1877, 2005, http://www.atmos-chem-phys.net/5/1855/2005/.

McCormick, M., Hamill, P., Pepin, T., Chu, W., Swissler, T., and McMaster, L.: Satellite Studies of the Stratospheric Aerosol, B. Am. Meteorol. Soc., 60, 1038–1046, 1979.

McElroy, C. T.: A spectroradiometer for the measurement of direct and scattered solar spectral irradiance from on-board the NASA ER-2 high-altitude research aircraft, Geophys. Res. Lett., 22, 1361–1364, 1995.

McElroy, C. T., Midwinter, C., Barton, D. V., and Hall, R. B.: A Comparison of J-values estimated by the composition and photodissociative flux measurement with model calculations, Geophys. Res. Lett., 22, 1365–1368, 1995.

McElroy, C. T., Nowlan, C. R., Drummond, J. R., Bernath, P. F., Barton, D. V., Dufour, D. G., Midwinter, C., Hall, R. B., Ogyu, A., Ullberg, A., Wardle, D. I., Kar, J., Zou, J., Nichitiu, F., Boone, C. D., Walker, K. A., and Rowlands, N.: The ACE-MAESTRO instrument on SCISAT: description, performance, and preliminary results, Appl. Optics, 46, 4341–4356, 2007.

McHugh, M., Magill, B., Walker, K. A., Boone, C. D., Bernath,

P. F., and Russell III, J. M.: Comparison of atmospheric retrievals from ACE and HALOE, Geophys. Res. Lett., 32, L10S10, doi:10.1029/2005GL022403, 2005.

McLinden, C., McConnell, J., Griffioen, E., and McElroy, C. T.: A vector radiative transfer model for the Odin/OSIRIS project, Can. J. Phys., 80, 375–393, 2002.

McLinden, C. A., Olsen, S. C., Hannegan, B., Wild, O., Prather, M. J., and Sundet, J.: Stratospheric ozone in 3-D models: A simple chemistry and the cross-tropopause flux, J. Geophys. Res., 105, 14 653–14 665, 2000.

McLinden, C. A., Haley, C. S., and Sioris, C. E.: Diurnal effects in limb scatter observations, J. Geophys. Res., 111(D14), 302, doi:10.1029/2005JD006628, 2006.

Melo, S. M. L., Strong, K., Bassford, M. R., Preston, K. E., McElroy, C. T., Rozanov, E. V., and Egorova, T.: Retrieval of Stratospheric NO_2 Vertical Profiles from Ground-based Zenith-Sky DOAS Measurements: Results for the MANTRA 1998 Field Campaign, Atmos.-Ocean, 43, 339–350, 2005.

Meyer, J., Bracher, A., Rozanov, A., Schlesier, A. C., Bovensmann, H., and Burrows, J. P.: Solar occultation with SCIAMACHY: algorithm description and first validation, Atmos. Chem. Phys., 5, 1589–1604, 2005, http://www.atmos-chem-phys.net/5/1589/2005/.

Moreau, G., Robert, C., Catoire, V., Chartier, M., Camy-Peyret, C., Huret, N., Pirre, M., Pomathiod, L., and Chalumeau, G.: SPIRALE: a multispecies in situ balloon-borne instrument with six tunable diode laser spectrometers, Appl. Optics, 44, 5972–5989, 2005.

Mount, G. H., Rusch, D. W., Zawodny, J. M., Barth, C. A., and Noxon, J. F.: Measurements of stratospheric NO_2 from the Solar Mesosphere Explorer satellite. I – An overview of the results, J. Geophys. Res., 89, 1327–1340, 1984.

Murcray, D. G., Kyle, T. G., Murcray, F. H., and Williams, W. J.: Nitric acid and nitric oxide in the lower stratosphere, Nature, 218, 1968.

Nakajima, H., Sugita, T., Yokota, T., Ishigaki, T., Mogi, Y., Araki, N., Waragai, K., Kimura, N., Iwazawa, T., Kuze, A., Tanii, J., Kawasaki, H., Horikawa, M., Togami, T., Uemura, N., Kobayashi, H., and Sasano, Y.: Characteristics and performance of the Improved Limb Atmospheric Spectrometer-II (ILAS-II) on board the ADEOS-II satellite, J. Geophys. Res., 111, D11S01, doi:10.1029/2005JD006334, 2006.

Newchurch, M. J., Allen, M., Gunson, M. R., Salawitch, R. J., Collins, G. B., Huston, K. H., Abbas, M. M., Abrams, M. C., Chang, A. Y., Fahey, D. W., Gao, R. S., Irion, F. W., Loewenstein, M., Manney, G. L., Michelsen, H. A., Podolske, J. R., Rinsland, C. P., and Zander, R.: Stratospheric NO and NO_2 abundances from ATMOS solar-occultation measurements, Geophys. Res. Lett., 23, 2373–2376, 1996.

Norton, H. and Beer, R.: New apodizing functions for Fourier spectrometry, J. Opt. Soc. Am., 66, 259–264, 1976; errata corrige J. Opt. Soc. Am., 67, 419, 1977.

Notholt, J., Toon, G., Stordal, F., Solberg, S., Schmidbauer, N., Meier, A., Becker, E., and Sen, B.: Seasonal variations of Atmospheric trace gases in the high Arctic at 79° N, J. Geophys. Res., 102, 12 855–12 861, 1997.

Noxon, J. F.: Nitrogen dioxide in the stratosphere and troposphere measured by ground-based absorption spectroscopy, Science, 187, 547–549, 1975.

Olsen, S., McLinden, C. A., and Prather, M. J.: Stratospheric N$_2$O-NO$_y$ system: Testing uncertainties in a 3-D framework, J. Geophys. Res., 106, 28 771–28 784, 2001.

Paton-Walsh, C., Jones, N. B., Wilson, S. R., Haverd, V., Meier, A., Griffith, D. W. T., and Rinsland, C. P.: Measurements of trace gas emissions from Australian forest fires and correlations with coincident measurements of aerosol optical depth, J. Geophys. Res., 110(D24), 305, doi:10.1029/2005JD006202, 2005.

Payan, S., Camy-Peyret, C., Jeseck, P., Hawat, T., Pirre, M., Renard, J.-B., Robert, C., Lefèvre, F., Kansawa, H., and Sasano, Y.: Diurnal and nocturnal distribution of stratospheric NO$_2$ from solar and stellar occultation measurements: Comparison with models and ILAS satellite measurements, J. Geophys. Res., 104, 21 585–21 593, 1999.

Platt, U.: Differential optical absorption spectroscopy (DOAS), in Sigrist, M., W.: Air Monitoring by Spectroscopic Techniques Chemical Analysis Series, 127, 27–84, Wiley, New York, 1994.

Platt, U. and Stutz, J.: Differential Optical Absorption Spectroscopy, Springer, Berlin, ISBN: 978-3-540-21193-8, 2008.

Pommereau, J. and Goutail, F.: O$_3$ and NO$_2$ Ground-Based Measurements by Visible Spectrometry during Arctic Winter and Spring 1988, Geophys. Res. Lett., 15, 891–894, 1988a.

Pommereau, J. and Goutail, F.: Stratospheric O$_3$ and NO$_2$ Observations at the Southern Polar Circle in Summer and Fall 1988, Geophys. Res. Lett., 15, 895–898, 1988b.

Pommereau, J. P. and Piquard, J.: Ozone, nitrogen dioxide and aerosol vertical distributions by UV-visible solar occultation from balloons, Geophys. Res. Lett., 21, 1227–1230, 1994.

Pougatchev, N. S. and Rinsland, C. P.: Spectroscopic study of the seasonal variation of carbon monoxide vertical distribution above Kitt Peak, J. Geophys. Res., 100, 1409–1416, 1995.

Pougatchev, N. S., Connor, B. J., and Rinsland, C. P.: Infrared measurements of the ozone vertical distribution above Kitt Peak, J. Geophys. Res., 100, 16 689–16 697, 1995.

Prather, M. J.: Catastrophic loss of stratospheric ozone in dense volcanic clouds, J. Geophys. Res., 97, 10 187–10 191, 1997.

Preston, K. E., Jones, R. L., and Roscoe, H. K.: Retrieval of NO$_2$ vertical profiles from ground-based UV-visible measurements: Method and validation, J. Geophys. Res., 102, 19 089–19 097, 1997.

Randall, C. E., Lumpe, J. D., Bevilacqua, R. M., Hoppel, K. W., Shettle, E. P., Rusch, D. W., Gordley, L. L., Kreher, K., Pfeilsticker, K., Boesch, H., Toon, G., Goutail, F., and Pommereau, J.-P.: Validation of POAM III NO$_2$ measurements, J. Geophys. Res., 107, 4432, doi:10.1029/2001JD001520, 2002.

Randall, C. E., Harvey, V. L., Manney, G. L., Orsolini, Y. J., Codrescu, M., Sioris, C., Brohede, S., Haley, C. S., Gordley, L. L., Zawodny, J. M., and Russell III, J. M.: Stratospheric effects of energetic particle precipitation in 2003–2004, Geophys. Res. Lett., 32, L05802, doi:10.1029/2004GL022003, 2005a.

Randall, C. E., Manney, G., Harvey, V., and Lumpe, J.: Update on the SOSST unified data base and occultation intercomparisons, Solar Occultation Satellite Science Team annual meeting, Columbia, MD, 2005b.

Randall, C. E., Harvey, V. L., Singleton, C. S., Bailey, S. M., Bernath, P. F., Codrescu, M., Nakajima, H., and Russell III, J. M.: Energetic particle precipitation effects on the Southern Hemisphere stratosphere in 1992–2005, J. Geophys. Res., 112, 8308, doi:10.1029/2006JD007696, 2007.

Raspollini, P., Belotti, C., Burgess, A., Carli, B., Carlotti, M., Ceccherini, S., Dinelli, B. M., Dudhia, A., Flaud, J.-M., Funke, B., Höpfner, M., López-Puertas, M., Payne, V., Piccolo, C., Remedios, J. J., Ridolfi, M., and Spang, R.: MIPAS level 2 operational analysis, Atmos. Chem. Phys., 6, 5605–5630, 2006, http://www.atmos-chem-phys.net/6/5605/2006/.

Richter, A., Wittrock, F., Weber, M., Beirle, S., Kühl, S., Platt, U., Wagner, T., Wilms-Grabe, W., and Burrows, J. P.: GOME observations of stratospheric trace gas distributions during the splitting vortex event in the Antarctic winter 2002 Part I: Measurements, J. Atmos. Sci., 62, 778–785, 2005.

Ridolfi, M., Carli, B., Carlotti, M., von Clarmann, T., Dinelli, B. M., Dudhia, A., Flaud, J.-M., Höpfner, M., Morris, P. E., Raspollini, P., Stiller, G., and Wells, R. J.: Optimised forward model and retrieval scheme for MIPAS near-real-time data processing, Appl. Optics, 39, 1323–1340, 2000.

Rinsland, C. P., Jones, N. B., Connor, B. J., Logan, J. A., Pougatchev, N. S., Goldman, A., Murcray, F. J., Stephen, T. M., Pine, A. S., Zander, R., Mahieu, E., and Demoulin, P.: Northern and southern hemisphere ground-based infrared spectroscopic measurements of tropospheric carbon monoxide and ethane, J. Geophys. Res., 103, 28 197–28 218, doi:10.1029/98JD02515, 1998.

Rinsland, C. P., Boone, C., Nassar, R., Walker, K., Bernath, P., McConnell, J. C., and Chiou, L.: Atmospheric Chemistry Experiment (ACE) Arctic stratospheric measurements of NO$_x$ during February and March 2004: Impact of intense solar flares, Geophys. Res. Lett., 32, L16S05, doi:10.1029/2005GL022425, 2005.

Rivière, E. D., Pirre, M., Berthet, G., Renard, J.-B., Taupin, F. G., Huret, N., Chartier, M., Knudsen, B., and Lefèvre, F.: On the interaction between nitrogen and halogen species in the Arctic polar vortex during THESEO and THESEO 2000, J. Geophys. Res., 108, 8311, doi:10.1029/2002JD002087, 2002.

Roche, A. E., Kumer, J. B., Mergenthaler, J. L., Ely, G. A., Uplinger, W. G., Potter, J. F., James, T. C., and Sterritt, L. W.: The cryogenic limb array etalon spectrometer (CLAES) on UARS: experiment description and performance, J. Geophys. Res., 98, 10 763–10 776, 1993.

Rodgers, C. D.: Inverse Methods for Atmospheric Sounding – Theory and Practise, vol. 2 of Series on Atmospheric, Oceanic and Planetary Physics/, World Scientific, ISBN-981-02-2740-X, 2000.

Rodgers, C. D. and Connor, B. J.: Intercomparison of remote sounding instruments, J. Geophys. Res., 108, 4116, doi:10.1029/2002JD002299, 2003.

Roscoe, H. K., Johnston, P. V., van Roozendael, M., Richter, A., Sarkissian, A., Roscoe, J., Preston, K. E., Lambert, J.-C., Hermans, C., Decuyper, W., Dzienus, S., Winterrath, T., Burrows, J. P., Goutail, F., Pommereau, J.-P., D'Almeida, E., Hottier, J., Coureul, C., Didier, R., Pundt, I., Bartlett, L. M., and McElroy, C. T.: Slant column measurements of O$_3$ and NO$_2$ during the NDSC intercomparison of zenith-sky UV-visible spectrometers in June 1996, J. Atmos. Chem., 32, 281–314, 1999.

Rothman, L. S., Jacquemart, D., Barbe, A., Chris Bennerc, D., Birk, M., Brown, L. R., Carleer, M. R., Chackerian Jr., C., Chance, K., Coudert, L. H., Dana, V., Devi, V. M., Flaud, J.-M., Gamache, R. R., Goldman, A., Hartmann, J.-M., Jucks, K. W., Maki, A. G., Mandin, J.-Y., Massie, S. T., Orphal, J., Perrin, A., Rinsland,

C. P., Smith, M. A. H., Tennyson, J., Tolchenov, R. N., Toth, R. A., Vander Auwera, J., Varanasi, P., and Wagner, G.: The HITRAN 2004 molecular spectroscopic database, J. Quant. Spectrosc. Ra., 96, 139–204, 2005.

Rozanov, A., Rozanov, V., Buchwitz, M., Kokhanovsky, A., and Burrows, J. P.: SCIATRAN 2.0 – A new radiative transfer model for geophysical applications in the 175–2400 nm spectral region, Adv. Space Res., 36, 1015–1019, 2005.

Russell III, J. M., Gordley, L. L., Park, J. H., Drayson, S. R., Hesketh, W. D., Cicerone, R. J., Tuck, A. F., Frederick, J. E., Harries, J. E., and Crutzen, P. J.: The Halogen Occultation Experiment, J. Geophys. Res., 98, 10 777–10 797, doi:10.1029/93JD00799, 1993.

SAGE ATBD Team: SAGE III Algorithm Theoretical Basis Document (ATBD) for transmission level 1b products version 2.1, Tech. rep., NASA Langley Res. Cent. (LaRC), Hampton, Virginia, 2002.

Sander, S. P., Friedl, R. R., Golden, D. M., Kuyolo, Huie, R. E., Orkin, V. L., Moortgat, G. K., Ravishankara, A. R., Kolb, C. E., Molina, M. J., and Finlayson-Pitts, B. J.: Chemical kinetics and photochemical data for use in stratospheric modeling, in Evaluation 14, Tech. Rep. 02-025, JPL, Pasadena, California, 2003.

Sasano, Y., Suzuki, M., Yokota, T., and Kanzawa, H.: Improved Limb Atmospheric Spectrometer (ILAS) for stratospheric ozone layer measurements by solar occultation technique, Geophys. Res. Lett., 26, 197–200, 1999.

Schneider, M., Blumenstock, T., Chipperfield, M., Hase, F., Kouker, W., Reddmann, T., Ruhnke, R., Cuevas, E., and Fischer, H.: Subtropical trace gas profiles determined by ground-based FTIR spectroscopy at Izaña (28° N, 16° W): Five year record, error analysis, and comparison with 3D-CTMs, Atmos. Chem. Phys., 5, 153–167, 2005,
http://www.atmos-chem-phys.net/5/153/2005/.

Strong, K., Bailak, G., Barton, D., Bassford, M. R., Blatherwick, R. D., Brown, S., Chartrand, D., Davies, J., Drummond, J. R., Fogal, P. F., Forsberg, E., Hall, R., Jofre, A., Kaminski, J., Kosters, J., Laurin, C., McConnell, J. C., McElroy, C. T., McLinden, C. A., Melo, S. M. L., Menzies, K., Midwinter, C., Murcray, F. J., Nowlan, C., Olson, R. J., Quine, B. M., Rochon, Y., Savastiouk, V., Solheim, B., Sommerfeldt, D., Ullberg, A., Werchohlad, S., Wu, H., and Wunch, D.: MANTRA - A Balloon Mission to Study the Odd-Nitrogen Budget of the Stratosphere, Atmos.-Ocean., 43, 283–299, 2005.

Strong, K., Wolff, M. A., Kerzenmacher, T. E., Walker, K. A., Bernath, P. F., Blumenstock, T., Boone, C., Catoire, V., Coffey, M., Mazière, M. D., Demoulin, P., Duchatelet, P., Dupuy, E., Hannigan, J., Höpfner, M., Glatthor, N., Griffith, D. W. T., Jin, J., Jones, N., Jucks, K., Kuttippurath, J., Lambert, A., Mahieu, E., McConnell, J. C., Mellqvist, J., Mikuteit, S., Murtagh, D., Notholt, J., Piccolo, C., Raspollini, P., Ridolfi, M., Robert, C., Schneider, M., Schrems, O., Semeniuk, K., Senten, C., Stiller, G. P., Strandberg, A., Taylor, J., Tétard, C., Toohey, M., Urban, J., Warneke, T., and Wood, S.: Validation of ACE-FTS N$_2$O Measurements, Atmos. Chem. Phys., 8, 4759–4786, 2008, http://www.atmos-chem-phys.net/8/4759/2008/.

Taylor, F. W., Rodgers, C. D., Whitney, J. G., Werrett, S. T., Barnett, J. J., Peskett, G. D., Venters, P., Ballard, J., Palmer, C. W. P., Knight, R. J., Morris, P., Nightingale, T., and Dudhia, A.: Remote sensing of the atmospheric structure and composi-

tion by pressure modulator radiometry from space: the ISAMS experiment on UARS, J. Geophys. Res., 98, 10 799–10 814, doi:10.1029/92JD03029, 1993.

Vandaele, A. C., Fayt, C., Hendrick, F., Hermans, C., Humbled, F., van Roozendael, M., Gil, M., Navarro, M., Puentedura, O., Yela, M., Braathen, G., Stebel, K., Tørnkvist, K., Johnston, P., Kreher, K., Goutail, F., Mieville, A., Pommereau, J.-P., Khaikine, S., Richter, A., Oetjen, H., Wittrock, F., Bugarski, S., Friess, U., Pfeilsticker, K., Sinreich, R., Wagner, T., Corlett, G., and Leigh, R.: An intercomparison campaign of ground-based UV-Visible measurements of NO$_2$, BrO, and OClO slant columns. Methods of analysis and results for NO$_2$, J. Geophys. Res., 110(D08), 305, doi:10.1029/2004JD005423, 2005.

Vigouroux, C., De Mazière M., Errera, Q, Chabrillat, S., Mahieu, E., Duchatelet, P., Wood, S., Smale, D., Mikuteit, S., Blumenstock, T., Hase, F., and Jones, N.: Comparisons between ground-based FTIR and MIPAS N$_2$O and HNO$_3$ profiles before and after assimilation in BASCOE, Atmos. Chem. Phys., 7, 377–396, 2007, http://www.atmos-chem-phys.net/7/377/2007/.

von Clarmann, T., Chidiezie Chineke, T., Fischer, H., Funke, B., García-Comas, M., Gil-López, S., Glatthor, N., Grabowski, U., Höpfner, M., Kellmann, S., Kiefer, M., Linden, A., López-Puertas, M., López-Valverde, M.-A., Mengistu Tsidu, G., Milz, M., Steck, T., and Stiller, G. P.: Remote Sensing of the Middle Atmosphere with MIPAS, in: Remote Sensing of Clouds and the Atmosphere VII, edited by: Schäfer, K., Lado-Bordowsky, O., Comerón, A., and Picard, R. H., 4882, 172–183, SPIE, Bellingham, WA, USA, 2003a.

von Clarmann, T., Glatthor, N., Grabowski, U., Höpfner, M., Kellmann, S., Kiefer, M., Linden, A., Mengistu Tsidu, G., Milz, M., Steck, T., Stiller, G. P., Wang, D. Y., Fischer, H., Funke, B., Gil-López, S., and López-Puertas, M.: Retrieval of temperature and tangent altitude pointing from limb emission spectra recorded from space by the Michelson Interferometer for Passive Atmospheric Sounding (MIPAS), J. Geophys. Res., 108, 4736, doi:10.1029/2003JD003602, 2003b.

Wetzel, G., Oelhaf, H., Friedl-Vallon, F., Kleinert, A., Lengel, A., Maucher, G., Nordmeyer, H., Ruhnke, R., Nakajima, H., Sasano, Y., Sugita, T., and Yokota, T.: Intercomparison and validation of ILAS-II version 1.4 target parameters with MIPAS-B measurements, J. Geophys. Res., 111, D11S06, doi:10.1029/2005JD006287, 2006.

Wetzel, G., Bracher, A., Funke, B., Goutail, F., Hendrick, F., Lambert, J.-C., Mikuteit, S., Piccolo, C., Pirre, M., Bazureau, A., Belotti, C., Blumenstock, T., De Mazière, M., Fischer, H., Huret, N., Ionov, D., López-Puertas, M., Maucher, G., Oelhaf, H., Pommereau, J.-P., Ruhnke, R., Sinnhuber, M., Stiller, G., Van Roozendael, M., and Zhang, G.: Validation of MIPAS-ENVISAT NO$_2$ operational data, Atmos. Chem. Phys., 7, 3261–3284, 2007, http://www.atmos-chem-phys.net/7/3261/2007/.

Wiacek, A., Jones, N. B., Strong, K., Taylor, J. R., Mittermeier, R. L., and Fast, H.: First detection of meso-thermospheric Nitric Oxide (NO) by ground-based FTIR solar absorption spectroscopy, Geophys. Res. Lett., 33(L03), 811, doi:10.1029/2005GL024897, 2006.

Wiacek, A., Taylor, J. R., Strong, K., Saari, R., Kerzenmacher, T., Jones, N. B., and Griffith, D. W. T.: Ground-Based solar absorption FTIR spectroscopy: characterization of retrievals and first results from a novel optical design instrument at a New NDACC

Complementary Station, J. Atmos. Oceanic Technol., 24, 432–448, 2007.

Wolff, M. A., Kerzenmacher, T., Strong, K., Walker, K. A., Toohey, M., Dupuy, E., Bernath, P., Boone, C., Brohede, S., Catoire, V., von Clarmann, T., Coffey, M., Daffer, W. H., Mazière, M. D., Duchatelet, P., Glatthor, N., Griffith, D. W. T., Hannigan, J., Hase, F., Höpfner, M., Huret, N., Jones, N., Jucks, K., Kagawa, A., Kasai, Y., Kramer, I., Kúllmann, H., Kuttippurath, J., Mahieu, E., Manney, G., McLinden, C., Mébarki, Y., Mikuteit, S., Murtagh, D., Piccolo, C., Raspollini, P., Ridolfi, M., Ruhnke, R., Santee, M., Senten, C., Smale, D., Tétard, C., Urban, J., and Wood, S.: Validation of HNO$_3$, ClONO$_2$ and N$_2$O$_5$ from the Atmospheric Chemistry Experiment Fourier Transform Spectrometer (ACE-FTS), Atmos. Chem. Phys., 8, 3529–3526, 2008, http://www.atmos-chem-phys.net/8/3529/2008/.

Wunch, D., Tingley, M. P., Shepherd, T. G., Drummond, J. R., Moore, G. W. K., and Strong, K.: Climatology and Predictability of the Late Summer Stratospheric Zonal Wind Turnaround over Vanscoy, Saskatchewan, Atmos.-Ocean, 43, 301–313, doi:10.3137/ao.430402, 2005.